الجامعة الأردنيـــــة
كلية الدراسات العليا

التاريـــخ: ٢٥ / ٧ / ٢٠١١م

نموذج رقم (١٨)
اقرار والتزام بالمعايير الأخلاقية والأمانة العلمية
وقوانين الجامعة الأردنية وأنظمتها وتعليماتها
لطلبة الماجستير

أنا الطالبة: رشا خالد الشويكي   الرقم الجامعي: (٨٠٧٠١٩٩)
تخصص: الكيمياء   الكليـــــــة: العلوم

عنوان الرسالة:

Preparation of some Ru(II) Complexes for Dye-sensitized Solar Cells

أعلن بأنني قد التزمت بقوانين الجامعة الأردنية وأنظمتها وتعليماتها وقراراتها السارية المفعول المتعلقة باعداد رسائل الماجستير عندما قمت شخصيا" باعداد رسالتي وذلك بما ينسجم مع الأمانة العلمية وكافة المعايير الأخلاقية المتعارف عليها في كتابة الرسائل العلمية. كما أنني أعلن بأن رسالتي هذه غير منقولة أو مستلة من رسائل أو كتب أو أبحاث أو أي منشورات علمية تم نشرها أو تخزينها في أي وسيلة اعلامية، وتأسيسا" على ما تقدم فانني أتحمل المسؤولية بأنواعها كافة فيما لو تبين غير ذلك بما فيه حق مجلس العمداء في الجامعة الأردنية بالغاء قرار منحي الدرجة العلمية التي حصلت عليها وسحب شهادة التخرج مني بعد صدورها دون أن يكون لي أي حق في التظلم أو الاعتراض أو الطعن بأي صورة كانت في القرار الصادر عن مجلس العمداء بهذا الصدد.

توقيع الطالب: ....   التاريخ: ٢٥ / ٧ /٢٠١١

تعتمد كلية الدراسات العليا
هذه النسخة من الرسالة

٢٥/٧/٢٠١١

The University of Jordan
Authorization Form

I, Rasha Khaled Al-Shwieki authorize the University of Jordan to supply copies of my Thesis/Dissertation to libraries or establishments or individuals on request.

Signature:
Date: ٢٠١١/٧/٢٥

PREPARATION OF SOME RUTHENIUM(II) COMPLEXES FOR DYE-SENSITIZED SOLAR CELLS

By
Rasha Khaled Al-Shwieki

Supervisor
Dr. Hamdallah A. Hodali, Prof.

This Thesis was Submitted in Partial Fulfillment of the Requirements for the Master's Degree in Chemistry

Faculty of Graduate Studies
The University of Jordan

July, 2011

Committee Decision

This Thesis (Preparation of some Ru(II) Complexes for Dye-Sensitized Solar Cells) was successfully defended and approved on Wednesday 13/7/2011.

Examination Committee	**Signature**
Dr. Hamdallah A. Hodali, Chairman Prof. of Inorganic Chemistry.	-------------
Dr. Musa Z. Nazer, Member Prof. of Organic Chemistry.	-------------
Dr. Afif M. Seyam, Member Prof. of Inorganic Chemistry.	-------------
Dr. Mahmoud S. Sunjuk, Member Assist. Prof. of Inorganic Chemistry (Hashemite University).	-------------

Dedication

To My

Mother, Father

Brothers and Sisters

And

To Whom I Love

AKNOWLEDGEMENTS

First and foremost I would like to thank God who has been my source of strength and to whom I owe all that I have been able to do and accomplish. Then my deepest appreciation and utmost gratitude goes to my supervisor Prof. Hamdallah A. Hodali for his invaluable support and patient guidance during the course of this work.

I would also like to thank the members of the committee composed of Prof. Musa Z. Nazer, Prof. Afif M. Seyam, and Dr. Mahmoud S. Sunjuk for their help and useful comments on this thesis.

Finally, sincere thanks to my parents for their endless support in everything I've ventured to in my life, and to my friends for their assistance, for listening to my complaints and particularly for all the fun we had during this period, and to all employees at the chemistry department, for the encouragement they provide at all times.

List of Contents

List of Tables

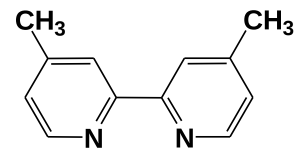
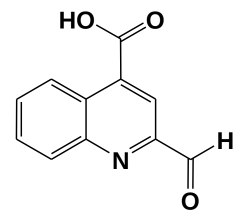
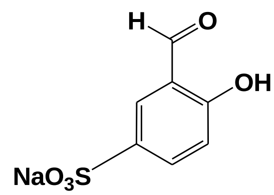
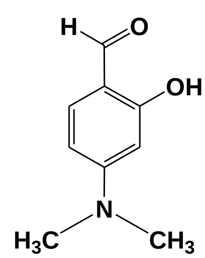
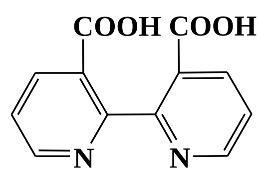
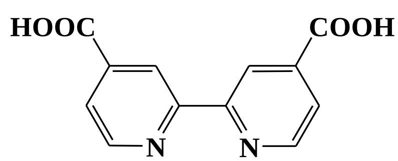
List of Figures

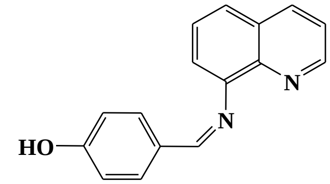
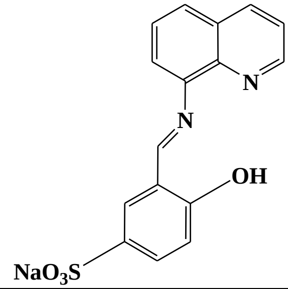
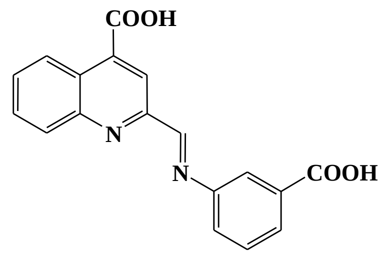
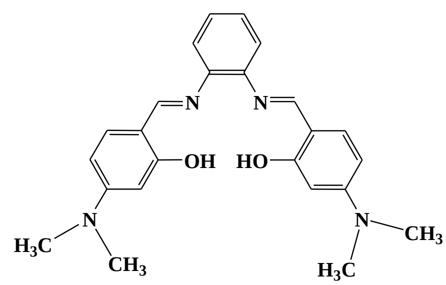
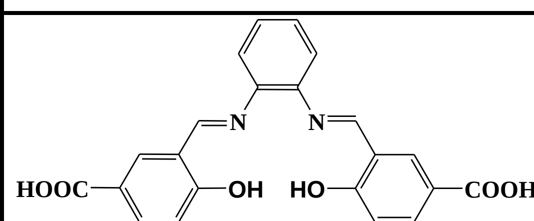
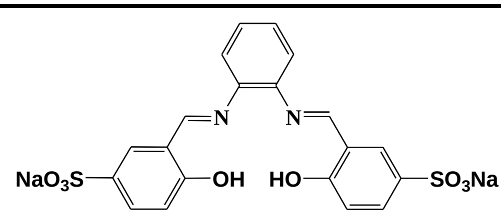
List of Schemes

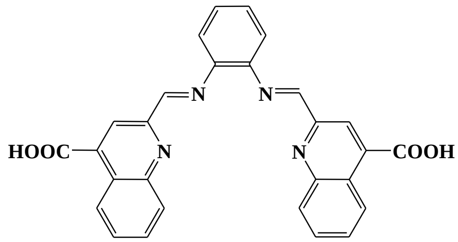
List of Abbreviations

DSSCs	Dye-Sensitized Solar Cells
FTO	Fluorine-doped Tin Oxide
HOMO	Highest Occupied Molecular Orbital
HTM	Hole Transport Material
LUMO	Lowest Unoccupied Molecular Orbital
MLCT	Metal-to-Ligand Charge Transfer
PV	Photovoltaic Cell
RT	Room Temperature
TW	Terawatt

List of Compounds and their ID. numbers

ID. No.	Name	Structure
I	4,4`-dimethyl-2,2`-bipyridine	
II	2-formyl-quinolinecarboxylic acid	
III	Sodium salt of salicylaldehyde-5-sulfonic acid	
IV	4-N,N-dimethylamino-2-hydroxybenzaldehyde	
V	3,3`-Dicarboxy-2,2`-bipyridine	
VI	4,4`-Dicarboxy-2,2`-bipyridine	

VII	4-[(8-quinolinylimino)methyl]phenol	
VIII	sodium salt of 4-hydroxy-3-[(quinolin-8-yl)carboximidoyl]benzenesulfonic acid	
IX	2-[(3-carboxyphenyl)carboximidoyl]quinolin-4-carboxylic acid	
X	2,2`-[1,2-phenylenebis(nitrilomethylidyne)]bis[5-dimethyamino]phenol	
XI	3,3`[1,2-phenylenebis(nitrilomethylidyne)]bis[4-hydroxy]benzoic acid	
XII	sodium salt of3,3`-[1,2-phenylenebis(nitrilomethylidyne)]bis[4-hydroxy]benzenesulfonic acid	

XIII	2,2`-(1,2-phenylenebis(azan-1-yl-1-ylidene))bis(methan-1-yl-1-ylidine)diquinoline-4-carboxylic acid	

PREPARATION OF SOME RUTHENIUM(II) COMPLEXES FOR DYE-SENSITIZED SOLAR CELLS

By

Rasha Khaled Al-Shweiki

Supervisor

Dr. Hamdallah A. Hodali, Prof.

Abstract

In this work a number of Schiff bases were prepared from: (a) condensation of 8-aminoquinoline with 4-hydroxybenzaldehyde to give **(1)** or with sodium salt of salicylaldehyde-5-sulfonic acid to give **(2)**, (b) condensation of 3-aminobenzoic acid with 2-formyl-4-quinolinecarboxylic acid to give **(3)**, (c) condensation of 1,2-phenylenediamine with 3-formyl-4-hydroxybenzoic acid to give **(4)**, with 4-N,N-dimethylamino-2-hydroxybenzaldehyde to give **(5)**, with sodium salt of salicylaldehyde-5-sulfonic acid to give **(6)**, and with 2-formyl-4-quinolinecarboxylic acid to give **(7)**. The isolated ligands were fully characterized using elemental analysis and IR, ^{1}H-NMR, ^{13}C-NMR and mass spectroscopy. Reaction of **1**, **2**, and **7** with dichlorotetrakis(dimethylsulphoxide)ruthenium(II), **$RuCl_2(DMSO)_4$**, gave the complexes [Ru(**1**)(AQ)Cl_2].5H_2O, [Ru(**2**-H)$_2$].4H_2O and [Ru(**7**)Cl_2].3H_2O, respectively. Reaction of **4**, **5**, and **6** with dichlorotris(triphenylphosphine)ruthenium(II), **$RuCl_2(PPh_3)_3$**, gave the complexes [Ru(**4**-3H)(PPh_3)(H_2O)], [Ru(**5**-2H)(PPh_3)(H_2O)].3H_2O and [Ru(**6**-2H)(PPh_3)(NEt_3)].3H_2O respectively. The complexes were characterized by microanalysis, IR spectra, electrical conductivity, and magnetic susceptibility measurements. All the complexes show absorption in the UV-Vis. region. The complexes [Ru(**1**)(AQ)Cl_2].5H_2O and [Ru(**2**-H)$_2$].4H_2O show absorption extending to 623 nm and 630 nm, respectively. The complexes [Ru(4-3H)(PPh_3)(H_2O)], [Ru(5-2H)(PPh_3)(H_2O)].3H_2O and [Ru(6-2H)(PPh_3)(NEt_3)].3H_2O show a strong absorption at λ = 466 nm (ε = 12,585 L.mol^{-1}.cm^{-1}), 412 nm (ε = 10,357 L.mol^{-1}.cm^{-1}), and 413 nm (ε = 16,553 L.mol^{-1}.cm^{-1}), respectively.

1. INTRODUCTION

1.1 Background

The quality of human life depends largely on the availability of energy. Now, more than ever before, energy is what makes our world continuously work (Ghoniem, 2011). Nowadays, fossil fuel resources meet most of the world's energy demand; supplying about 82% of all energy consumed worldwide (Ghoniem, 2011). However, this energy source is facing rapid depletion, and its combustion is accompanied by many dangerous effects, such as accumulation of CO_2 gas in the atmosphere (Gaffney and Marely, 2009) that leads to negative effects on climate (global warming), environment and health (Omer, 2009). The need for clean, cheap and renewable resources of energy becomes urgent. This is also important because the worldwide energy consumption is expected to expand, due to the increase in world population and the rising demand of the energy in the developing countries (Gratzel, 2009).

Several forms of renewable energy compete for an appropriate role in global energy supply (Grossmann et.al, 2010). Among these, solar energy is inexhaustible, freely available and has the capacity to meet increasing world energy needs without potentially destructive environmental consequences (Eisenberg and Nocera, 2005; Armaroli and Balzani, 2007). The Sun is in fact the primary source of energy for nearly all forms of life on earth. It provides about

120,000 TWs (TW=10^{12} watts) to the earth's surface, which amounts to 6000 times the present rate of the world’s energy consumption (Gratzel, 2007).

Solar energy cannot be employed as such; it must be captured and converted into useful forms of energy. Solar cells, which commonly referred to as Photovoltaic (PV) cells, are the most attractive system among the different solar energy conversion systems (Kuznetsov and Edwards, 2010), since it converts solar energy (photo) directly into electricity (voltaic). Solar cells cause no environmental pollution in operation and can generate power locally where it is needed. Covering only 0.1% of the earth’s surface with solar cells with an efficiency of 10% would satisfy the energy needs for the whole world (Gratzel, 2001).

1.2 Solid-State Solar Cells

Photovoltaic devices to date have been dominated by solid-state junction devices, usually made of silicon. The first silicon solar cell was developed at the Bell Laboratories in 1954 with an efficiency of about 6% *(*Chapin et al., 1954). Silicon has been and still is the most important material that dominates the present world market of PV production by 85% as a base material; particularly in its crystalline form (Sivoththaman and Baroughi, 2006), and with a recorded efficiency for a laboratory cell of about 25% (Green et al., 2010). However, the efficiency of commercial silicon solar cells (currently available) is in the best case not more than 15% (Shah et al., 1999). Although silicon technology is nowadays

the most mature and current market leader (Bosi and Pelosi); however, silicon has a low optical absorption coefficient (Goetzberger et al., 2002). In practice this means that the Si wafers (layers) need to be greater than 50 μm thick to absorb most of the incident light (Ribeiro et al., 2009). Therefore, to be useful in solar cells, Si must be refined to an extremely high degree of purity. The process of purification is expensive and the material cost nearly 50% of the total cost (Sivoththaman and Baroughi, 2006).

The above problems associated with the solid-state solar cells diverted efforts to a new type of solar cell devices, known as Dye-Sensitized Solar Cells (DSSCs). These devices offer the prospect of very low-cost fabrication and present a range of attractive features that will facilitate market entry.

1.3 Dye-Sensitized Solar Cell (DSSC)

In contrast to the solid-state solar cells where the light absorption and charge transport occurs in the same material (semiconductor), DSSC separates these functions, the optical absorption is carried out by the dye molecules, and charge separation is carried out in a wide-band gap semiconductor and an electrolyte (O`Regan and Gratzel, 1991). In general, the used wide band-gap semiconductors (like TiO_2) are cheap, photochemically stable, and their spectral sensitivity is limited to UV, which make them suitable for PV applications. Usually, a chromophoric compound, the sensitizer, is adsorbed onto the semiconductor's

surface to expand the absorption spectrum range, and thus increasing light harvesting efficiency.

The DSSC technology offers the following unique characteristics (Luque and Hegedus, 2003; Hagfeldt et al., 2010):

a. Relatively high energy conversion efficiency (photo-to-energy efficiency is over 11%) (Nazeeruddin et al., 2006).
b. Low cost fabrication: the DSSC is very simple to construct and it's made of low cost and abundantly available materials.
c. Low potential for environmental pollution since it's made of nontoxic materials, good recyclability and flexibility.

1.3.1 History of Dye Sensitization

Sensitization of wide-band gap semiconductors using dyes has a long history, dating back to early days of photography, where mixtures of several organic dyes are used to extend the spectral range of silver halide grains (McEvoy and Gratzel, 1994; Kalynanasundaram and Gratzel, 1998).

The systematic studies of dye-sensitized solar cells started in the 1960's with the work of dye-sensitization process on ZnO and SnO_2 electrodes, carried by Gerischer and Memming (Markvart and Castaner, 2005). However, due to the limited amount of dye that could be adsorbed (mostly physisorbed) on the semiconductor surface and the too narrow spectral absorbance range of the dyes, the conversion efficiencies remained below 1% for these systems. Attempts to

harvest more light by using multilayer of dyes were unsuccessful. The basic problem was the belief that only smooth semiconductor surfaces could be used (Hagfeldt et al., 2010). Incremental improvements were then achieved by increasing the efficiency of dye via chemisorption on the surface of the semiconductors (Tsubomura et al., 1976; Anderson et al., 1979).

Most semiconductors such as CdS, CdSe, GaP and Si facing serious photocorrosion or even normal corrosion in the dark, thus a stable wide band gap semiconductor, such as TiO_2, became the material of choice.

The breakthrough of dye-sensitized devises as solar cells was achieved in 1991. A dye-sensitized solar cell with 7% efficiency was constructed, based on nanocrystalline TiO_2 and tris(2,2`-bipyridyl-4,4`-dicarboxylic acid)ruthenium(II) (O'Regan and Gratzel, 1991). Subsequent work by the Gratzel group pushed the efficiency to 10% by the use of cis-bis(isothiocyanato)-bis(2,2`-bipyridyl-4,4`-dicarboxylic acid)ruthenium(II) sensitizer, adsorbed onto mesoporous film of TiO_2, and with I^-/I_3^- electrolyte (Nazeeruddin et al., 1993). The evolution has continued progressively since then, with certified efficiencies now over 11% (Nazeeruddin et al., 2006).

1.3.2 DSSC Structure and Operating Principle

The DSSCs are composed of: (1) Photoelectrode (working electrode): the most commonly used is glass coated with fluorine-doped tin oxide (FTO), (2) Mesoporous oxide layer, composed of a network of TiO_2 nanoparticles deposited

on the Photoelectrode, (3) Dye, which is visible light absorbing substance spread on the TiO_2 surface, (4) A redox electrolyte (usually a solution containing the I^-/I_3^- pair), located in the space between the dye and the counter electrode, (5) Counter electrode, which is coated with a thin layer of platinum.

The basic DSSC operating principles are presented in Figure 1.1. The incoming photon is absorbed by the dye molecule and an electron is excited from the molecular ground state S to the excited state S*.

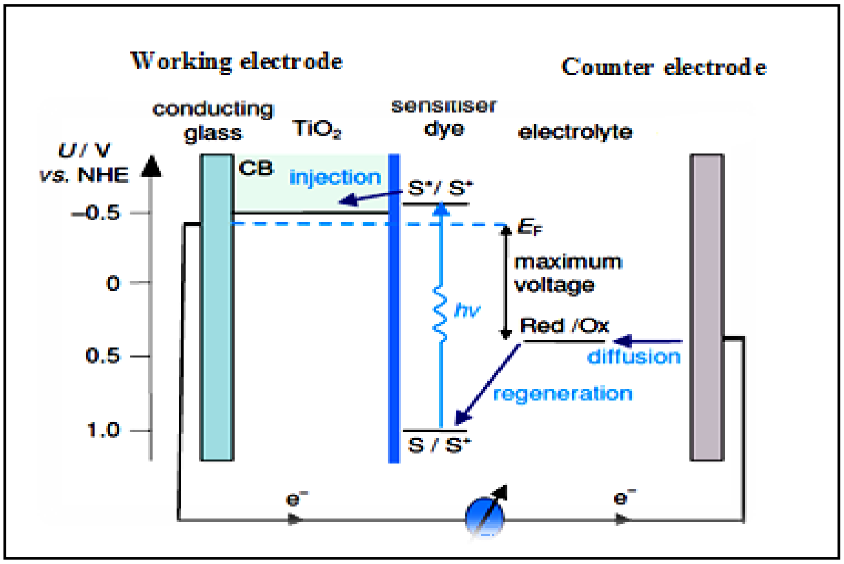


Figure 1.1: Schematic representation of the DSSC operating principles and energy levels

The excited electron is injected into the conduction band of TiO_2 particle leaving the dye molecule in an oxidized state S^+. After injection, electrons diffuse in the nanocrystalline TiO_2 network to the conductive coating of the substrate, from which they can be transferred to an external circuit to the counter electrode.

In order for the current generation to continue, the dye must be reduced back to its ground state; this is done by the redox couple in the electrolyte, the oxidized dye gets electrons from the iodide ions which, in turn, get oxidized to triiodide in process. The triiodide ions then diffuse to the counter electrode, where they get reduced back to iodide by the electrons returning from the external load. Thus, the cell operation is based on consecutive oxidation/ reduction cycles. The chemical reactions going on in the cell can be summarized as follows:

❖ Light absorption	$S + h\nu \rightarrow S^*$	(1)
❖ Electron injection	$S^* \rightarrow S^+ + e^- (TiO_2)$	(2)
❖ Dye regeneration	$2S^+ + 3I^- \rightarrow 2S + I_3^-$	(3)
❖ Triiodide reduction	$I_3^- + 2e^-_{(Pt)} \rightarrow 3I^-$	(4)

1.4 DSSC Basic Components

1. Photoelectrode (working electrode).
2. Electrolyte.
3. Dye (photosensitizer).

1.4.1 Photoelectrode (working electrode)

The Photoelectrode consists of a wide band gap, porous semiconductor of high surface area that is sensitized for the visible spectrum by a dye adsorbed onto its surface. Metal oxide semiconductors are preferential in DSSC because of their exceptional stability against photo-corrosion on optical excitation (Kalyanasundaram and Gratzel, 1998). Furthermore, the large band gap (> 3eV) of the oxide semiconductors is needed in DSSC for the transparency of the semiconductor electrode for the large part of the solar spectrum.

Titanium dioxide (TiO_2) offers some unique properties making it the preferred semiconductor for DSSC, it has a good chemical stability under visible irradiation in solution (Luque and Hegedus, 2003), its conduction band edge lies slightly below the excited state energy level of many dyes, it`s relatively cheap, nontoxic and biocompatible (Hagfeldt et al., 2010). TiO_2 exists naturally in three crystalline forms; anatase, rutile and brookite, of which the anatase structure is the most suitable for DSSC applications (Jose et al., 2009).

Many other metal oxide systems (Jose et al., 2009); have been tested as an alternative of TiO_2 semiconductor, such as ZnO, SnO_2, Nb_2O_5. However, TiO_2

has been and still the cornerstone semiconductor for dye-sensitized nanostructured electrodes for DSSCs.

The surface morphology of the semiconductor film is critical for the performance of the cell. A large surface area of the semiconductor allows strong absorption of solar irradiation to be achieved by only a monolayer of adsorbed dye. The use of a mesoporous film of the semiconductor enhances the surface area by up to a 1000-fold for a 10μm thick film, leading to high visible light absorption (Hagfeldt et al., 2010).

1.4.2 Electrolyte

The electrolyte is the responsible for regeneration of the dye at the Photoelectrode with the charge collected at the counter electrode (Longo and De Paoli, 2003). Since the discovery of the DSSC, and up till now, I^-/I_3^- system is still the best electrolyte for DSSCs, and appears very hard to replace; it simply performs better than all alternatives tested so far (Hagfeldt et al., 2010), since it exhibits an electrochemical redox potential suitable for regeneration of several oxidized dyes, and the best kinetic properties in DSSC (Goncalves et al., 2008).

1.4.3 Dye (Photosensitizer)

The dye is the key component in the DSSC; it serves as the light absorber whose properties decide the ability to create electrons and photoelectric conversion efficiency, thus in order to optimize the performance of such devices, it is important to design suitable dyes with tunable spectroscopic and electrochemical properties (Xie and Guo, 2007). To achieve a high light-to-energy conversion efficiency, dyes must accomplish a number of essential requirements:

1. The dye must have strong absorption and cover a broad range in solar spectrum up to about 900 nm (Gratzel, 2000).
2. They must have an anchoring groups (-COOH, -H_2PO_3, -SO_3H, etc.) to bind strongly to TiO_2 film, to ensure efficient electron injection into the TiO_2 conduction band (Robertson, 2006).
3. The LUMO of the dye must be sufficiently high in energy (slightly above the conduction band edge of TiO_2) for efficient electron injection and the HOMO must be sufficiently low in energy (slightly below the redox potential of the electrolyte) for efficient regeneration of the ground state of the dye by the redox couple (Hagfeldt and Gratzel, 1995).
4. The adsorbed dye molecule should be stable enough in the working environment (at the semiconductor-electrolyte interface) to sustain about 20 years of operation at exposure to natural daylight, i.e. at least 10^8 redox turnovers without decomposition (Hagfeldt and Gratzel, 2000).

5. Electron injection from the excited state to the conduction band of the semiconductor should be fast in comparison with electron relaxation to the ground state.
6. The dye should be photostable, and electrochemical and thermal stability are also required.

Based on these requirements thousands of dyes have been investigated, including a wide range of organic dyes and transition metal complexes (Hagfeldt et al., 2010).

When considering organic dyes for use in DSSCs, many dyes including porphyrins, phthalocyanines, coumarine, indoline, triarylamine, carbazole, hemicyanine, squaraine, perylene, oligothiophene and many others, have been adapted to act as photosensitizers, and have obtained impressive efficiencies (Hagfeldt et al., 2010). The best performing organic dye to date is an indoline (Figure 1.2), which showed efficiency reaching up to 9.2 % (Ito et al., 2006).

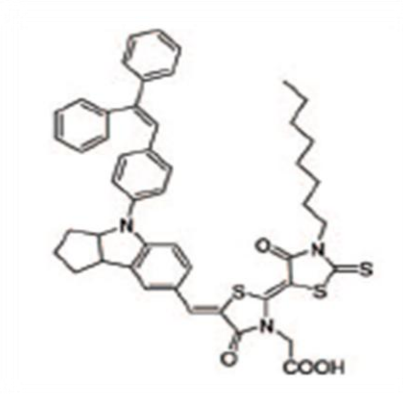


Figure 1.2: Indoline organic dye with 9.2 % conversion efficiency

However, the aggregation of organic dyes and their poor stabilities limit their practical application in solar cells (Xie and Guo, 2007). Accordingly, many researchers directed their efforts to the use of metal complexes as alternatives to organic dyes.

Transition metal complexes and ruthenium complexes, in particular, have been investigated intensively for DSSC application because of their broad absorption spectra and favorable photovoltaic properties (Ardo and Meyer, 2009).

Generally, metal complexes employed as photosensitizers consist of a central metal ion with ancillary ligands having at least one anchoring group. Ancillary ligands are not directly attached onto the semiconductor surface and can be tuned to change the photophysical and electrochemical properties of the complexes (Polo et al., 2004). Anchoring ligands of the complex are responsible for chemisorption onto the semiconductor surface. The anchoring group of the dye ensures the uniform (mononuclear) distribution of dye molecules on the oxide surface, and most importantly, increases the strength of the electronic coupling between the donor levels of the excited dye and the acceptor levels of the semiconductor (conduction band) (Kalyanasundaram and Gratzel, 1998), and ensures a high probability that the excited state of the dye molecule will relax by electron injection into the semiconductor conduction band (Gratzel, 2000).

The majority of the metal complexes photosensitizers are bound to the TiO_2 surface through acidic groups; mostly carboxylic acid or, less commonly,

phosphonic acid linkers (Wang et al., 2004). Some other linkers like esters, acid chlorides, carboxylate salts, amides, sulphonic acid, silanes, ethers, and acetylacetonate (Hou et al., 1999; Galoppini, 2004; Altobello et al., 2004), were found to have poorer adsorption on the semiconductor oxide surfaces compared to the carboxylic acid groups. However, it has been shown that the chemisorption at semiconductor oxide through carboxylic group can occur through a variety of binding modes Figure 1.3.

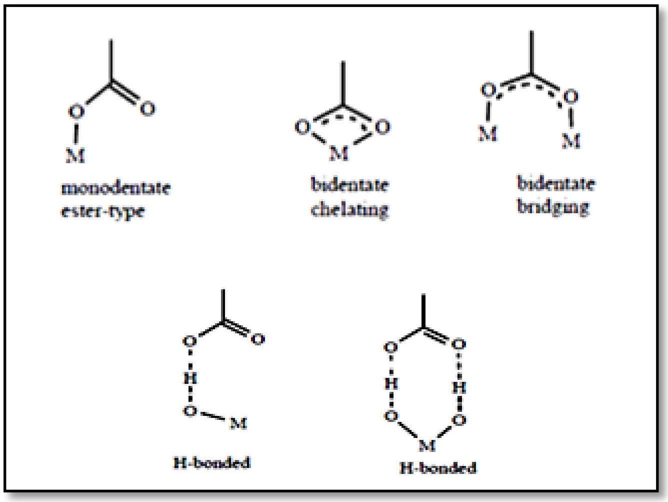


Figure 1.3: Binding modes for carboxylate unit on TiO_2 surface.

1.4.3.1 Ruthenium (Ru) Complexes as Photosensitizers

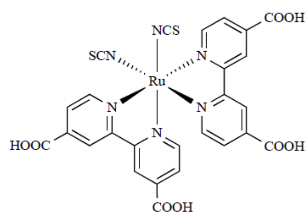
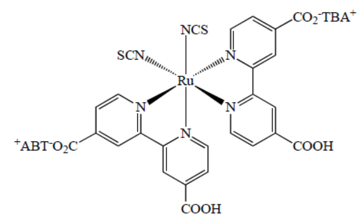
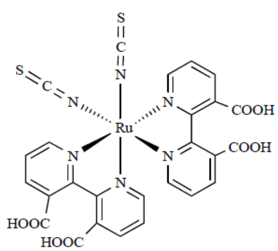
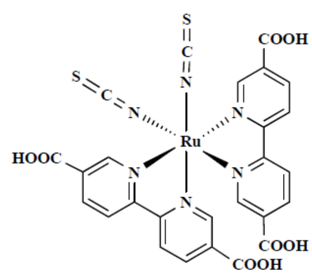
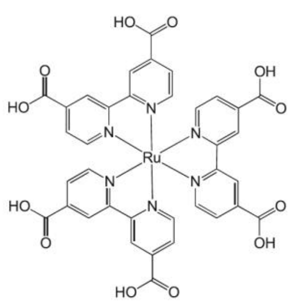
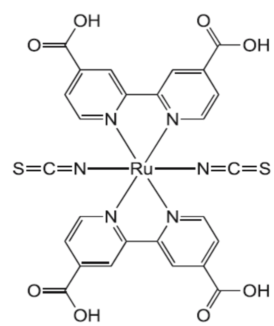
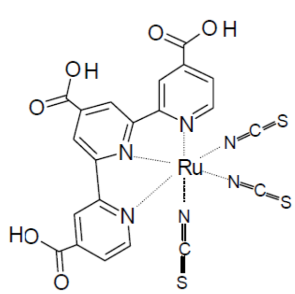
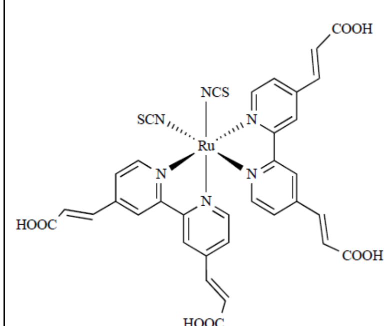
Among the transition metal complexes, Ru(II) complexes (d^6- metal complexes) have shown the best photovoltaic properties (Haque et al., 2005; Kuang et al., 2006; Kuang et al., 2007). The choice of Ru metal is of interest for a number of reasons:

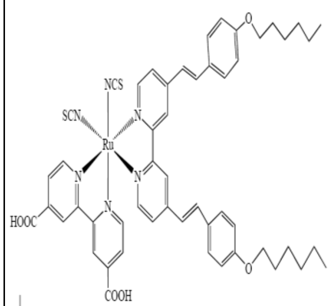
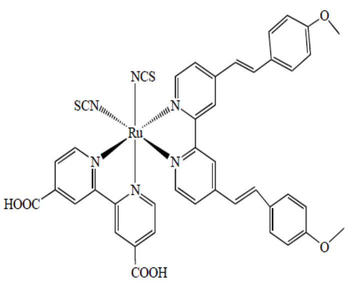
- Because of its octahedral geometry specific ligands can be introduced in a controlled manner.
- The photophysical and electrochemical properties of Ru complexes can be tuned in a predictable way.
- The Ru metal center possesses two stable and accessible oxidation states II to III.

Among the Ru(II) complexes, the best photovoltaic performance in terms of both conversion efficiency and long-term stability has so far been achieved with carboxylated bipyridyl complexes of Ru(II). These complexes show a strong and broad absorption band in the visible region (Longo and De Paoli, 2003). The excited states of these complexes have long lifetimes and they do not have the tendency to aggregate or decompose (Balzani et al., 1996).

The classic sensitizer dye employed in DSSCs is ruthenium(II) bipyridyl dye, cis-bis(isothiocyanato)-bis(2,2`-bipyridyl-4,4`-dicarboxylic acid)ruthenium(II) , (known as **N3**) (Nazeeruddin, 1993), which shows superior performance and has been the top choice for DSSCs (Hagfeldt et al., 2010). The structure of this dye **1** is shown in Table 1.1.

Table 1.1: Collection of Some Representative Ru-Complex Photosensitizers

Dye	Structure	λ_{max} (nm)	Dye	Structure	λ_{max} (nm)
1		**535**	**2**		**538**
3		**570**	**4**		**580**
5		**465**	**6**		**582**
7		**620**	**8**		**555**

Dye	Structure	λ_{max} (nm)	Dye	Structure	λ_{max} (nm)
9		**543**	**10**		**545**

Changing the protonation of the acid groups of **1** had influence on the efficiency of the solar cell. Partial deprotonation of **1** to form a di-tetrabutylammonium salt **2** in Table 1.1 exhibited improved power conversion efficiency (Nazeeruddin et al., 1999).

Besides the protonation state of the carboxylic acid group, the sites of these linkers on the 2,2`-bipyridyl ligand would affect the photophysical and photoelectric properties of the Ru(II) complexes (Hou et al., 1999; Galoppini, 2004). The carboxylic groups of Ru complexes could be on one of three different sites of the 2,2`-bipyridyl which are 3,3` position, 4,4` position or 5,5` position. The Ru complexes with carboxylic groups in the 3,3` or 5,5` positions of the 2,2`-bipyridyl ligand **3** and **4** in Table 1.1 exhibited poorer performance in DSSC than the complex **1** (Galoppini, 2004). The steric hindrance of the two carboxylic groups in the 3,3` positions and the relatively high oxidation potential of the

ground state of 5,5`-bipyridyl complex **4**, were the reasons for the low DSSCs performance.

In bipyridyl complexes of Ru(II), metal-to-ligand charge transfer (MLCT) transitions account for nearly all the visible light absorption. The MLCT corresponds to promotion of an electron from a molecular orbital (MO) that is largely Ru(II) based (filled t_{2g} level) (Highest occupied Molecular Orbital, HOMO) to a MO that is largely ligand based (empty π* orbital of the bipyridyl ligand) (Lowest unoccupied Molecular Orbital, LUMO) Figure1.4. Thus the smaller the energy gap, the more red-shifted is the related MLCT transition. The energies of the MLCT states can be altered systematically by modifying the anchoring ligands as well as by changing the ancillary ligands (Polo et al., 2004).

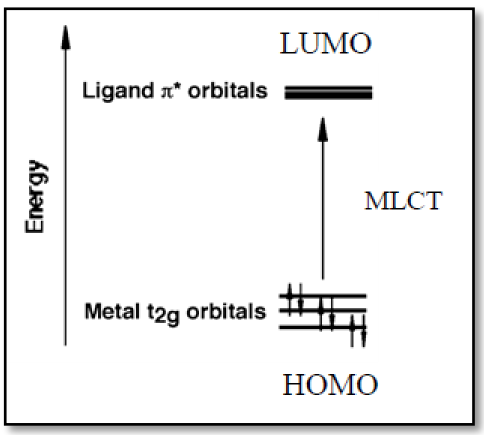


Figure 1.4: Schematic representation of the HOMO (t_{2g}) and the LUMO (π*) molecular orbitals

Although scientists have made great progress in the studies on dye-sensitized nanocrystalline TiO_2 films using **N3** or **N719**, the main disadvantages of these sensitizers were the weak absorption in the red region of the solar spectrum and

the relatively low molar extinction coefficient (Nazeeruddin et al., 1993). Many efforts have been made to overcome these shortcomings (Hagfeldt et al., 2010).

The spectral properties of ruthenium bipyridyl complexes can be tuned in two ways Figure 1.5. Firstly, by raising the energy (destabilization) of the HOMO (metal-t_{2g}) secondly, by decreasing the energy of LUMO (ligand-π^*). This is done by using donor or acceptor ligands, respectively (Anderson et al., 1994; Nazeeruddin and Gratzel, 2007).

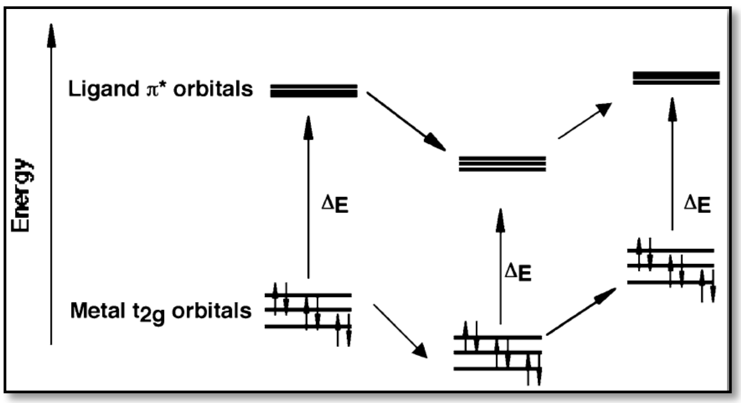


Figure 1.5: Schematic representation of tuning the (t_{2g}) and (π^*) orbitals energies

The energies of the MLCT states can be modified systematically by changing the ancillary ligands. The MLCT absorption bands of the bis-chelated complexes, cis-[Ru(dcbpy)$_2$(L)$_2$] (L = Cl^-, Br^-, I^-, NCS^- and CN^-), shift to lower energy by changing L from π accepting to π donating ones (Table 1.2). This is due to a direct perturbation of the electronic density at the metal center (increasing the HOMO level) (Xie and Guo, 2007).

Table 1.2: Absorption Properties of the (RuL_2X_2) Complexes

Complex	λ_{max} (nm) (ε / 10^4 $M^{-1}cm^{-1}$)
[$RuL_2(NCS)_2$]	534 (1.42), 396 (1.40), 313 (3.12)
[$RuL_2(CN)_2$]	493 (1.45), 365 (1.20), 310 (3.90)
[RuL_2Cl_2]	534 (0.96), 385 (1.01), 309 (4.13)
[RuL_2Br_2]	530 (0.84), 382 (0.80), 309 (2.30)
[RuL_2I_2]	536 (0.68), 384 (0.66), 310 (2.50)
[$RuL_2(OH_2)_2$]	500 (1.19), 365 (1.09), 306 (4.90)

L: 2,2`-bipyridyl-4,4`-dicarboxylic acid

The energy of MLCT transition of Ru polypyridyl complexes of the type tris-[Ru(4,4`-dicarboxy-2,2`-bipyridine)$_3$] , can be lowered so that it absorbs more in the red region of the visible spectrum by replacing one 4,4-dicarboxy-2,2-bipyridine (dcbpy) with two thiocyanate ligands [Ru(dcbpy)$_2$(NCS)$_2$] Figure 1.6.

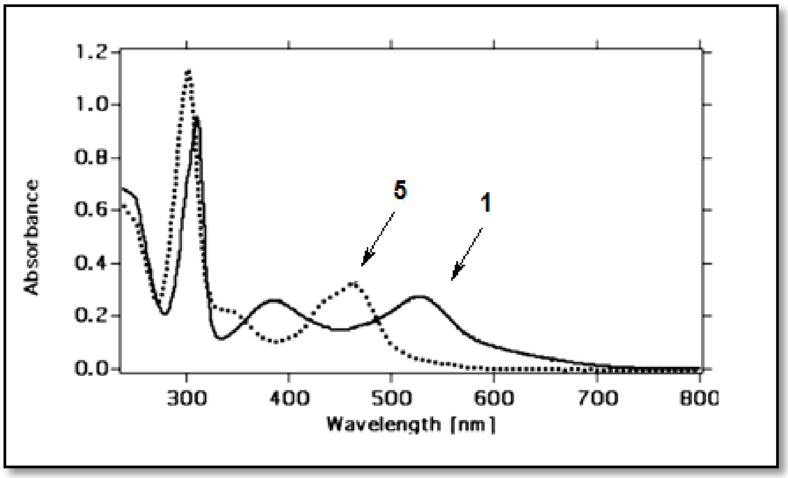


Figure 1.6: Comparison of absorption spectra of complexes **1** and **5**

Transforming the complex **1** from its cis-configuration to the trans-configuration to form complex **6** causes a shift from 538 to 582 nm upon isomerization (Figure 1.7). This red-shift is believed to be due to the destabilization of the ruthenium t_{2g} orbital (Zakeeruddin et al., 1999; Wang et al., 2000). However, disadvantages such as poor solubility and the tendency to photoinduced isomerization of the trans isomer limit its practical application.

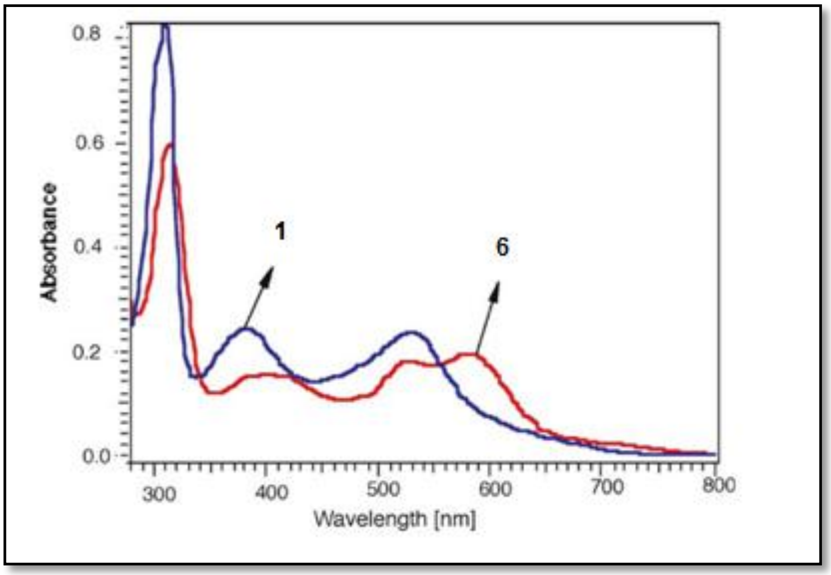


Figure 1.7: Absorption spectra of cis-Ru (**1**) and trans-Ru (**6**)

The photovoltaic performance of complex **1** has been unmatched by virtually hundreds of other complexes that have been synthesized and tested. However, the tri(isothiocyanato)-(2,2`2``-terpyridyl-4,4`4``-tricarboxylate)Ru(II) (known as black dye); with structure **7** in Table 1.1, achieved solar-to-power conversion efficiency of 10.4% over the whole visible range extending into the near-IR region up to 920 nm (Nazeeruddin et al., 2001). The red shift in the MLCT band

is due to the decrease in the π* level of the terpyridine ligand and an increase in the energy of the t_{2g} metal orbital (Nazeeruddin et al., 2001).

A large number of ruthenium based sensitizers have been investigated in order to improve the photovoltaic performance and the stability of the DSSCs (Hara et al., 2001; Gratzel, 2005). Recently, complexes with structures **8**, **9** and **10** in Table 1.1, attract more attention in research as they have higher molar extinction coefficients as compared with **1**. For DSSC, increasing the molar extinction coefficients of the sensitizers will enhance the light harvesting. High extinction coefficients have been achieved by using of extended delocalized ligands for Ru complexes (Xie and Guo, 2007). Molar extinction coefficient for **8**, **9** and **10** for example are: $\varepsilon = 18000\ M^{-1}\ cm^{-1}$ ($\lambda_{max} = 555$ nm), $\varepsilon = 18200\ M^{-1}\ cm^{-1}$ ($\lambda_{max} = 543$ nm) and $\varepsilon = 18000\ M^{-1}\ cm^{-1}$ ($\lambda_{max} = 545$) respectively were found to be much higher than that of **1** $\varepsilon = 13600\ M^{-1}\ cm^{-1}$($\lambda_{max}$= 535 nm,) (Klein et al., 2005; Kang et al., 2005).

The most common synthetic approach to the preparation of bipyridyl complexes is by the reaction of bipyridyl ligand and $RuCl_3.3H_2O$ as starting material in refluxed DMF (Juris et al., 1988). However, with thermally sensitive ligands, $Ru(DMSO)_4Cl_2$ (where DMSO is dimethylsulphoxide) has been used as starting material (Xie et al., 2000). The structures of bipyridyl complexes are best described as distorted octahedrons (Xie et al., 2000).

Although, the work in DSSCs has been focused on Ru(II) bipyridyl complexes, many attempts, however, have been made to construct sensitizers with other metal

ions, such as Os(II), Re(I), Fe(II), Pt(II) and Cu(I) (Polo et al., 2004; Hagfeldt et al., 2010). Among these, Os(II) complexes appear to be promising photosensitizers. For example the replacement of the Ru(II) metal center with Os(II) metal center, extends the light absorption to higher wavelength values without sacrifying the good photovoltaic performance (Kuciauskas et al., 2002).

1.5 Ruthenium Schiff base Complexes

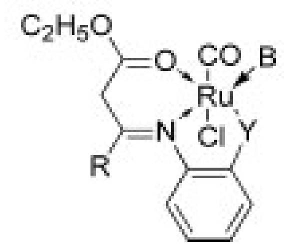
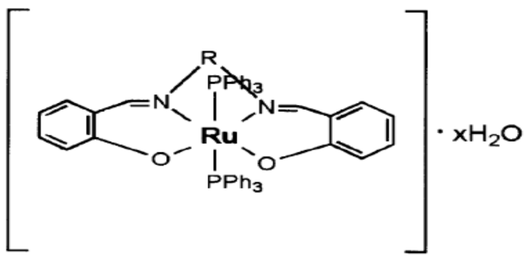
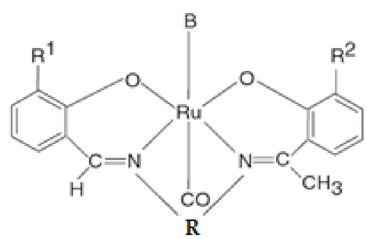
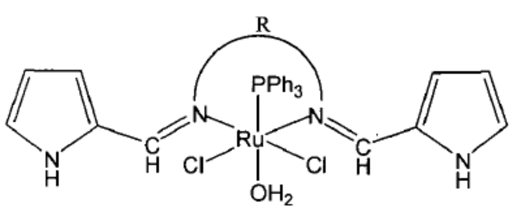
Schiff bases are compounds that result from the condensation of a primary amine and a ketone or an aldehyde according to (Eq. 1).

$$RNH_2 + R_1R_2C{=}O \longrightarrow R\text{-}N{=}CR_1R_2 + H_2O \;\ldots\ldots\ldots\; \mathbf{(1)}$$

Schiff bases make up a very large group of compounds of variable structures, depending on the amines and the carbonyl compounds (aldehydes or ketones) involved. All Schiff bases are characterized by having one or more azomethine groups (-RC=N-) and forming stable metal complexes. A large number of the Schiff bases are often used as ligands in coordination chemistry owing to their metal binding ability. The first Schiff base complex was isolated in 1840 from the reaction of Cu(II) acetate, salicylaldehyde and aqueous ammonia. It was later characterized to be bis(salicylaldimino) copper(II) (Holm et al., 1966).

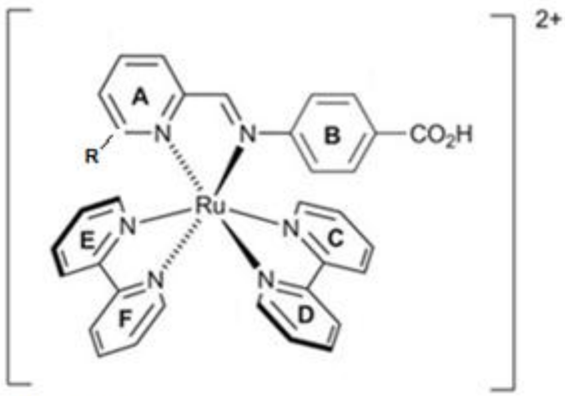
There has been considerable interest in the chemistry of ruthenium, primarily because of its fascinating electron-transfer and photoelectrochemical properties. As the coordination environment around the central metal ion directs properties of the complexes, complexation of ruthenium by ligands of different types has been of significant importance. The easy synthesis of inexpensive Schiff base ligands (usually through one-step process and often in quantitative yields) and because of the ease of adjusting their donor-acceptor properties via appropriate selection of the substituents on their backbone makes them an attractive alternative to the bipyridyl ligands (Bozic-Weber et al., 2010). Many Ru(II) Schiff base complexes have been prepared and some representative examples are shown in Table 1.3.

Table 1.3: Collection of some Representative Ru(II) Schiff base complexes

Ru-Schiff base complex	λ_{max} (nm)	Reference
 **(R = CH_3,C_6H_5; Y= O,S; B = PPh_3, $AsPh_3$**	**255-670**	(Sathya et al., 2010)
 **R = C_6H_4, X = 2**	**384**	(Bhowon et al., 1999)
 **B = $AsPh_3$, PPh_3; R^1= H, OCH_3, R^2= H, C_4H_4; R = $(CH_2)_2$, C_6H_4**	**222-379**	(Gowri et al., 2008)
 **R = C_6H_4, $C_6H_3(CH_3)$**	**256, 310** **232, 301, 463**	(Bhowon et al., 2004)

However, these complexes and many others were mainly utilized in the catalytic reactions and biological applications (Singh et al., 2005; Naskar et al., 2009).

There is only one report (Bozic-Weber et al., 2010), on the use of Ru(II) complexes based on Schiff base ligands; as photosensitizers. These Ru(II) complexes were prepared from *N*-phenylpyridin-2-ylmethanimine Schiff base ligands decorated with carboxylic acid functionalities (Figure 1.8). They show a weak absorption at λ = 481 nm (ε =7100 $L.mol^{-1}.cm^{-1}$) and at λ = 480 nm (ε = 3500 $L.mol^{-1}.cm^{-1}$).



R = H, CH_3

Figure 1.8: Ru(II) complex based on of *N*-phenylpyridin-2-ylmethanimine ligand

1.6 Purpose of the work:

The research in this work is directed towards the photosensitizer (dye) component of the DSSC. The main idea is the preparation of Schiff base ruthenium complexes as alternative dyes for bipyridyl ruthenium complexes.

Schiff base ligands based on quinoline and phenylenediamine moieties, bearing carboxylic, sulfonyl and hydroxyl groups will be prepared and characterized. Complexes of the above Schiff base ligands with Ru(II) will be prepared and studied. The complexes will be characterized by their microanalysis, infrared (IR) spectra, magnetic susceptibility and electrical conductivity. Their UV-Vis. spectra will be measured and compared with those of standard bipyridyl complexes.

2. EXPERIMENTAL

2.1 Materials

All procedures were performed under an atmosphere of dry, purified nitrogen. Solvents were distilled and dried by standard methods (Perrin and Armarego, 1988). 2-Amino-4-picoline, 4-hydroxybenzaldehyde and Isatin were purchased from Acros, USA. 3-Aminobenzoic acid and 8-aminoquinoline were purchased from Riedel-deHaen. Selenium dioxide (SeO_2) was purchased from BDH chemicals, England. Ruthenium(III) chloride trihydrate and 1,2-phenylenediamine were purchased from Fluka, Switzerland.

2.2 Physical measurements

The IR Spectra were recorded, as KBr discs, on Nicolet Impact-400 FT-IR spectrometer (Madison, WI, USA). The NMR spectra were recorded on a bruker DPX 300 MHz spectrometer (Wissembourg Cedex, France). Melting points were determined with Philip-Harris melting point apparatus and are uncorrected. Conductivity measurements were carried out for 1.0×10^{-3} M solutions at 25 ^{o}C. Magnetic susceptibility measurements were measured by Gouy Method. Microanalyses of ligands were performed by using Perkin-Elmer Euro-Vector 8910 Elemental Analyzer. Microanalyses of the new ruthenium complexes were performed at Technical University of Munich in Germany. UV-Vis spectra were carried out for 1.0×10^{-4} M solutions at 25 ^{o}C by using Cary 100 Bio UV-Vis spectrophotometer.

2.3 Preparation of starting materials

2.3.1 Preparation of 4,4`-Dimethyl-2,2`-biyridine, (I)

This compound was prepared from the following precursors.

2.3.1a Preparation of 2-Bromo-4-methylpyridine.

The compound was prepared following literature procedure with some modifications (Case, 1946). 2-amino-4-methylpyridine (12.0 g, 0.111 mol) was added gradually to a stirred solution of 47% hydrobromic acid (70 mL). The mixture was cooled to 0 ^{o}C and then 17 mL of bromine was added slowly. To the resulting pale-orange solution, a solution of sodium nitrite (21.0 g, 0.304 mol) in 30 mL of water was added gradually, keeping the temperature at 0 ^{o}C until near the end of the reaction when it rose spontaneously to 10 ^{o}C. A solution of sodium hydroxide (45.0 g in 115 mL of H_2O) was drop wise added at a rate keeping the temperature below 25 ^{o}C. The resulting oil was extracted with diethyl ether (50 mL×4). Ether was then removed under reduced pressure, and the oil was distilled in vacuum to give colorless oil (Yield: 14.34 g, 75 %). ^{1}H NMR (300 MHz, $CDCl_3$, in ppm): δ = 2.27 (s, 3H); 7.01 (d, 1H); 7.25 (s, 1H); 8.15 (d, 1H). ^{13}C NMR (75 MHz, $CDCl_3$, in ppm): δ = 20.7 (primary C); 123.9, 128.7, 149.7 (tertiary C); 142.3, 150.3 (quaternary C). m/z =171.98 (+M).

2.3.1b Preparation of Tetraethylammonium iodide.

The compound was prepared following literature procedure (Vernon and Sheard, 1948). A sample of triethylamine (10.7 g, 0.106 mol) was placed in flask

rapped with aluminum foil. Ethyliodide (16.46 g, 0.106 mol) was added gradually with stirring. The mixture was then stored overnight. The crude product was then collected, washed with petroleum ether and dried. The product was then dissolved in boiling absolute ethanol and treated with alcoholic potassium hydroxide until pink to phenolphthalein. The mixture was then cooled in ice bath, filtered and the white product was then recrystallized twice from absolute ethanol (Yield: 19.00 g, 70%). Mp. 300 ^{o}C (lit. 300 ^{o}C), ^{1}H NMR (300 MHz, D_2O, in ppm): δ = 1.14 (t, 12H); 3.14 (q, 8H). ^{13}C NMR (75 MHz, D_2O, in ppm): δ = 6.84 (primary C); 52.00 (secondary C).

2.3.1c Preparation of dichlorobis(triphenylphosphine)nickel(II), $NiCl_2(PPh_3)_2$

The compound was prepared following literature procedure (Venanzi, 1958; Cotton et al., 1961). A solution of nickel chloride hexahydrate (23.8 g, 0.100 mol) in water (20 mL) was added to a solution of triphenylphosphine (52.5 g, 0.200 mol) in warm glacial acetic acid (750 mL). The Olive-green microcrystalline precipitate was kept in contact with its mother liquor for 24 hours to give dark blue crystals. The crystals were filtered off, washed with glacial acetic acid, diethyl ether and dried in vacuum at 50 ^{o}C (Yield: 53.5 g, 82 %). Mp. > 350 ^{o}C (lit. > 300 ^{o}C) . Elemental analysis for $C_{36}H_{30}Cl_2NiP_2$ (%): C, 66.10; H 4.62, Found: C, 66.00; H, 4.59 %. Mp. > 350 ^{o}C.

2.3.1d Preparation of 4,4`-Dimethyl-2,2`-bipyridine, (I)

The compound was prepared following literature procedure with some modifications (Rajalakshmanan and Alexander, 2005). To a solution of $Ni(PPh_3)_2Cl_2$ (22.3 g, 30 mmol) and Et_4NI (25.7 g, 100 mmol) in dry DMF (200 mL) under argon, was added zinc dust (9.81 g, 150 mmol). After 30 min of stirring at room temperature, the reaction mixture (red-brown slurry) was heated to 50 ^oC. A solution of 2-bromo-4-methylpyridine (17.2 g, 100 mmol) in dry DMF (40 mL) was added dropwise. After 14 hours at 50^o C, the reaction mixture was poured over 2 M aqueous ammonia (300 mL). The reaction mixture was filtered, and the filtrate was extracted with ether (150 mL) and then benzene (150 mL). The organic layer was separated and the aqueous layer was again extracted with ether/benzene (1:1, 2×100 mL). The combined organic extracts were washed with water (2×100 mL) and brine (100 mL), dried over anhydrous $MgSO_4$, and evaporated under reduced pressure. The residue was purified by silica-gel column chromatography, using petroleum ether-ethylacetate (98:2, v/v) as the eluent. The second band was eluted and upon evaporating to dryness gave the product as a white solid (Yield: 3.68 g, 40 %). Mp. 174 ^oC (lit. 174 ^oC). ^1H NMR (300 MHz, $CDCl_3$, in ppm): δ = 2.39 (s, 6H); 7.09 (2H); 8.19 (d, 2H); 8.49 (d, 2H). ^{13}C NMR (75 MHz, $CDCl_3$, in ppm): δ = 21.23 (primary C); 122.04, 124.69, 148.94 (tertiary C); 148.20, 156.03 (quaternary C). m/z = 185.11 (+M).

2.3.2 Preparation of 2-formyl-4-quinolinecarboxylic acid, (II)

This compound was prepared from the following precursors.

2.3.2a Preparation of 2-methyl-4-quinolinecarboxylic acid

The compound was prepared following literature procedure with some modifications (Tietze, 2000). A sample of Isatin (10.0 g, 0.068 mol) was added to a 33% solution of potassium hydroxide (60.0 g). The mixture was stirred for 5 min until it turned to a pale-orange solution. Acetone (60.5 g) was then added gradually, and the mixture was then refluxed for 16 h. The mixture was cooled, poured over 200 g of ice, and then washed twice with diethyl ether (200 mL) to get rid of excess acetone. The aqueous phase was then acidified to pH~3 with conc. hydrochloric acid (40 mL) to produce a white precipitate. The ppt. was filtered off, washed with ice water and then recrystallized from water and dried in vacuo at 50 ^{o}C (Yield: 10.50 g, 83 %). Mp. 244 ^{o}C (lit. 242-244 ^{o}C). ^{1}H NMR (300 MHz, DMSO-d_6, in ppm): δ = 2.66 (s, 3H, -CH_3); 7.58 (t, 1H); 7.73 (t, 1H); 7.79 (s, 1H); 7.97 (d, 1H); 8.59 (d, 1H). ^{13}C NMR (75 MHz, DMSO-d_6, in ppm): δ = 25.16 (primary C); 123.24, 125.82, 127.42, 129.32, 130.14 (tertiary C); 123.28, 136.63, 148.58, 159.19, 168.14 (quaternary C). m/z = 188.07 (+M).

2.3.2b Preparation of 2-methyl-4-quinolinecarboxylic acid, methyl ester

The compound was prepared following literature procedure (Sarkis and Axamawaty, 2003). To a mixture of 2-methyl-4-quinolinecarboxylic acid (9.36 g, 0.050 mol) and conc. sulfuric acid (7.4 mL), methanol (30 mL) was slowly added

with stirring. The mixture was heated to reflux for 12 h, and then was cooled to room temperature and left standing overnight. The reaction mixture was poured into crushed ice (100 g) and neutralized by ammonia solution (28 %, 20 mL). The ester was extracted with $CHCl_3$ (3×50 mL), dried over anhydrous $MgSO_4$ and filtered. Solvent was removed under reduced pressure to give the ester as a white solid that needed no further purification (Yield: 8.40 g, 83 %). Mp. 59 ^{o}C (lit. 59-60 ^{o}C). ^{1}H NMR (300 MHz, $CDCl_3$, in ppm): δ = 2.72 (s, 3H); 3.96 (s, 3H); 7.52 (dd, 1H); 7.67 (dd, 1H); 7.73 (s, 1H); 8.01 (d, 1H); 8.63 (d, 1H). ^{13}C NMR (75 MHz, CDCl3, in ppm): δ = 25.29, 52.69 (primary C); 123.31, 125.39, 127.22, 129.23, 129.74 (tertiary C); 134.91, 148.82, 158.47, 166.77 (quaternary C). m/z = 202.09 (+M).

2.3.2c Preparation of 2-formyl-4-quinolinecarboxylic acid, methylester

A solution of 2-methy-4-quinolinecarboxylic acid, methyl ester (8.00 g, 0.0398 mol) in dioxane (40 mL) was heated to reflux. A sample of SeO_2 (8.83 g, 0.0796 mol) was added and refluxing was continued for 30 min. The reaction mixture was cooled, diluted with ether (40 mL), filtered, and the ethereal phase was washed with water, 10 % $NaHCO_3$ (2×50 mL), brine (100 mL) and then dried over anhydrous Na_2SO_4. Solvent was removed under reduced pressure. The aldehyde was obtained as pale-yellow solid that needed no further purification (Yield: 7.28g, 85 %). ^{1}H NMR (300 MHz, $CDCl_3$, in ppm): δ = 4.03 (s, 3H); 7.74-7.85 (m, 2H); 8.26 (dd, 1H); 8.45 (s, 1H); 8.81 (dd, 1H); 10.20 (s, 1H). ^{13}C NMR (75 MHz, $CDCl_3$, in ppm): δ = 52.79 (primary C); 118.65, 125.88, 130.59,

130.72, 131.08, 192.83 (tertiary C); 126.92, 136.16, 148.95, 152.18, 165.92 (quaternary C). m/z = 216.07 (+M).

2.3.2d Preparation of 2-formyl-4-quinolinecarboxylic acid, (II)

2-formyl-4-quinolinecarboxylic acid, methylester (2.75 g, 12.8 mmol) was dissolved in a mixture solvent (THF: H_2O, 1:1, 200 mL), and KOH (1.10 g, 19.2 mmol) was added with stirring at room temperature for 15 min. Completion of the reaction was tested by TLC. THF was removed under reduced pressure and the resulting aqueous solution was acidified to a pH 1-2 with 1 M HCl solution. The product was extracted with ethylacetate (3×100 mL). The organic layer was dried over anhydrous Na_2SO_4. Solvent was removed under reduced pressure to give the product as pale-yellow solid (Yield: 1.90 g, 74 %). Mp. 243-244 ^oC (lit. 241-242 ^oC).

2.3.3 Preparation of sodium salt of salicylaldehyde-5-sulfonic acid (III)

This compound was prepared from the following precursors.

2.3.3a Preparation of N-phenylsalicylaldimine

The compound was prepared following literature procedure (Khera et al., 1983). Aniline (22.3 g, 0.240 mol) in absolute ethanol (150 mL) was added dropwise under vigorous stirring to a solution of salicylaldehyde (24.4 g, 0.200 mol) in absolute ethanol (100 mL) over a period of one hour. The mixture was refluxed for 2 h, and then cooled to 0 ^{o}C. The precipitate was filtered off and dried in vacuo at 25 ^{o}C (Yield: 31.83 g, 80.70 %). Mp. 49 ^{o}C.

2.3.3b Preparation of N-phenylsalicyldimine-5-sulphonic acid and the sodium salt of salicylaldehyde-5-sulfonic acid

These compounds were prepared following literature procedures (Berry et al., 1982; Botsivali et al., 1985). N-phenylsalicylaldimine (17.7 g, 90.0 mmol) was added to conc. sulfuric acid (47.5 mL) and the mixture was kept at a temperature of 100 ± 5 ^{o}C with occasional stirring for 2 h. After cooling to room temperature, the solution was added slowly to ice water (600 mL) with vigorous stirring. The mixture was reheated until all the solids had dissolved. The solution was then allowed to cool to room temperature and the solid product was filtered off and dried in vacuum at 50 ^{o}C (Yield:17.90 g, 71.8 %).

N-phenylsalicylaldimine-5-sulphonic acid (25.0 g, 90.0 mmol) was added to an aqueous solution (150 mL) of anhydrous sodium carbonate (13.8 g) and the

solution was then boiled vigorously to remove aniline. Aniline was efficiently removed by simple distillation of the solution with occasional addition of hot water to compensate for the distilled water. Distillation continued till complete removal of aniline (3 h). The solution was then cooled and glacial acetic acid (100 mL) was slowly added to bring the pH to about 5. Ethanol (100 mL) was added to precipitate the product. The solution was cooled to 0 ^{o}C and the pale-yellow solid product (sodium salt of salicylaldehyde-5-sulfonic acid) was filtered off, recrystallized from water-ethanol (1:1) and finally air dried (Yield: 16.21 g, 80.4 %). Mp. > 350 ^{o}C (lit. > 350 ^{o}C).

2.3.4 Preparation of 4-N,N-dimethylamino-2-hydroxybenzaldehyde, (IV)

The compound was prepared following literature procedure with some modifications (Flašík et al., 2009). Vielsmeier Haack adduct was prepared by addition of $POCl_3$ (15 mL, 0.16 mol) dropwise to dry DMF (30.4 mL) at 0 ^{o}C, and the mixture was then stirred for 30 min at the same temperature. To the adduct a solution of 3-N,N-dimethylaminophenol (11.00 g, 0.08 mol) in dry DMF (22.9 mL) was added dropwise at 0 ^{o}C. The reaction mixture was then slowly warmed to room temperature and stirred for another 4 h, then was heated at 85-90 ^{o}C for 30 min, then was kept at room temperature with stirring overnight. The reaction mixture was then poured into crushed ice, and neutralized with saturated aqueous solution of Na_2CO_3 (~120 mL). The precipitate was filtered off, washed with water and dried in vacuo at 25 ^{o}C, and needed no further purification (Yield: 9.00 g, 68 %). Mp. 78-79 ^{o}C (lit. 80.5-81 ^{o}C).

2.4 Preparation of the ligands

2.4.1 Preparation of 3,3`-Dicarboxy-2,2`-bipyridine, (V)

The compound was prepared following literature procedure (Kanungo et al., 2003). To a solution of sodium hydroxide (2.0 g, 0.05 mol) in 300 mL distilled water, 1,10-phenanthroline (5.0 g, 0.025 mol) was added, then potassium permanganate (11.85 g, 0.075 mol) was added to the above mixture slowly (within 15 min) with a good stirring at RT. The mixture was then heated to reflux for 6 h. The brown precipitate (MnO_2) was filtered while hot. The volume of the filtrate was reduced to ~120 mL in a rotary evaporator. The solution (pale-yellow) was boiled with ~2 g of decolorizing charcoal and filtered. Conc. HCl (11-12 mL) was added dropwise to the filtrate and at pH ~ 3 fine crystals started to precipitate. Addition of HCl continued till the pH of the solution reached ~2. The white crystalline solid was filtered off, washed with water, then with ethanol and dried in vacuo at 50 ^{o}C. The filtrate was collected and the volume was reduced to half and was left undisturbed overnight while more crystals separated out. This process of concentration was repeated with the filtrates till no more crystals came out (Yield: 4.62 g, 75 %), Mp. 260 ^{o}C d (lit. 262 ^{o}C d)

2.4.2 Preparation of 4,4`-Dicarboxy-2,2`-bipyridine, (VI)

The compound was prepared following literature procedure (Hoertz et al., 2006). A mixture of 4,4`-dimethyl-2,2`-bipyridine (2.50 g, 0.0136 mol) in conc. H_2SO_4 (62.5 mL) was heated at 70-80 ^{o}C. To the mixture was slowly added solid

potassium dichromate (12.00 g). The temperature was held consistently between 70 and 80 ^{o}C during the transfer. The deep green mixture was then poured over 800 mL of ice/water, affording a light yellow precipitate that was isolated by filtration and washed with water. The solid was then refluxed in 50 % HNO_3 (150 mL) for 4 h. The cooled pale green solution was then poured over ice and diluted with water (800 mL). A white powder was filtered off, washed with water and dried in vacuo at 50 ^{o}C (Yield: 3.20 g, 96 %). Mp. > 350 ^{o}C.

2.4.3 Preparation of Schiff base ligands

2.4.3a Preparation of 4-[(8-quinolinylimino)methyl]phenol, (VII)

A solution of 4-hydroxybenzaldehyde (2.00 g, 0.0164 mol) in dry ethanol (25 mL) was introduced into a 250-mL two-necked round bottomed flask connected with a nitrogen inlet and equipped with a dropping funnel and a condenser connected to a bubbler. 8-aminoquinoline (2.36 g, 0.0164 mol) in dry ethanol (25 mL) was added dropwise. After the addition was complete, the solution was refluxed for 2 h. After cooling, the solid was collected and washed with small amount of cold ethanol. The product was recrystallized from ethanol to give yellow fine crystals. The product was dried in vacuo at 50 ^{o}C (Yield: 3.91 g, 96 %). Mp. 210 ^{o}C.

2.4.3b Preparation of sodium salt of 4-hydroxy-3-[(quinolin-8-yl)carboximidoyl]benzenesulfonic acid, (VIII)

This compound was prepared by a procedure similar to 2.4.3a above. The product was separated as intense orange solid (Yield: 96 %). Mp. > 350 ^oC

2.4.3c Preparation of 2-[(3-carboxyphenyl)carboximidoyl]quinolin-4-carboxylic acid, (IX)

To a solution of 2-formyl-4-quinolinecarboxylic acid (1.05 g, 5.22 mmol) in dry methanol (25 ml), introduced into a 250-ml two-necked round bottomed flask equipped with a dropping funnel and a condenser with a nitrogen inlet, 3-aminobenzoic acid (0.72 g, 5.22 mmol) in dry methanol (20 ml) was added dropwise. After the addition was complete, the solution was heated to reflux for 1 hour. After cooling, the solid was collected, washed with methanol, recrystallized from methanol and dried in vacuo at 50 ^oC to give a white solid product (Yield: 1.72g, 83 %). Mp. > 350 ^oC.

2.4.3d Preparation of 2,2`-[1,2-phenylenebis(nitrilomethylidyne)]bis[5-dimethyamino]phenol, (X)

A solution of 4-N,N-dimethylamino-2-benzaldehyde (1.00 g, 6.05 mmol) in dry ethanol (25 mL) was introduced into a 150-mL two-necked round bottomed flask equipped with a dropping funnel, a condenser, a nitrogen inlet and connected to a bubbler. 1,2-phenylenediamine (0.327 g, 3.025 mmol) in dry ethanol (20 mL) was added dropwise. After the addition was complete, the

reaction mixture was refluxed for 4 h. After cooling the solid was collected, washed with small amount of cold ethanol and recrystallized from ethanol. The intense yellow product was dried at 50 ^{o}C in vacuo (Yield: 1.13 g, 93 %). Mp. 200-202 ^{o}C

2.4.3e Preparation of 3,3`[1,2-phenylenebis(nitrilomethylidyne)]bis[4-hydroxy]benzoic acid, (XI)

To a solution of 3-formyl-4-hydroxybenzoic acid (0.60 g, 3.61 mmol) in dry methanol (25 mL) was introduced into a 150-mL two-necked round bottomed flask equipped with a dropping funnel, a condenser, a nitrogen inlet and connected to a bubbler. 1,2-phenylenediamine (0.20 g, 1.81 mmol) in dry methanol (20 mL) was added dropwise. After the addition was complete, the reaction mixture was refluxed for 2 h. The mixture was cooled and the solid product was filtered, washed with cold methanol and recrystallized from methanol. The intense orange product was dried at 40 ^{o}C in vacuo (Yield: 0.65 g, 89 %). Mp. > 350 ^{o}C.

2.4.3f Preparation of sodium salt of 3,3`-[1,2-phenylenebis(nitrilomethylidyne)]bis[4-hydroxy]benzenesulfonic acid, (XII)

This compound was prepared according to the procedure of 2.4.3e above (sodium salicylaldehyde-5-sulfonic acid (2.00 g, 8.92 mmol) in dry methanol (40 mL) with 1,2-phenylenediamine (0.48 g, 4.46 mmol) in dry methanol (20 mL). the product was separated as intense yellow solid (Yield: 2.14 g, 92 %). Mp. > 350 ^oC.

2.4.3g Preparation of (XIII)

This compound was prepared according to the procedure of 2.4.3f above (2-formyl-4-quinolinecarboxylic acid (1.86 g, 9.24 mmol) in dry methanol (40 mL) with 1,2-phenylenediamine (0.50 g, 4.62 mmol) in dry methanol (20 mL). the product was separated as pale-yellow solid (Yield: 1.91 g, 87 %). Mp. > 350 ^oC.

2.5 Preparation of Ru(II) Complexes

2.5.1 Preparation of Dichlorotetrakis(dimethylsulphoxide)ruthenium(II) $RuCl_2(DMSO)_4$

The compound was prepared following literature procedure (Evans et al., 1973). Ruthenium(III) chloride trihydrate $RuCl_3.3H_2O$ (2.00 g, 7.65 mmol) placed in a 50 mL round-bottomed flask, was refluxed in degassed dimethylsulphoxide (20 mL) for 5 min only (the mixture will turn to brown-orange color when the reaction is complete). The volume was then reduced to half under reduced pressure. Acetone (40 mL) was slowly added and the mixture was cooled in an ice bath for 10-15 min. The yellow complex was filtered off, washed with acetone and diethyl ether, and dried in vacuo at 50 ^{o}C (Yield: 2.82 g, 76 %). Mp. 190-191 ^{o}C (lit. 193 ^{o}C).

2.5.2 Preparation of Dichlorotris(triphenylphosphine) ruthenium(II) $RuCl_2(PPh_3)_3$

The compound was prepared following literature procedure (Hallman et al., 1970). Ruthenium(III) chloride trihydrate (1.0 g, 3.8 mmol) was dissolved in methanol (250 mL) and the solution was filtered. The filtrate was refluxed under nitrogen for 5 min. After cooling, triphenylphosphine (6.0 g, 22.9 mmol) was added and the solution was again refluxed under nitrogen for 3 h. The complex was precipitate from the hot solution as a chocolate-brown solid. The solution mixture was left to cool and the complex was filtered off under nitrogen, washed

several times with degassed diethyl ether, and dried in vacuo at 50 ^{o}C (Yield: 2.7 g, 74 %). Mp. 132-134 ^{o}C (lit. 132-134 ^{o}C).

2.5.3 Preparation of Ru(II)-bipyridyl complexes

2.5.3a Preparation of cis-Dichloro-N,N`-bis(2,2`-bipyridyl-4,4`-dicarboxylic acid)ruthenium(II), $Ru(VI)_2Cl_2$

The compound was prepared following literature procedure (Xie et al., 2000). To a solution of $RuCl_2(DMSO)_4$ (0.484 g, 1 mmol) in chloroform (40 mL) was added 4,4`-dcbpy (0.488 g, 2 mmol) in dry ethanol (30 mL). The mixture was refluxed with stirring under reduced light (using aluminum foil) and under N_2 atmosphere for 24 h. The reaction mixture was allowed to cool and then filtered. The filtrate was evaporated to dryness, and the solid was dissolved in dry methanol (30 mL) and filtered, diethyl ether was added to the condensed methanolic solution to precipitate the product. The red powder was collected and dried in vacuo at 50 ^{o}C (Yield: 0.58 g, 88 %). Mp. > 350 ^{o}C.

2.5.3b Preparation of cis-Di(thiocyanato)-N,N-bis(2,2`-bipyridyl-4,4`-dicarboxylic acid)ruthenium(II), cis-$Ru(VI)_2(NCS)_2$

The compound was prepared following literature procedure (Nazeeruddin et al., 1993). Ru(4,4`-dcbpy)$_2$Cl$_2$ (0.565 g, 0.856 mmol) was dissolved in dry DMF (50 mL) under reduced light. To this solution 0.1 M aqueous NaOH (40 mL) was added in order to deprotonate the carboxyl groups. Sodium thiocyanate (NaNCS) (0.70 g, 9.04 mmol) was separately dissolved in distilled water (4 mL) and

subsequently added to the above solution. The reaction mixture was then refluxed for 6 h under N_2 atmosphere. Then, the reaction mixture was allowed to cool, and the solvent was removed in vacuo. The resulting solid was dissolved in water (40 mL) and filtered through a sintered glass crucible. The pH of this filtrate was lowered to 2.5 by adding dilute $HClO_4$, and the filtrate was placed in a refrigerator overnight. After reaching room temperature, the microcrystalline solid was isolated by suction filtration, washed well with water, acetone-ether mixture (1:10) followed by anhydrous diethyl ether, and dried in vacuum at 50^{o}C (Yield: 0.48 g, 79 %). Mp. > 350 ^{o}C.

2.5.3c Preparation of cis-Dichloro-N,N`-bis(2,2`-bipyridyl-3,3`-dicarboxylic acid)ruthenium(II) and cis-Di(thiocyanato)-N,N-bis(2,2`-bipyridyl-3,3`-dicarboxylic acid)ruthenium(II), cis-Ru(V)$_2$Cl$_2$ and cis-Ru(V)$_2$(NCS)$_2$

Complex cis-Ru(V)$_2$Cl$_2$ was prepared as in 2.5.3a using ligand **(V)** and $RuCl_2(DMSO)_4$ (Yield: 89 %), complex cis-Ru(V)$_2$(NCS)$_2$ was prepared as in 2.5.3b using Ru(V)$_2$Cl$_2$ with NaNCS (Yield: 79 %). Mp. > 350 ^{o}C.

2.5.4 Preparation of Ru(II)-Schiff base complexes

2.5.4a Preparation of [Ru(VII)(aminoquinoline)Cl$_2$].5H$_2$O

$RuCl_2(DMSO)_4$ (0.58 g, 1.21 mmol) was dissolved in dry 2-methoxyethanol (30 mL). To this solution **(VII)** (0.60 g, 2.42 mmol) in 2-methoxyethanol (30 mL) was added. The mixture was refluxed with stirring under reduced light (using aluminum foil) and under N_2 atmosphere for 8 h. After the reaction mixture was

cooled, the volume of the solvent was reduced in vacuo till 10 mL. Diethyl ether was added slowly to precipitate the product as fine green solid, which was filtered, washed thoroughly with diethyl ether and dried in vacuo at 50 ^{o}C. Mp. 225 ^{o}C.

2.5.4b Preparation of [Ru(VIII-H)$_2$].4H$_2$O

RuCl$_2$(DMSO)$_4$ (0.55 g, 1.14 mmol) was added to a solution of **(VIII)** (0.80 g, 2.28 mmol) and Et$_3$N (0.23 g, 2.28 mmol) in dry 2-methoxy ethanol (40 mL). The mixture was refluxed under reduced light (using aluminum foil) and under N$_2$ atmosphere for 8 h. After the reaction mixture was cooled, the volume of the solvent was reduced in vacuo till 10 mL. Diethyl ether was added slowly to precipitate the product as fine black solid, which was filtered, washed thoroughly with diethyl ether and dried in vacuo at 50 ^{o}C. Mp. > 350 ^{o}C.

2.5.4c Preparation of [Ru(X-2H)(PPh$_3$)(H$_2$O)].3H$_2$O

RuCl$_2$(PPh$_3$)$_3$ (0.958 g, 1 mmol) was added to a solution of **(X)** (0.402 g, 1 mmol) and Et$_3$N (0.303 g, 3 mmol) in dry 2-methoxy ethanol (40 mL). The solution mixture was refluxed under reduced light (using aluminum foil) and under N$_2$ atmosphere for 4 h. After the reaction mixture was cooled, the volume of the solvent was reduced in vacuo till 10 mL. Diethyl ether was added slowly to precipitate the product as red solid, which was filtered, washed thoroughly with diethyl ether and dried in vacuo at 50 ^{o}C. Mp. 250-252 ^{o}C.

2.5.4d Preparation of [Ru(XI-3H)(PPh_3)(H_2O)]

This compound was prepared as in 2.5.4c procedure above(using ($RuCl_2(PPh_3)_3$ (0.948 g, 0.989 mmol) and **(XI)** (0.40 g,0.989 mmol)). The complex was separated as brown solid. Mp. > 350 ^oC.

2.5.4e Preparation of [Ru(XII-2H)(PPh_3)(NEt_3)].3H_2O

This compound was prepared as in 2.5.4d procedure above (using ($RuCl_2(PPh_3)_3$ (0.55 g, 0.574 mmol) and **(XII)** (0.30 g, 0.574 mmol)). The complex was separated as pale brown solid. Mp. > 350 ^oC.

2.5.4f Preparation of [Ru(XIII)Cl_2].3H_2O

$RuCl_2(DMSO)_4$ (0.51 g, 1.05 mmol) was dissolved in dry 2-methoxyethanol (30 mL). To this solution **(XIII)** (0.50 g, 1.05 mmol) in 2-methoxyethanol (30 mL) was added. The mixture was refluxed under reduced light (using aluminum foil) and under N_2 atmosphere for 4 h. After the reaction mixture was cooled, the volume of the solvent was reduced in vacuo till 10 mL. Diethyl ether was added slowly to precipitate the product as violet solid, which was filtered, washed thoroughly with diethyl ether and dried in vacuo at 50 ^oC. Mp. > 350 ^oC.

3. RESULTS

The results of melting points (or decomposition points), mass spectral data (m/z) and solubility, for the starting materials are listed in Table 3.1 and Table 3.2.

Table 3.1: Colors, molecular weights, melting points and mass spectral data for the starting materials

Starting material	Color	M.P (^oC)	M.W	m/z
4,4`-Dimethyl-2,2`-bipyridine **(I)**	White	171-173	184.24	185.11 (+M)*
2-formyl-4-quinolinecarboxylic acid **(II)**	Pale-Yellow	243-244	201.18	200.03 (-M)**
sodium salt of Salicylaldehyde-5-sulfonic acid **(III)**	Pale-Yellow	> 350	224.17	200.99 (-M)***
4-N,N-dimethylamino-2-hydroxybenzaldehyde **(IV)**	Pale-Yellow	78-79	165.19	166.09 (+M)

*(+M): positive mode (+H), ** (-M): negative mode (-H), *** (-M): negative mode (-Na)

Table 3.2: Solubility chart for the starting materials*

Starting material	H_2O	Acetone	MeOH	EtOH	CH_2Cl_2	$CHCl_3$	THF	Pet. ether	Diethyl ether	hexane	Ethyl acetate
(I)	-	-	+	±	+	+	±	-	-	-	-
(II)	-	-	+	-	-	-	+	-	±	-	+
(III)	+	-	±	-	-	-	-	-	-	-	±
(IV)	-	±	+	±	+	+	+	-	±	-	+

*- : insoluble, +: soluble, ±: slightly soluble

The results of elemental analysis, melting points (or decomposition points), mass spectral data (m/z) and solubility for bipyridyl and Schiff base ligands are listed in Tables 3.3-3.5, respectively.

Table3.3: Elemental analysis for the bipyridyl and Schiff base ligands

Ligand (Formula)	**C % Calculated (found)**	**H % Calculated (found)**	**N % Calculated (found)**
(V) ($C_{12}H_8N_2O_4$)	59.01 (58.30)	3.30 (3.23)	11.47 (11.50)
(VI) ($C_{12}H_8N_2O_4$)	59.01 (58.43)	3.30 (3.29)	11.47 (11.33)
(VII) ($C_{16}H_{12}N_2O$)	77.40 (77.22)	4.87 (4.93)	11.29 (11.31)
(VIII) ($C_{16}H_{11}N_2O_4S.Na$)	54.85 (54.77)	3.17 (3.21)	7.99 (7.93)
(IX) ($C_{18}H_{12}N_2O_4$)	67.50 (67.39)	3.78 (3.75)	8.75 (8.69)
(X) ($C_{24}H_{26}N_4O_2$)	71.62 (71.57)	6.51 (6.52)	13.92 (14.01)
(XI) ($C_{22}H_{16}N_2O_6$)	65.35 (65.24)	3.99 (3.94)	6.93 (6.85)
(XII) ($C_{20}H_{14}N_2O_8S_2.2Na$)	46.15 (46.04)	2.71 (2.69)	5.38 (5.26)
(XIII) ($C_{28}H_{18}N_4O_4$)	70.88 (70.90)	3.82 (3.95)	11.81 (11.81)

Table 3.4: Colors, melting points and mass spectral data for the bipyridyl and Schiff base ligands

Ligand	Color	M.W	m/z	M.P (^oC)
(V)	White	244.20	245.06 (+M)	260 (d)*
(VI)	White	244.20	245.06 (+M)	> 350
(VII)	Yellow	248.28	249.10 (+M)	210
(VIII)	Orange	350.33	-	> 350
(IX)	White	320.31	319.07 (-M)	> 350
(X)	Intense- yellow	402.50	403.21 (+M)	200-202
(XI)	Orange	404.38	403.09 (-M)	> 350
(XII)	Intense-yellow	520.45	-	> 350
(XIII)	Pale-yellow	474.48	475.14 (+M)	> 350

*d: decomposition point

Table 3.5: Solubility chart for the bipyridyl and Schiff base ligands

Ligand	H_2O	Acetone	MeOH	EtOH	CH_2Cl_2	$CHCl_3$	THF	Pet. ether	Diethyl ether	hexane	DMSO	DMF
(V)	-	-	-	-	-	-	-	-	-	-	+	+
(VI)	-	-	-	-	-	-	-	-	-	-	-	±
(VII)	-	-	±	±	-	-	±	-	-	-	+	+
(VIII)	+	-	±	±	-	-	±	-	-	-	+	+
(IX)	-	-	±	-	-	-	-	-	-	-	+	+
(X)	-	-	+	±	+	+	+	-	-	-	+	+
(XI)	-	-	-	-	-	-	±	-	-	-	+	+
(XII)	+	-	±	±	-	-	±	-	-	-	+	+
(XIII)	-	-	-	-	-	-	-	-	-	-	-	±

Table 3.6: ^{1}H-NMR spectral data for the starting materials

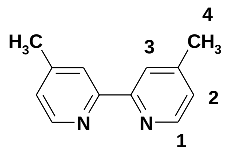
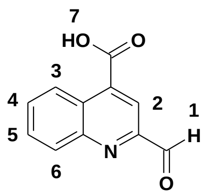
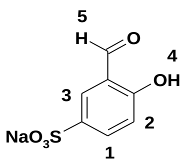
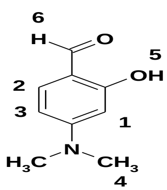
Starting materials		Chemical Shift δ (ppm)						
		1	**2**	**3**	**4**	**5**	**6**	**7**
 (I)	^{1}H	8.49 (d, 2 H) J = 4.84 Hz	7.09 (d, 2 H) J = 3.39 Hz	8.19 (s, 2 H)	2.39 (s, 6 H)	-	-	-
 (II)	^{1}H	8.78 (d, 1 H) J = 8.52 Hz	**3**	**6**	**2**	**4**	**5**	10.10 (s, 1 H)
			8.26 (d, 2 H) J = 6.83 Hz		7.83-7.96 (m, 3 H)			
 (III)	^{1}H	7.73 (dd, 1 H)	6.87 (d, 1 H) J= 8.77 Hz	7.91 (s, 1 H)	-	9.76 (s, 1 H)	-	-
 (IV)	^{1}H	6.24 (dd, 1 H)	7.23 (d, 1 H) J= 6.4 Hz	6.02 (d, 1 H) J= 2.36 Hz	3.01 (s, 6 H)	11.58 (s, 1 H)	9.47 (s, 1 H)	-

Table 3.7: ^{13}C-NMR spectral data for the starting materials

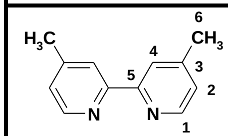
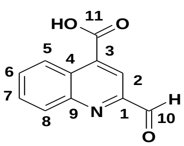
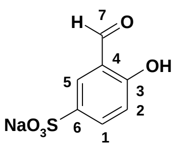
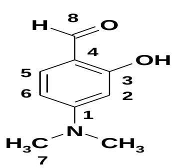
Starting materials		Chemical Shift δ (ppm)										
		1	**2**	**3**	**4**	**5**	**6**	**7**	**8**	**9**	**10**	**11**
 **(I)**	^{13}C	148.9	122.0	148.2	124.7	156.0	21.2	-	-	-	-	-
 **(II)**	^{13}C	148.1	118.3	138.2	126.3	126.6-131.5 (126.7; 131.1; 131.2;131.5)				152.5	193.6	167.4
 **(III)**	^{13}C	133.9	117.9	161.8	120.3	130.8	134.6	196.6	-	-	-	-
 **(IV)**	^{13}C	156.2	97.2	164.1	111.7	135.2	104.7	40.1	192.4	-	-	-

Table 3.8: ^{1}H-NMR and ^{13}C-NMR spectral data for the bipyridyl ligands

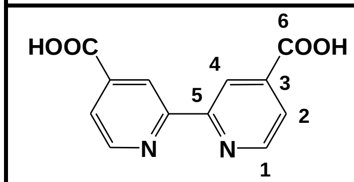
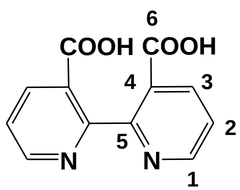
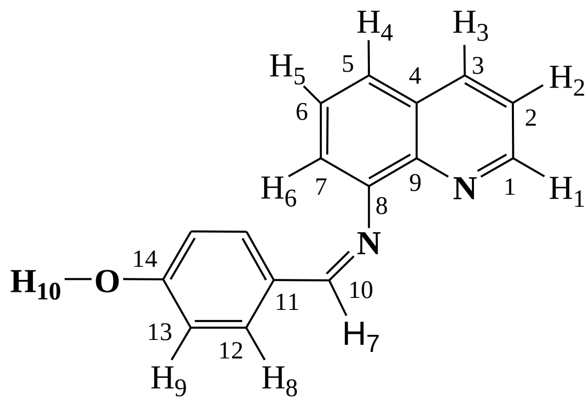
Ligand	Chemical Shift δ (ppm)						
		1	**2**	**3**	**4**	**5**	**6**
 **(VI)**	^{1}H	8.59(d) J = 4.9 Hz 2 H	7.68 (d) J = 4.9 Hz 2 H	-	8.19 (s) 2 H	-	-
	^{13}C	149.7	121.2	146.3	123.3	155.7	172.9
 **(V)**	^{1}H	8.65 (dd) J = 3.14 Hz 2 H	7.48 (dd) J = 4.81 Hz 2 H	8.24 (dd) J = 6.19 Hz 2 H	-	-	-
	^{13}C	151.1	123.2	138.2	127.0	159.4	167.4

Table 3.9: ^{1}H-NMR and ^{13}C-NMR spectral data for (VII)

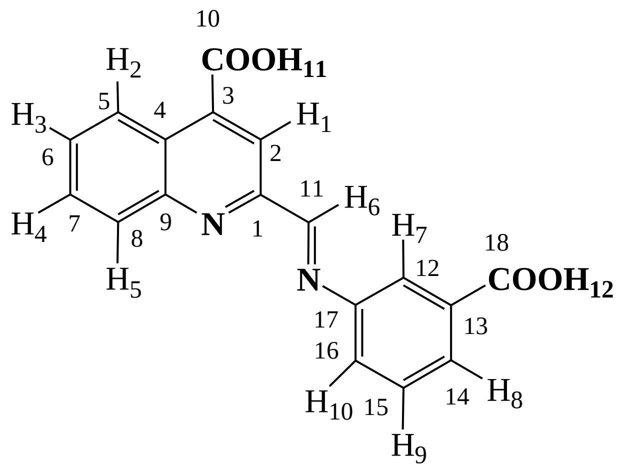
\



Chemical Shift δ (ppm)										
	1	**2**	**5**	**3**	**4**	**6**	**7**	**8**	**9**	**10**
^{1}H	8.83 (dd, 1 H)	7.49-7.56 (m, 2 H)		8.33 (dd, 1 H)	7.71 (d, 1 H) J= 8.14 Hz	7.26 (dd, 1 H)	8.44 (s, 1H)	7.80 (d, 2 H) J= 8.58 Hz	6.89 (d, 2 H) J= 8.55 Hz	10.14 (s, 1 H)

	C-1	**C-2**	**C-3**	**C-4**	**C-5**	**C-6**	**C-7**	**C-8**	**C-9**	**C-10**	**C-11**	**C-12**	**C-13**	**C-14**
^{13}C	150.2	119.1	136.6	129.3	124.7	127.3	122.1	150.7	141.9	162.7	128.2	131.3	116.1	161.1

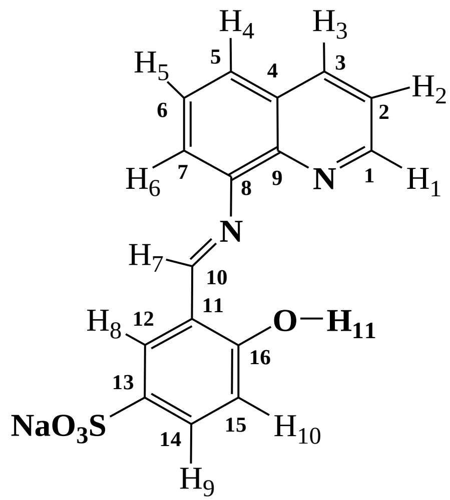
Table 3.10: ^{1}H-NMR and ^{13}C-NMR spectral data for (IX)



Chemical Shift δ (ppm)												
	1	2	3	4	5	6	7	8	9	10	11	12
^{1}H	8.62 (s, 1 H)	8.75 (d, 1 H) J = 7.99 Hz	7.84-7.89 (m, 3 H)			8.79 (s, 1 H)	8.16 (d, 1 H) J = 7.99 Hz	7.58 (d, 1 H) J = 7.6 Hz	7.73-7.78 (m, 1 H)	7.66 (d, 1 H) J = 8.24 Hz	13.40 (bs, 2 H)	

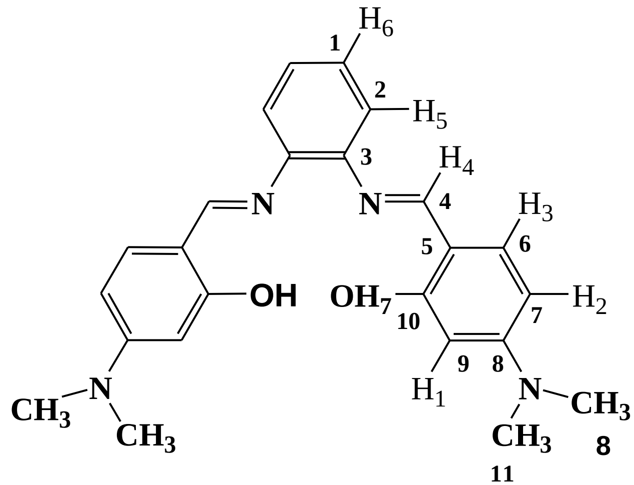
	C-1	C-2	C-3	C-4	C-5	C-6	C-7	C-8	C-9	C-10	C-11	C-12	C-13	C-14	C-15	C-16	C-17	C-18
^{13}C	148.8	119.6	137.4	126.0	125.6	128.4	130.5	129.9	150.7	167.7	161.7	154.4	122.8	132.6	130.2	130.9	126.3	167.4

Table 3.11: ^{1}H-NMR and ^{13}C-NMR spectral data for (VIII)



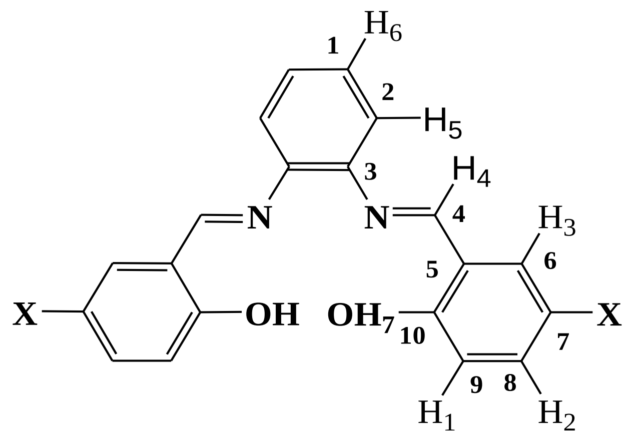
	Chemical Shift δ (ppm)															
^{1}H	1		3		4	6		2	5	9	7	8		10		11
	8.95 (dd, 1 H)		8.40 (dd, 1 H)		7.89 (dd, 1 H)	7.77 (d, 1 H) J= 7.46 Hz		7.57-7.68 (m, 3 H)			9.14 (s, 1 H)	7.93 (d, 1H) J= 2.17 Hz		6.89 (d, 1 H) J= 8.58 Hz		14.18 (s, 1 H)
^{13}C	C-1	C-2	C-3	C-4	C-5	C-6	C-7	C-8	C-9	C-10	C-11	C-12	C-13	C-14	C-15	C-16
	151.1	118.7	136.7	129.2	127.4	130.3	127.1	144.8	142.2	164.4	118.4	122.7	139.8	131.6	116.8	162.4

Table 3.12: ^{1}H-NMR and ^{13}C-NMR spectral data for (X)



Chemical Shift δ (ppm)											
^{1}H	1	2	3		4	6	5	7		8	
	6.06 (s) 2 H	6.30 (dd) 2 H	7.22 (dd) 2 H		8.62 (s) 2 H	7.29-7.32 (m) 4 H		13.46 (s) 2 H		2.96 (s) 12 H	
^{13}C	C-1	C-2	C-3	C-4	C-5	C-6	C-7	C-8	C-9	C-10	C-11
	126.90	119.64	142.55	162.31	109.85	134.37	104.63	154.47	98.16	163.80	40.29

Table 3.13: ¹H-NMR and ¹³C-NMR spectral data for (XI) and (XII)



Chemical Shift δ (ppm)												
^{1}H	**Ligand**	**X**	**1**		**2**	**3**	**4**	**5**	**6**	**7**		**9***
	XI	**COOH**	7.01 (d, 2 H) J= 5.3 Hz		7.92 (s) 2 H	8.31 (s) 2 H	9.03 (s) 2 H	7.44 (d, 4 H) J= 23.0 Hz		13.65 (s) 2 H		12.7 (bs) 2 H
	XII	**SO_3Na**	6.88 (d, 2 H) J= 8.55 Hz		7.60 (dd)	7.92 (d, 2 H)	8.96 (s) 2 H	7.36-7.49 (m) 4 H		13.17 (s) 2 H		-
^{13}C	**Ligand**	**X**	**C-1**	**C-2**	**C-3**	**C-4**	**C-5**	**C-6**	**C-7**	**C-8**	**C-9**	**C-10**
	XI	***COOH**	128.6	122.1	142.2	164.3	119.5	134.9	120.4	135.0	117.6	164.8
	XII	**SO_3Na**	130.4	120.4	142.5	164.9	118.5	128.4	140.1	131.5	116.4	161.1

* δ of carboxyl group proton. * δ of carboxyl group carbon = 167.0 ppm

Table 3.14: Infrared spectral data for the Schiff base ligands

Mode	VII	VIII	IX	X	XI	XII	XIII
Azomethine C=N str.	1599(s)	1633(s)	1625 (s)	1629	1611(s)	1620(s)	1629(w)
O-H str.	3436(w)	3447(br)	-		3424 (br)	3446(v.br)	-
C=O str.	-	-	1710	-	1695(s)	-	1702(s)
C-H str.	3054, 2805	3047	2954 (w)	2896	3060, 2915(w)	3055	2953(s)
Aromatic C=C str.	1521(m)	1513(s)	1587	1599	1513(m)	1569(w)	1585(m)
Sulphonyl group vibrations	-	596(s), 1027(s), 1108(s), 1167	-	-	-	606(s), 1041(s), 1112(s), 1186(s)	-

The results of melting points (or decomposition points) and solubility, for Ru(II) precursors and the bipyridyl complexes are listed in Table 3.15 and Table 3.16.

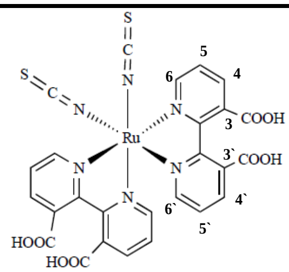
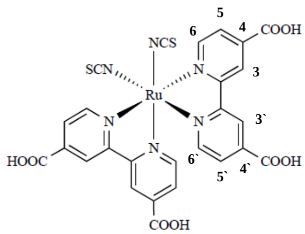
Table 3.15: Colors, melting points and molecular weights for Ruthenium precursors and the Ruthenium bipyridyl complexes

Complex (Formula)	**Color**	**M.W**	**MP. (^{o}C)**
$Ru(DMSO)_4Cl_2$ ($C_8H_{24}S_4O_4Cl_2Ru$)	Yellow	484.52	190-191
$RuCl_2(PPh_3)_3$ ($C_{56}H_{45}Cl_2P_3Ru$)	Chocolate -brown	982.89	132-134
$Ru(V)_2Cl_2$ ($C_{24}H_{16}N_4O_8Cl_2Ru$)	Purple-red	660.38	> 350
$Ru(VI)_2Cl_2$ ($C_{24}H_{16}N_4O_8Cl_2Ru$)	Red	660.38	> 350
$Ru(V)_2(NCS)_2$ ($C_{26}H_{16}N_6S_2O_8Ru$)	Black	705.64	> 350
$Ru(VI)_2(NCS)_2$ ($C_{26}H_{16}N_6S_2O_8Ru$)	Intense-red	705.64	> 350

Table 3.16: Solubility chart of Ru-precursors and Ru-bipyridyl complexes

Complex	**H_2O**	**Acetone**	**MeOH**	**EtOH**	**CH_2Cl_2**	**$CHCl_3$**	**THF**	**Pet. ether**	**Diethyl ether**	**hexane**	**DMSO**	**DMF**
$Ru(DMSO)_4Cl_2$	-	-	+	+	+	+	±	-	-	-	+	+
$Ru (PPh_3)_3Cl_2$	-	-	±	±	+	+	+	-	-	-	+	+
$Ru(V)_2Cl_2$	-	-	±	-	-	-	±	-	-	-	+	+
$Ru(VI)_2Cl_2$	-	-	±	-	-	-	±	-	-	-	+	+
$Ru(V)_2(NCS)_2$	-	-	±	-	-	-	±	-	-	-	±	+
$Ru(VI)_2(NCS)_2$	-	-	±	-	-	-	±	-	-	-	±	+

Table 3.17: ^{1}H-NMR spectral data of $Ru(4,4`\text{-dcbpy})_2(NCS)_2$ and $Ru(3,3`\text{-dcbpy})_2(NCS)_2$

Complex	Chemical Shift δ (ppm)					
	4	**5**	**6**	**4`**	**5`**	**6`**
 $Ru(V)_2(NCS)_2$	8.54 (d, 2 H) J= 6.46 Hz	8.15 (d, 2 H) J= 7.51 Hz	9.53 (d, 2 H) J= 4.88 Hz	8.07-8.01 (m, 6 H)		
	3	**5**	**6**	**3`**	**5`**	**6`**
 $Ru(VI)_2(NCS)_2$	9.07 (s) 2 H	9.30 (d, 2 H) J= 5.82 Hz	9.58 (d, 2 H) J= 6.02 Hz	8.97 (s) 2 H	8.13 (d, 2 H) J= 1.52 Hz	8.27 (d, 2 H) J= 4.39 Hz

The results of elemental analysis, melting points (or decomposition points), solubility, IR spectra and UV-Vis absorption data for Ru(II) Schiff base complexes are listed in Tables 3.18-3.21 respectively.

Table 3.18: Elemental analysis for the Ruthenium Schiff base complexes

Complex (Formula)	**C % Calculated (found)**	**H % Calculated (found)**	**N % Calculated (found)**
[Ru(VII)(AQ)Cl_2].5H_2O $C_{25}H_{29}Cl_2N_4O_6Ru$	45.95 (44.97)	4.47 (4.39)	8.57 (8.49)
[Ru(VIII-H)$_2$].4H_2O $C_{32}H_{28}N_4Na_2O_{12}RuS_2$	44.04 (43.02)	3.21 (3.41)	6.42 (6.41)
[Ru(X-2H)(PPh_3)(H_2O)].3H_2O $C_{42}H_{47}N_4O_6PRu$	60.29 (60.19)	5.62 (5.82)	6.70 (6.81)
[Ru(XI-3H)(PPh_3)(H_2O)] $C_{46}H_{46}N_3O_7PRu$	62.43 (62.68)	5.42 (5.70)	4.75 (4.49)
[Ru(XII-2H)(PPh_3)(NEt_3)].3H_2O $C_{44}H_{48}N_3Na_2O_{11}PRuS_2$	50.91 (49.26)	4.63 (4.40)	4.05 (3.86)
[Ru(XIII)Cl_2].3H_2O $C_{28}H_{24}Cl_2N_4O_5Ru$	47.96 (48.14)	3.43 (3.47)	7.99 (8.13)

Table 3.19: Colors, molecular weights and melting points for the Ruthenium Schiff base complexes

Complex	Color	M.W	MP. (^oC)
[Ru(VII)(AQ)Cl_2].5H_2O	Green	653.5	225
[Ru(VIII-H)$_2$].4H_2O	Black	871.76	>350
[Ru(X-2H)(PPh_3)(H_2O)].3H_2O	Red	835.89	250-252
[Ru(XI-3H)(PPh_3)(H_2O)]	Brown	884.92	>350
[Ru(XII-2H)(PPh_3)(NEt_3)].3H_2O	Brown	1037.02	>350
[Ru(XIII)Cl_2].3H_2O	Violet	700.62	>350

Table 3.20: Solubility chart for the Ruthenium Schiff base complexes

Complex	H_2O	Acetone	MeOH	EtOH	CH_2Cl_2	$CHCl_3$	THF	Pet. ether	Diethyl ether	hexane	DMSO	DMF.
[Ru(VII)(AQ)Cl_2].5H_2O	-	-	±	±	-	-	-	-	-	-	±	±
[Ru(VIII-H)$_2$].4H_2O	+	-	±	-	-	-	-	-	-	-	±	±
[Ru(X-2H)(PPh_3)(H_2O)].3H_2O	-	-	±	±	-	-	-	-	-	-	±	±
[Ru(XI-3H)(PPh_3)(H_2O)]	-	-	-	-	-	-	-	-	-	-	±	±
[Ru(XII-2H)(PPh_3)(NEt_3)].3H_2O	+	-	±	-	-	-	-	-	-	-	±	±
[Ru(XIII)Cl_2].3H_2O	-	-	-	-	-	-	-	-	-	-	±	±

Table 3.21: Infrared and electronic* spectral data for the Ruthenium bipyridyl and Schiff base complexes

Complex	$\nu_{C=N}$ (cm^{-1})	$\nu_{C=O}$ (cm^{-1})	$\nu_{C=C}$ (cm^{-1})	$\nu_{sulfonyl}$ (cm^{-1})	λ_{max} (nm) ((ε) $L.mol^{-1}.cm^{-1}$)
$Ru(V)_2(NCS)_2$	-	1715	1577	-	580.0
$Ru(VI)_2(NCS)_2$	-	1717	1563	-	552.0 (10190)*
$[Ru(VII)(AQ)Cl_2].5H_2O$	1587(m)	-	1507(m)	-	623 (6834)
$[Ru(VIII\text{-}H)_2].4H_2O$	1600(s)	-	1507(m)	614, 1030, 1111 1178.	399 (13,012) 630 (6310)
$[Ru(X\text{-}2H)(PPh_3)(H_2O)].3H_2O$	1605(s)	-	1559(s)	-	371 (12,484), 466 (12,585)
$[Ru(XI\text{-}3H)(PPh_3)(H_2O)]$	1596(s)	1664(s)	1564(m)	-	412 (10,357), 494.7 (5045)
$[Ru(XII\text{-}2H)(PPh_3)(NEt_3)].3H_2O$	1598(s)	-	1572(w)	613, 1031, 1112 1183	413.0 (16,553)
$[Ru(XIII)Cl_2].3H_2O$	1592	1717	1544	-	365 (19510) 499.0 (4786)

* In 10^{-4} DMF solution. * λ= 534 nm (ε = 14200 $L.mol^{-1}.cm^{-1}$)(Nazeeruddin et al, 1993), λ= 535 nm (ε = 13600 $L.mol^{-1}.cm^{-1}$) (Xie and Guo, 2007).

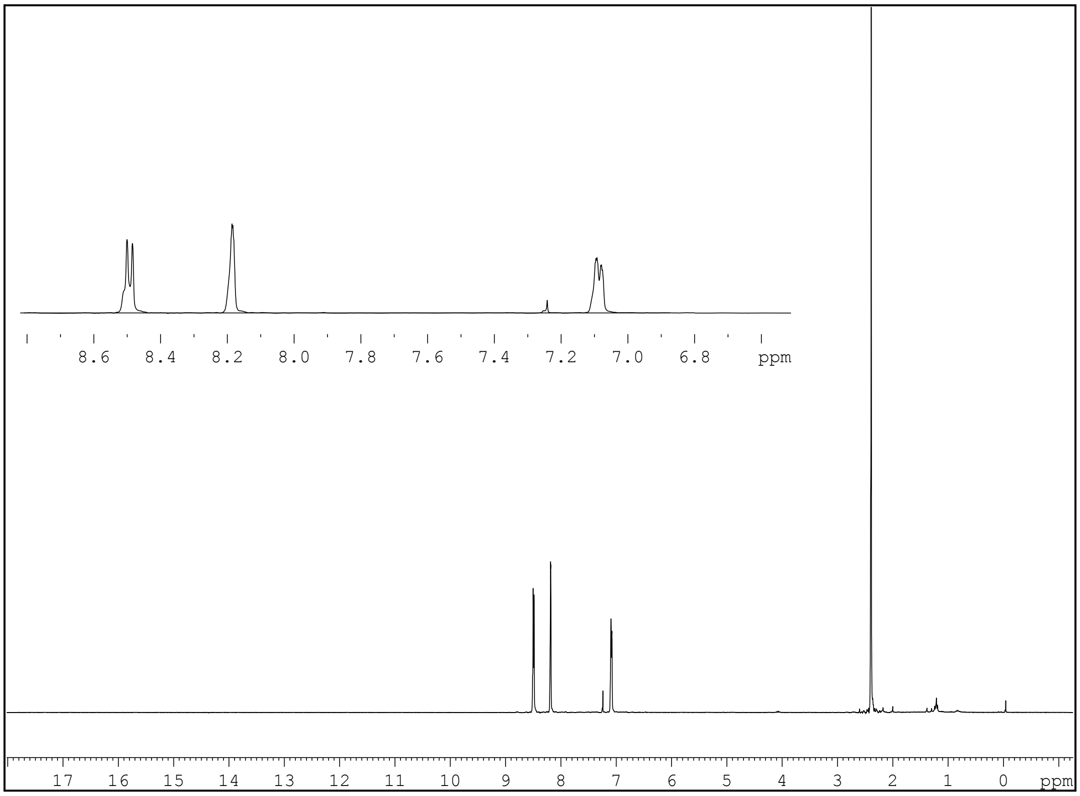


Figure 3.1: ^{1}H-NMR spectrum of 4,4`-dimethyl-2,2`-bipyridine **(I)** in $CDCl_3$

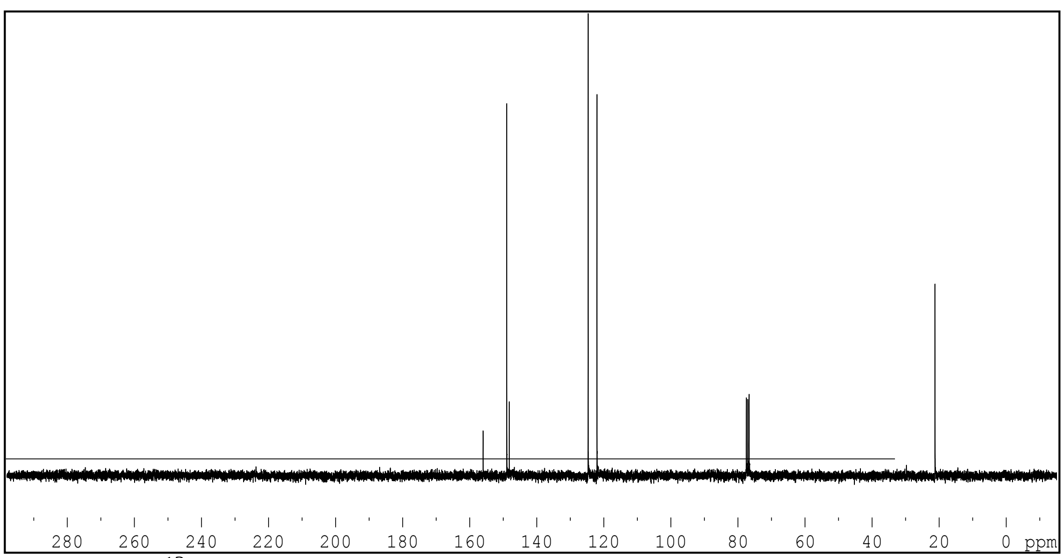


Figure 3.2: ^{13}C-NMR spectrum of 4,4`-dimethyl-2,2`-bipyridine in $CDCl_3$

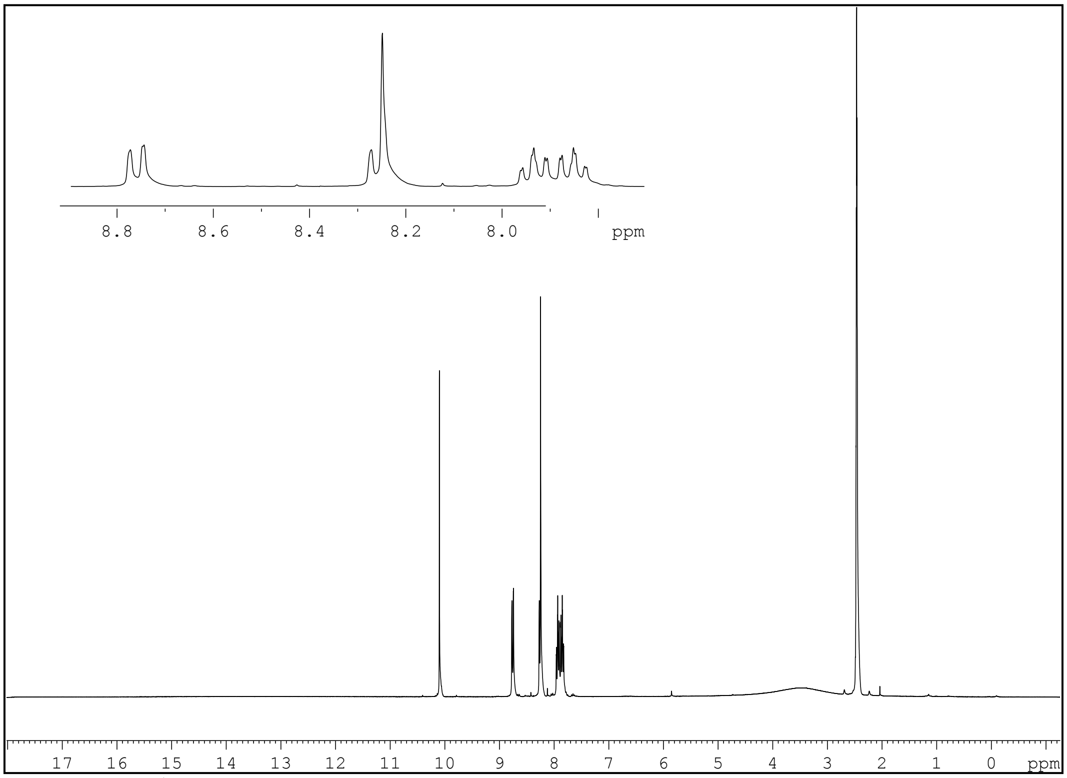


Figure 3.3: ^{1}H-NMR spectrum of 2-formyl-4-quinolinecarboxylic acid **(II)** in DMSO-d_6

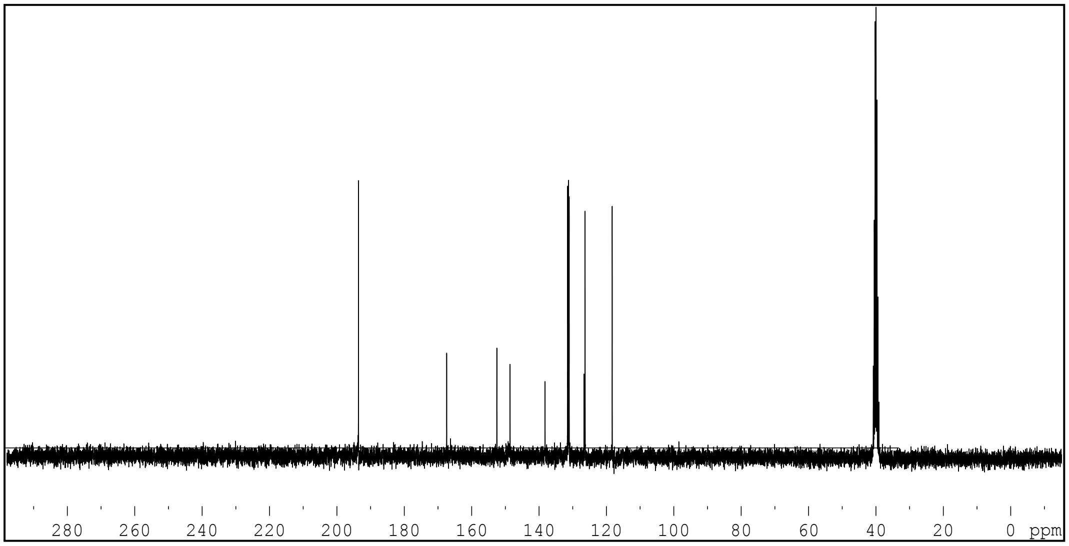


Figure 3.4: ^{13}C-NMR spectrum of 2-formyl-4-quinolinecarboxylic acid in DMSO-d_6

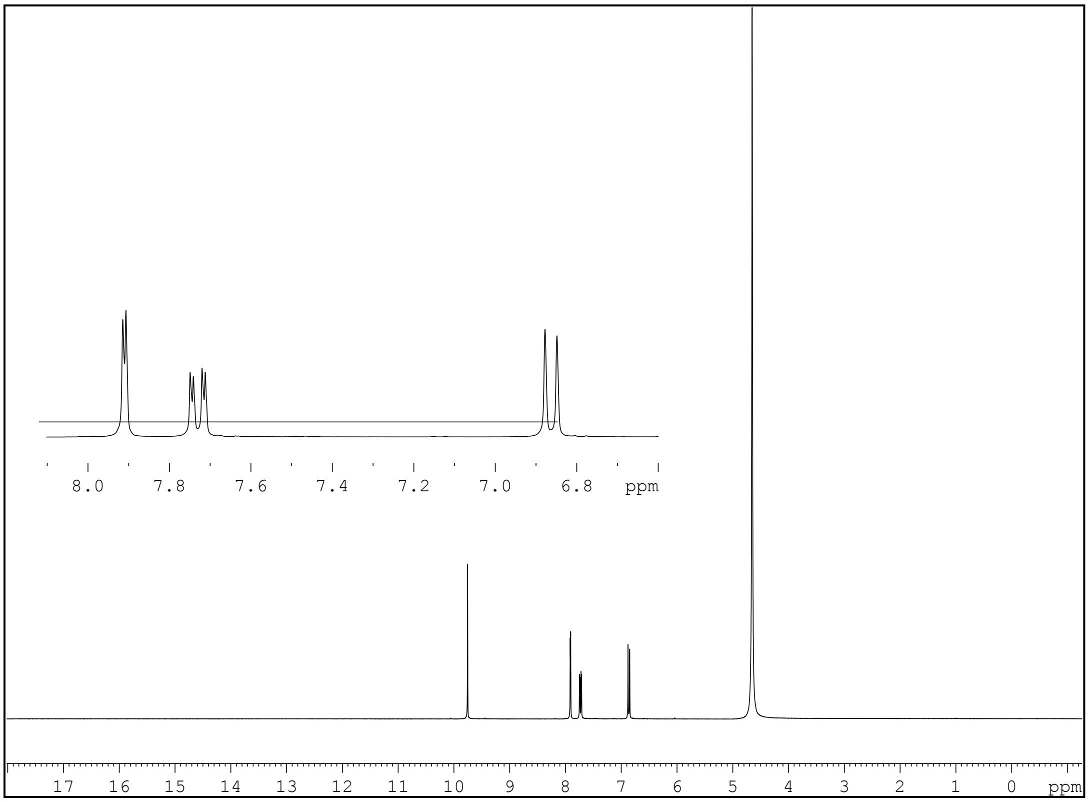


Figure 3.5: ^{1}H-NMR of sodium salt of Salicylaldehyde-5-sulfonic acid **(III)** in D_2O

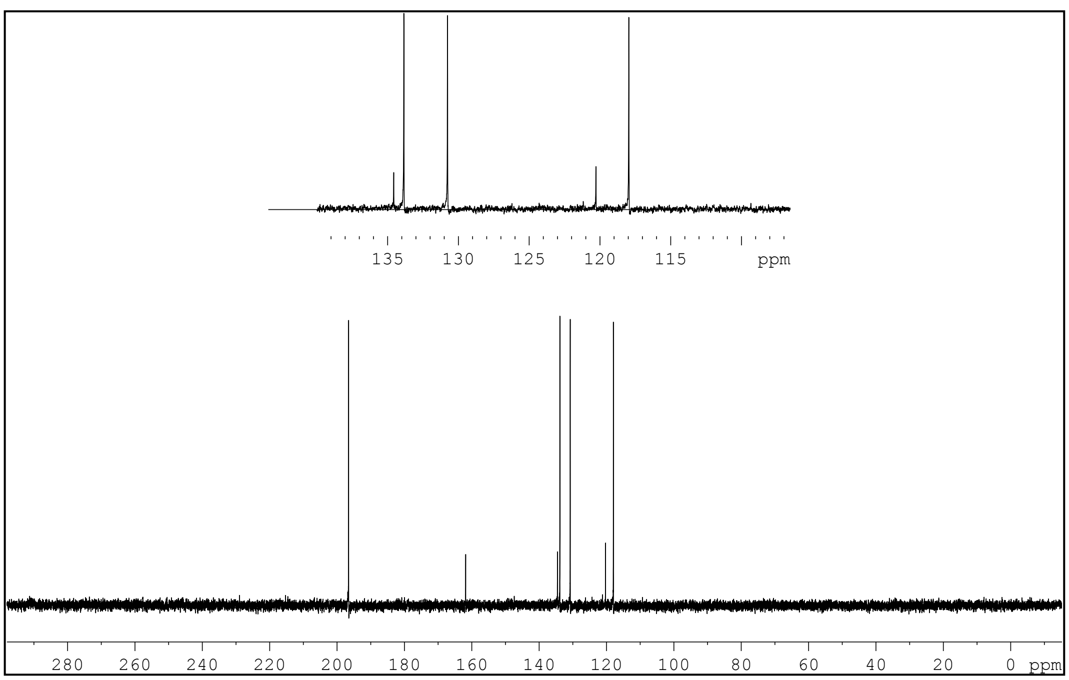


Figure 3.6: ^{13}C-NMR of sodium salt of Salicylaldehyde-5-sulfonic acid in D_2O

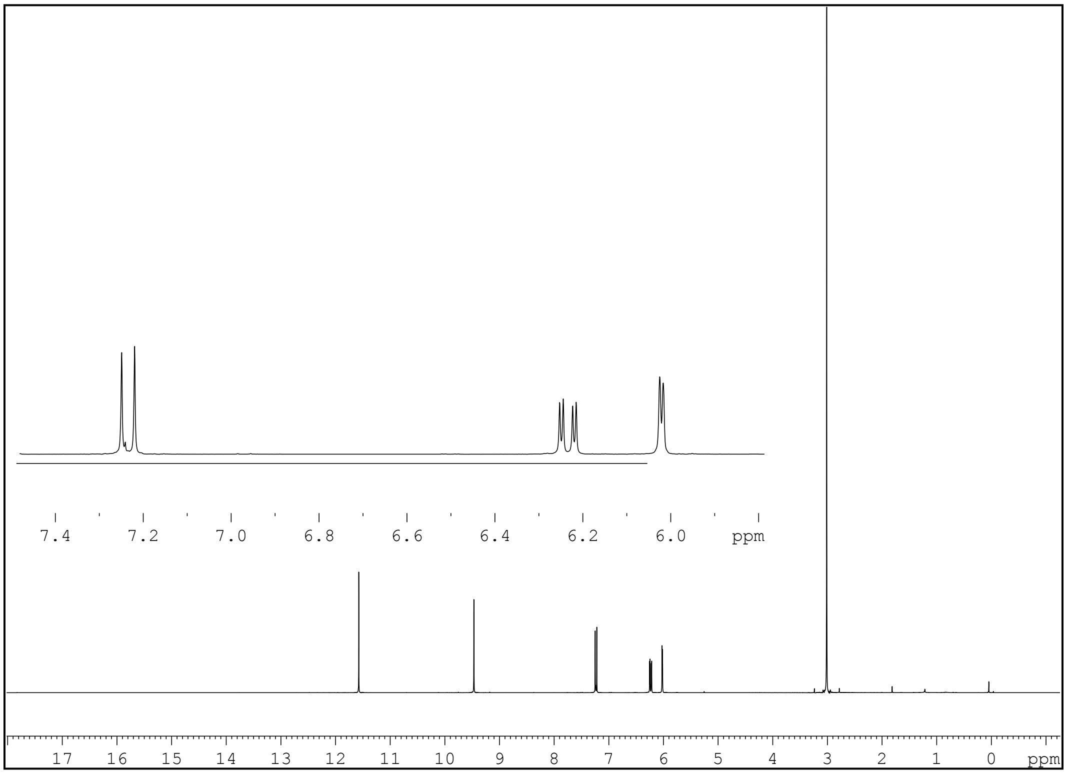


Figure 3.7: ^{1}H-NMR spectrum of 4-N,N-dimethylamino-2-hydroxybenzaldehyde **(VI)** in $CDCl_3$

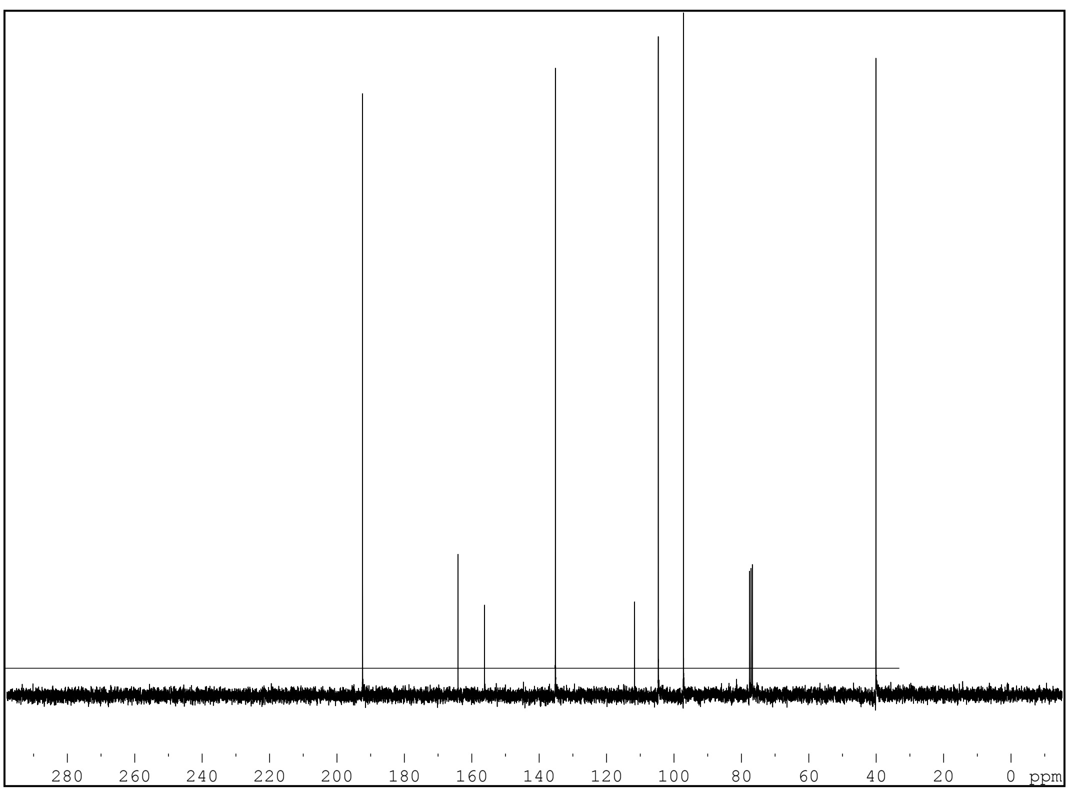


Figure 3.8: ^{13}C-NMR spectrum of 4-N,N-dimethylamino-2-hydroxybenzaldehyde in $CDCl_3$

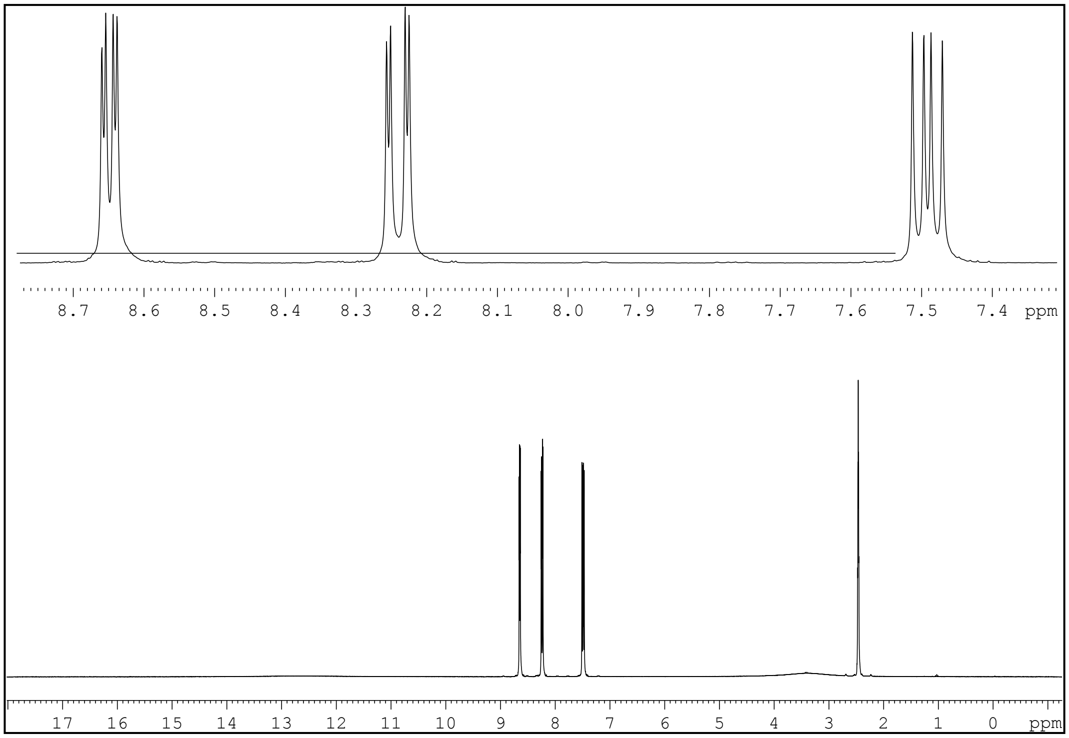


Figure 3.9: ^{1}H-NMR spectrum **(V)** in DMSO-d_6

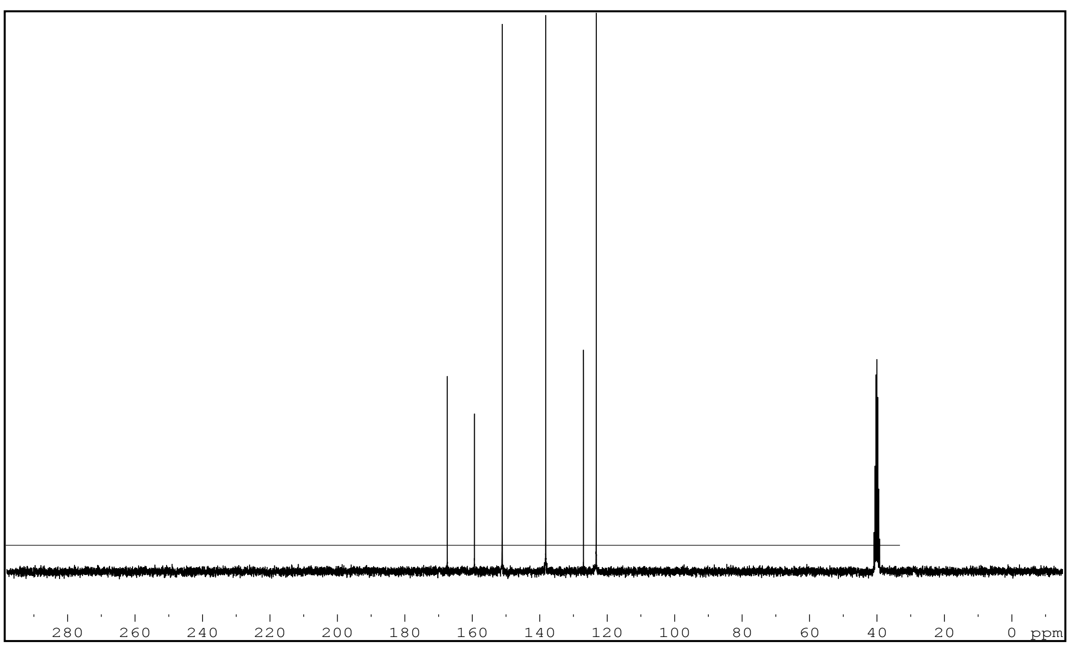


Figure 3.10: ^{13}C-NMR spectrum of **(V)** in DMSO-d_6

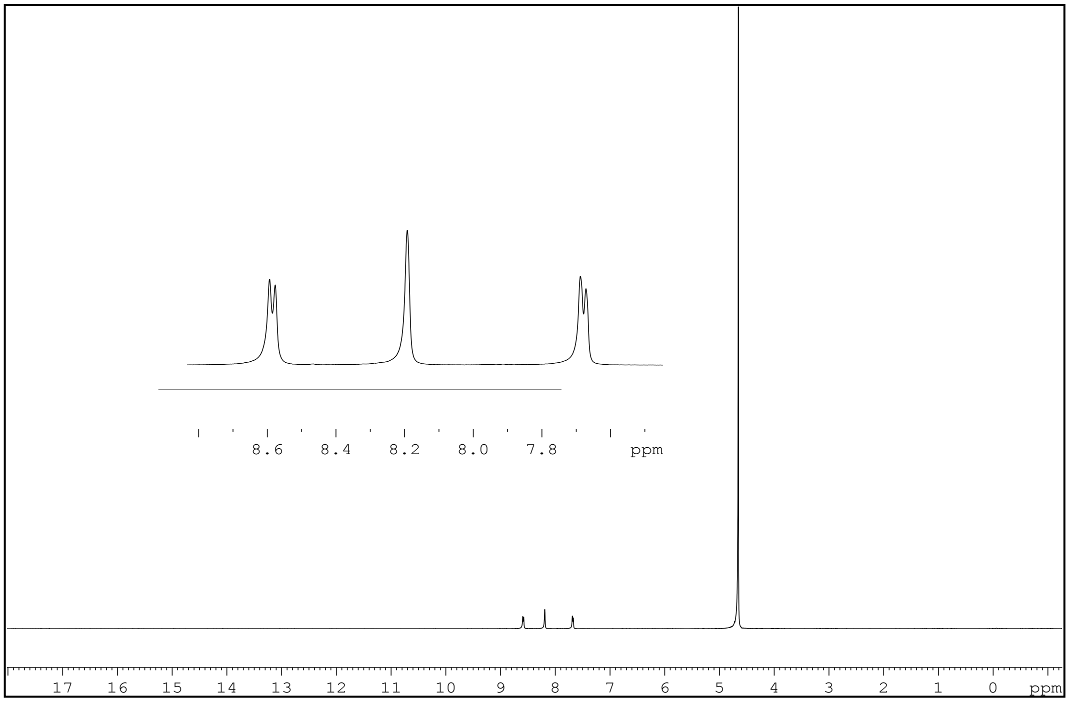


Figure 3.11: ^{1}H-NMR spectrum of sodium salt of **(VI)** in D_2O

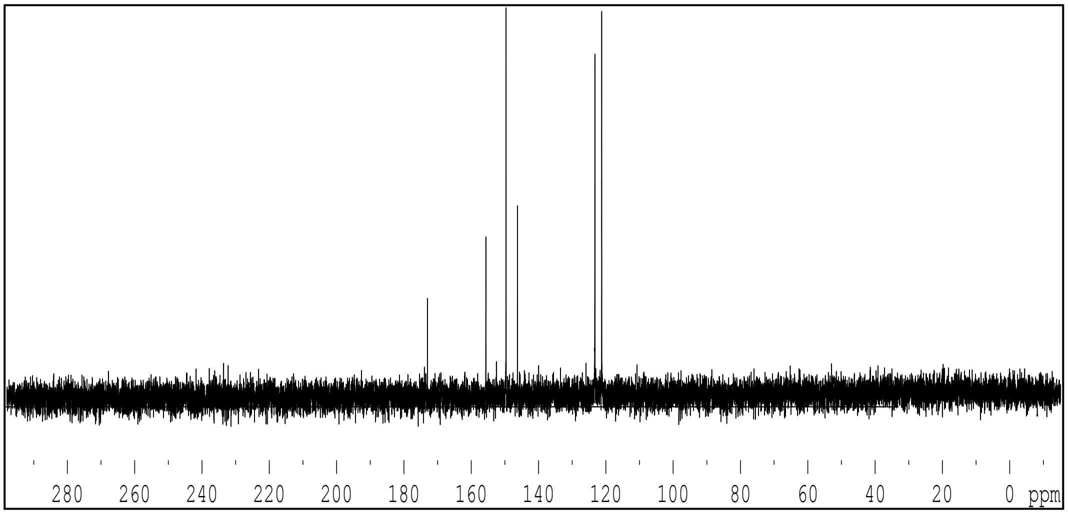


Figure 3.12: ^{13}C-NMR spectrum of sodium salt of **(VI)** in D_2O

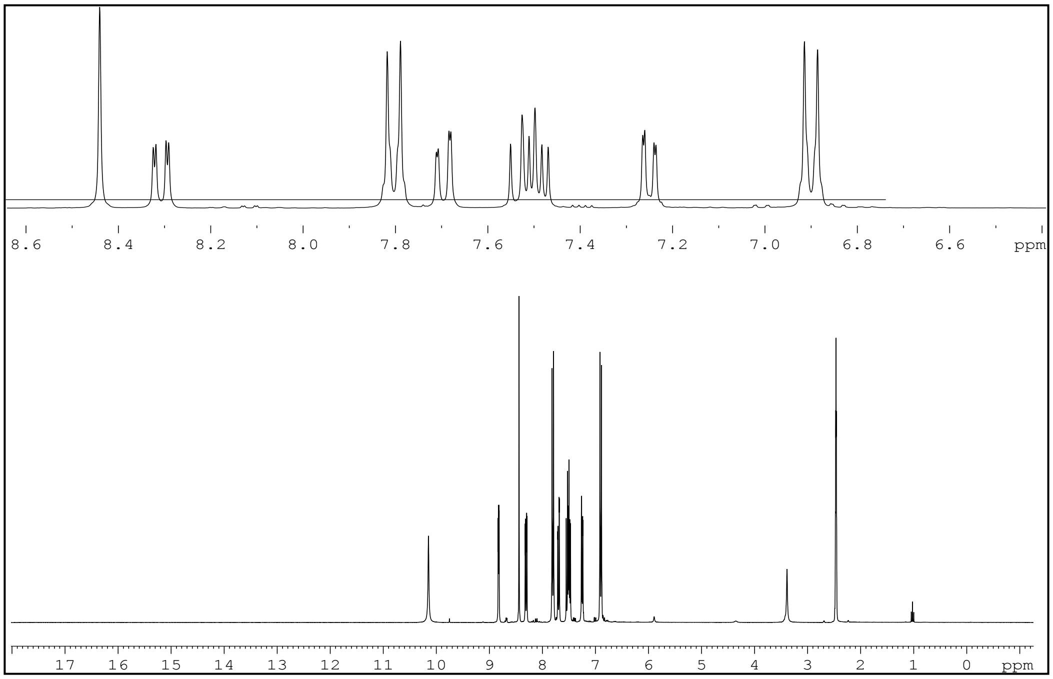


Figure 3.13: ^{1}H-NMR spectrum of **(VII)** in DMSO-d_6

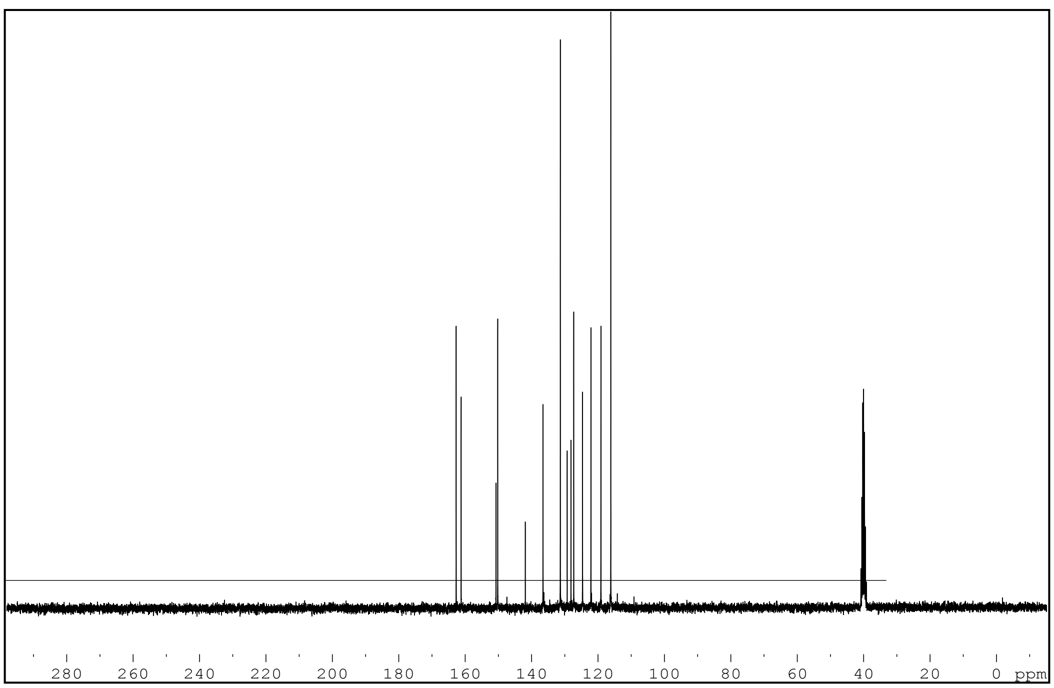


Figure 3.14: ^{13}C-NMR spectrum of **(VII)** in DMSO-d_6

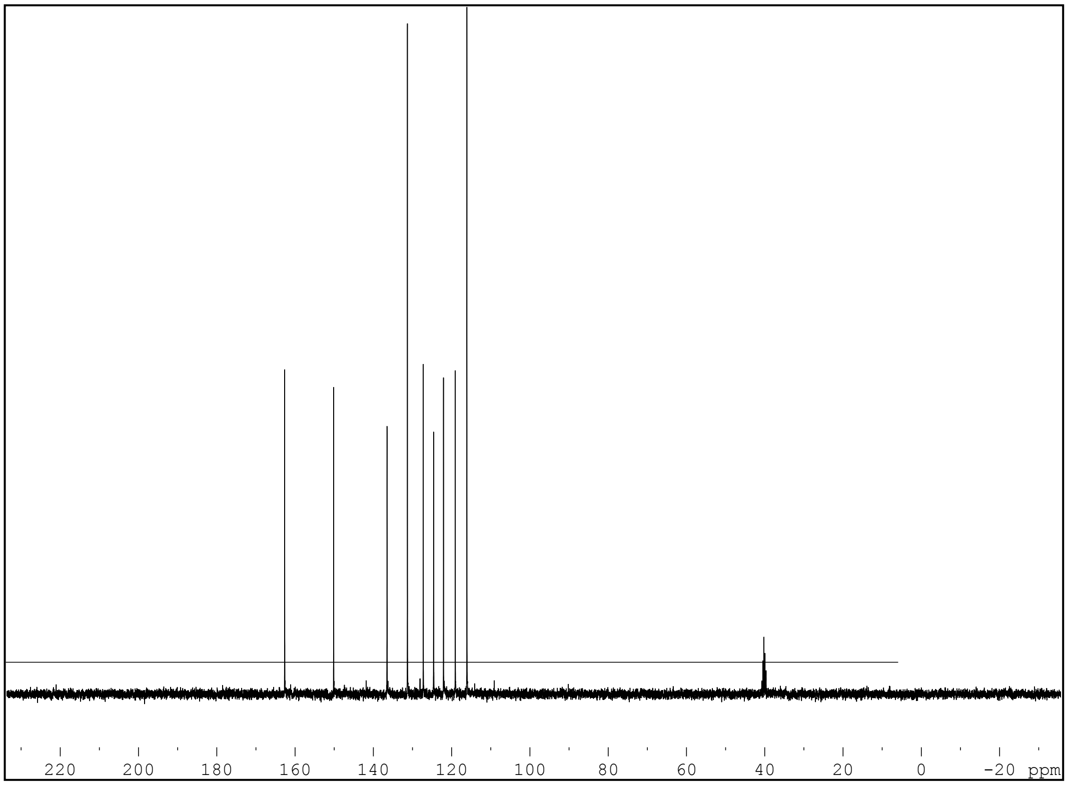


Figure 3.15: Dept-135 ^{13}C-NMR spectrum of **(VII)** in DMSO-d_6

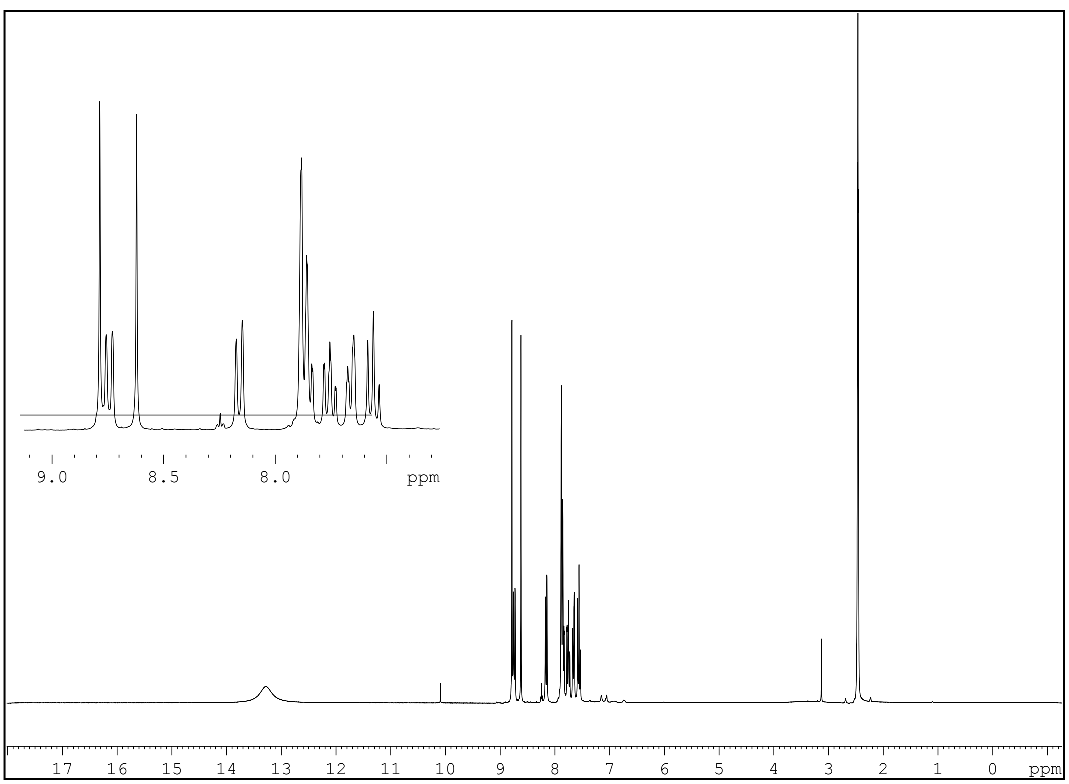


Figure 3.16: ^{1}H-NMR spectrum of **(IX)** in DMSO-d_6

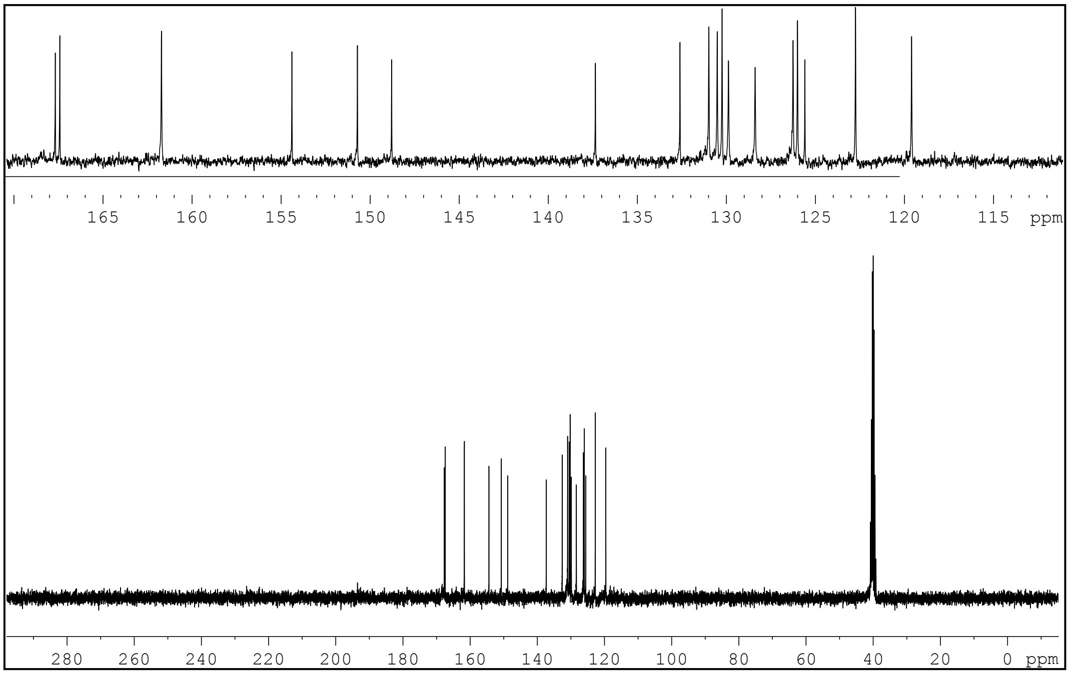


Figure 3.17: ^{13}C-NMR spectrum of **(IX)** in DMSO-d_6

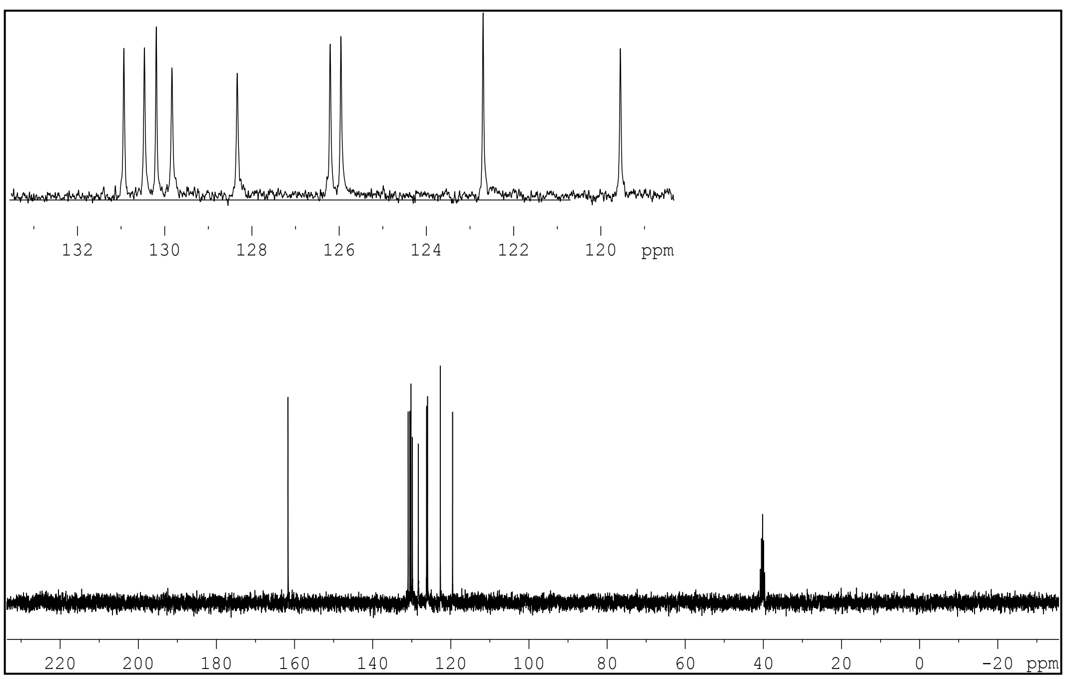


Figure 3.18: Dept-135 ^{13}C-NMR spectrum of **(IX)** in DMSO-d_6

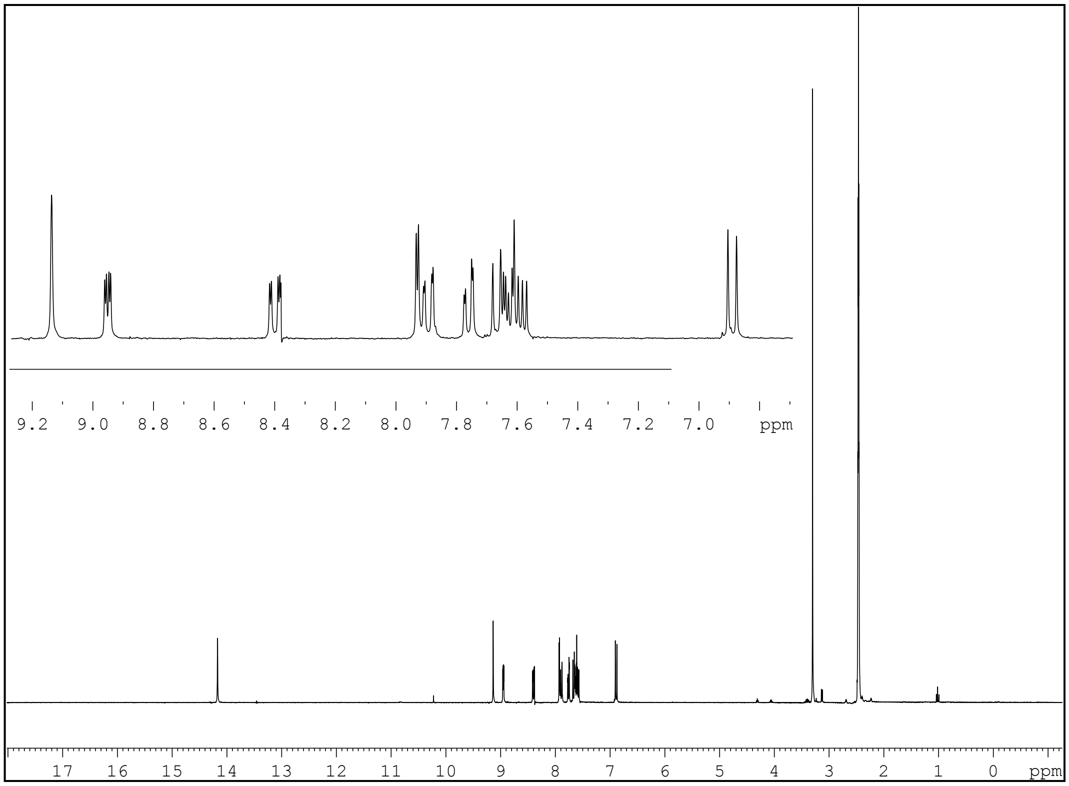


Figure 3.19: ^{1}H-NMR spectrum of **(VIII)** in DMSO-d_6

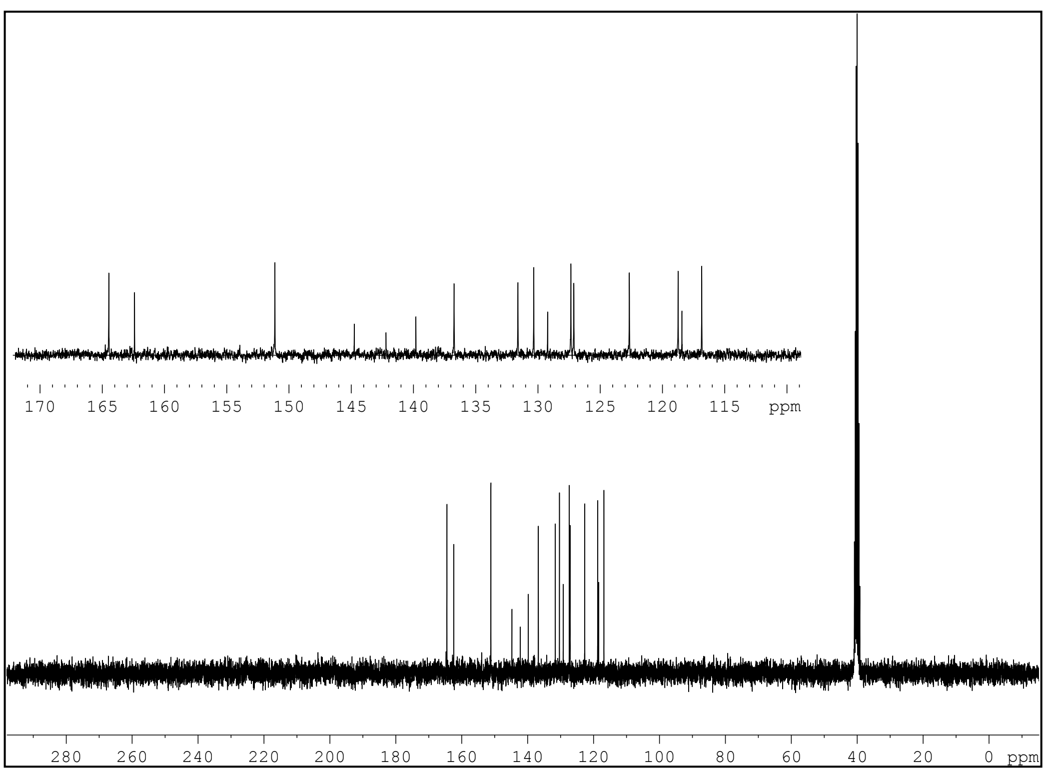


Figure 3.20: ^{13}C-NMR spectrum of **(VIII)** in DMSO-d_6

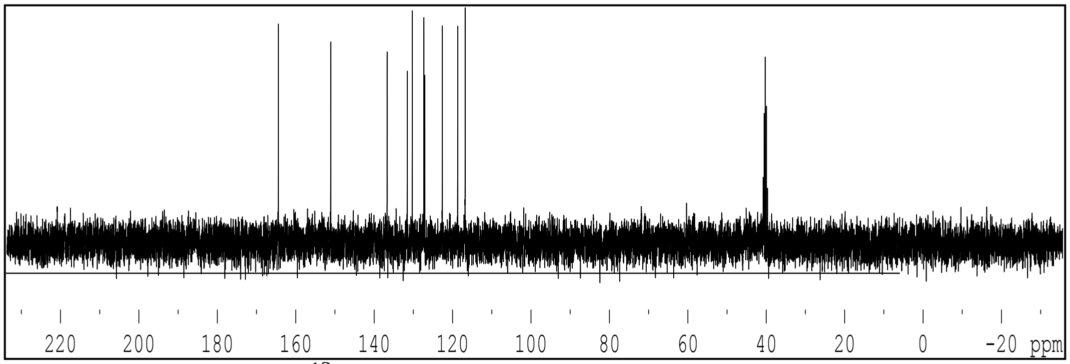


Figure 3.21: Dept-135 ^{13}C-NMR spectrum of **(VIII)** in DMSO-d_6

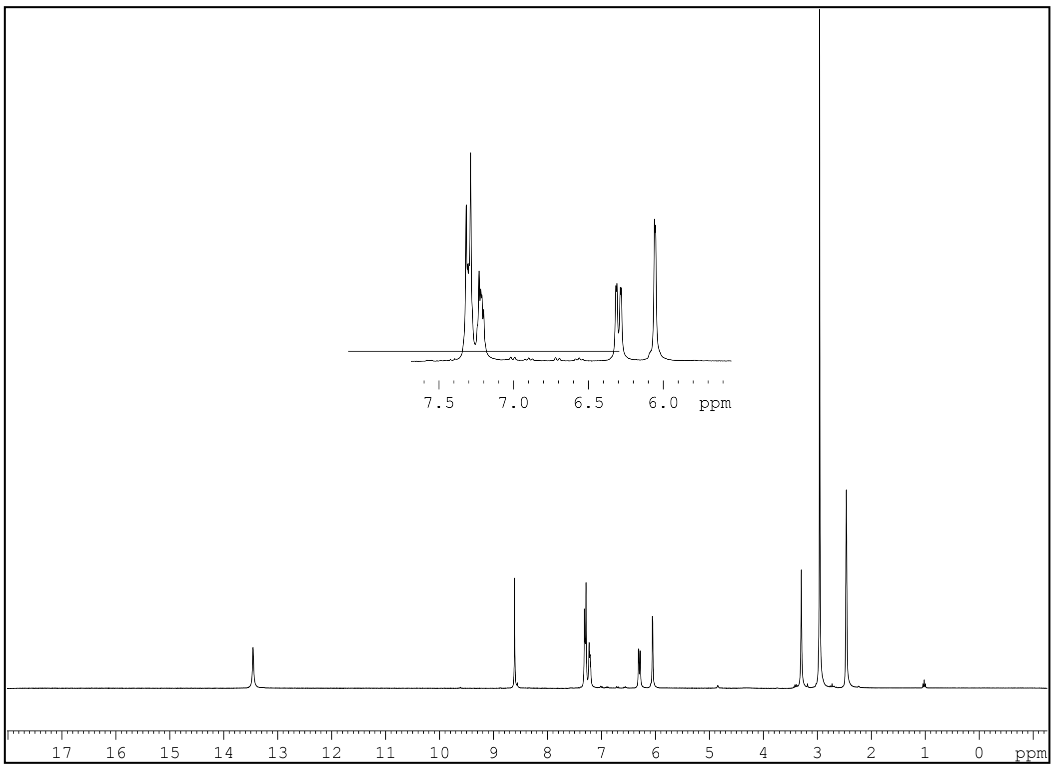


Figure 3.22: ^{1}H-NMR spectrum of **(X)** in DMSO-d_6

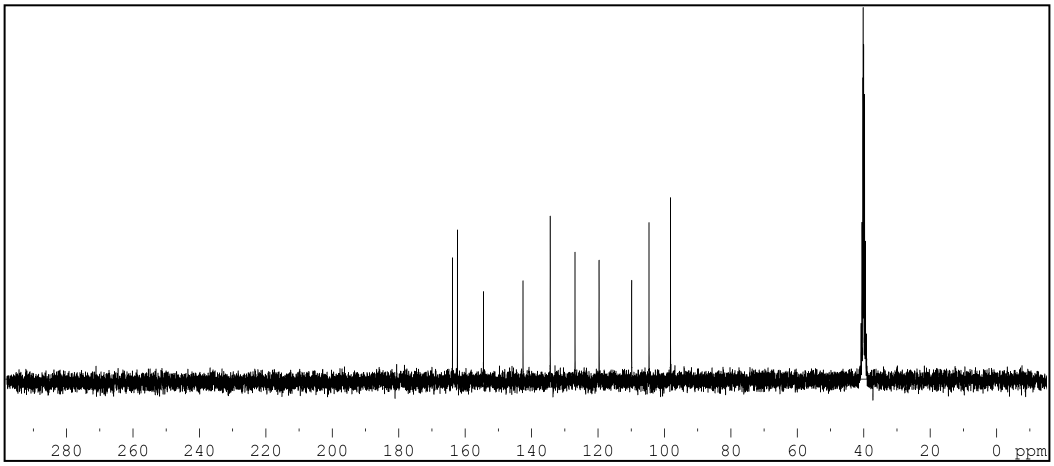


Figure 3.23: ^{13}C-NMR spectrum of **(X)** in DMSO-d_6

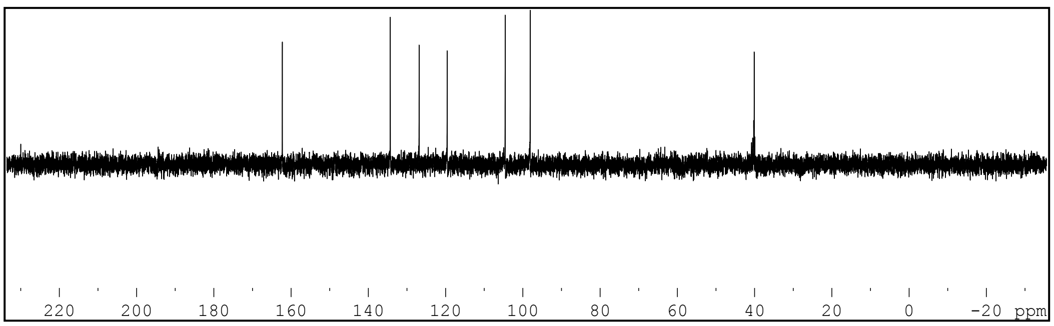


Figure 3.24: Dept-135 ^{13}C-NMR spectrum of **(X)** in DMSO-d_6

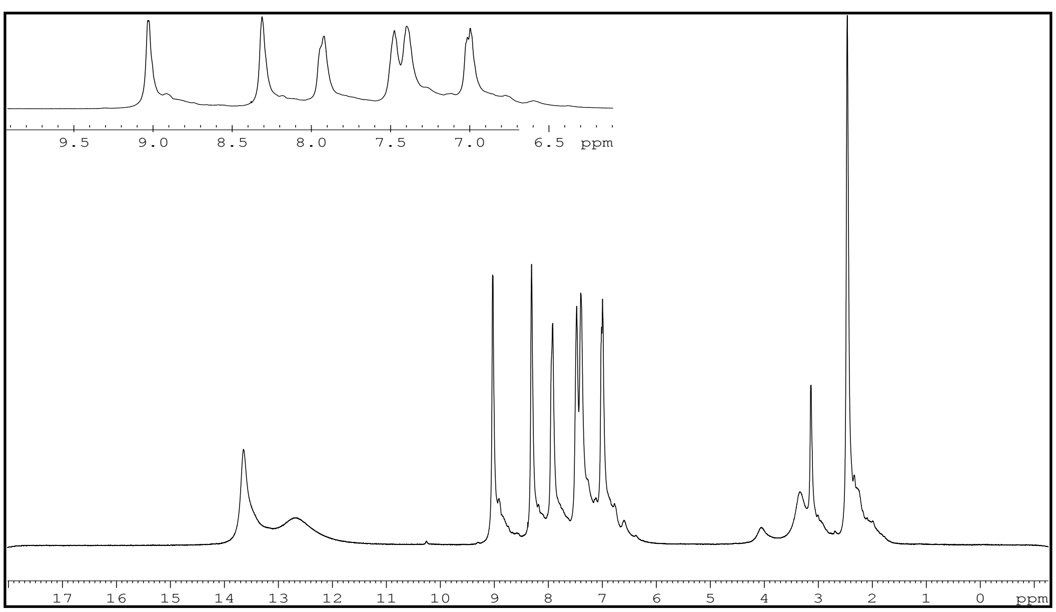


Figure 3.25: ^{1}H-NMR spectrum of **(XI)** in DMSO-d_6

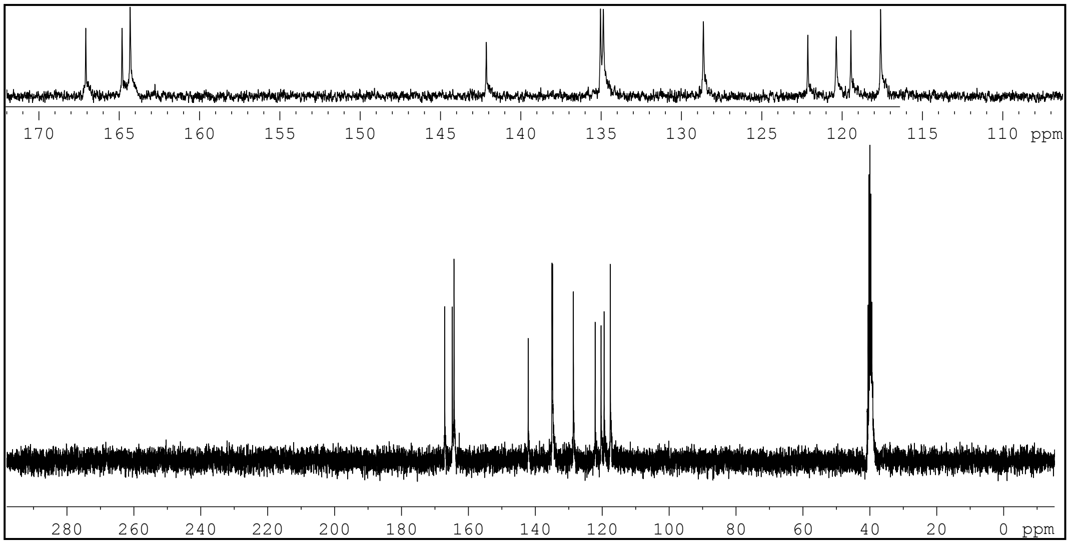


Figure 3.26: ^{13}C-NMR spectrum of **(XI)** in DMSO-d_6

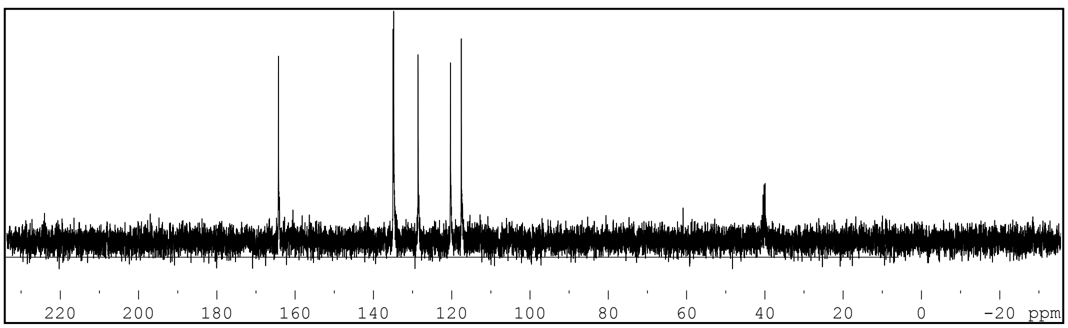


Figure 3.27: Dept-135 ^{13}C-NMR spectrum of **(XI)** in DMSO-d_6

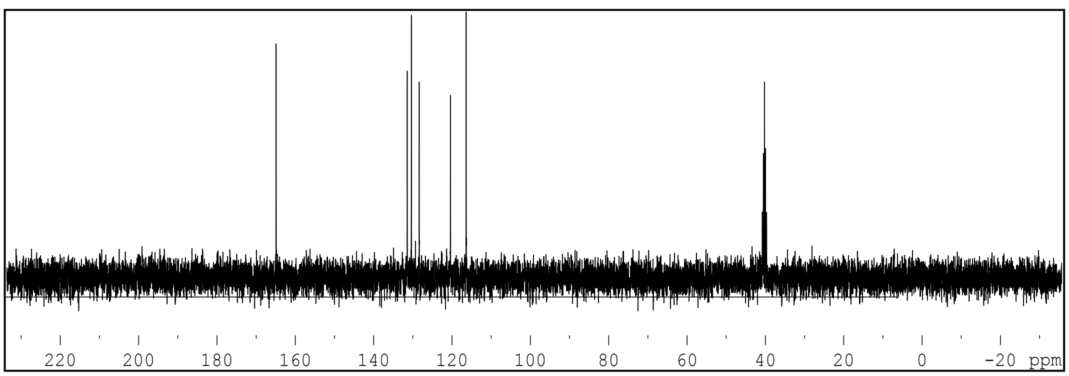


Figure 3.28: Dept-135 ^{13}C-NMR spectrum of **(XII)** in DMSO-d_6

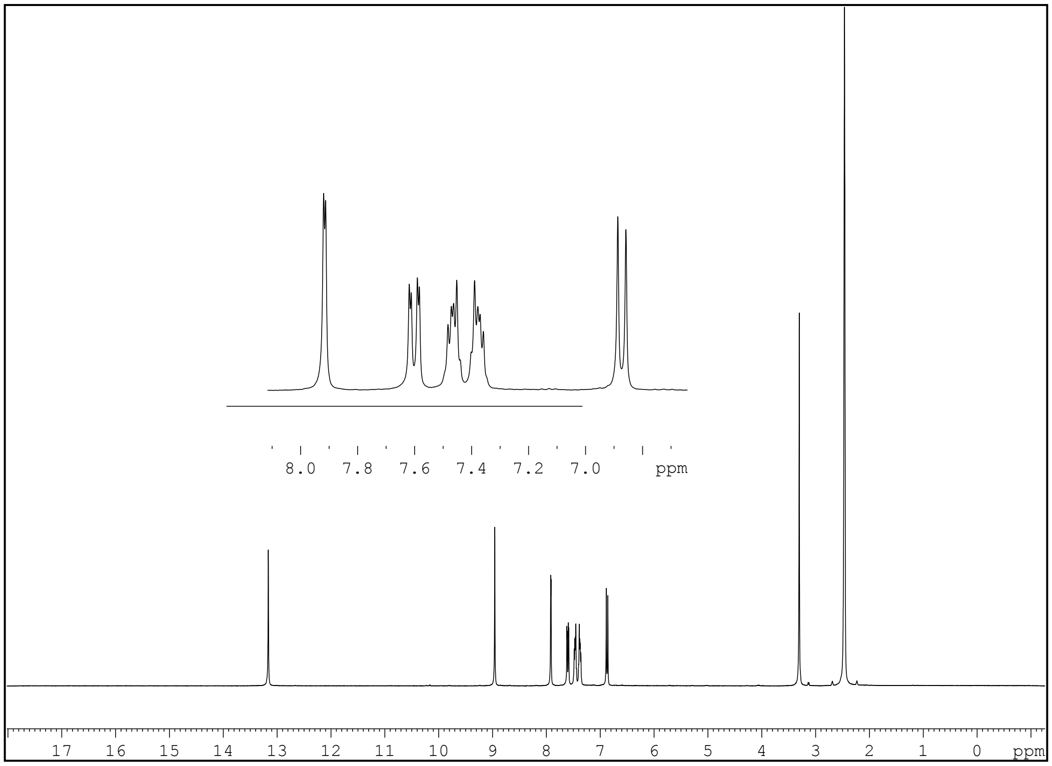


Figure 3.29: ^{1}H-NMR spectrum of **(XII)** in DMSO-d_6

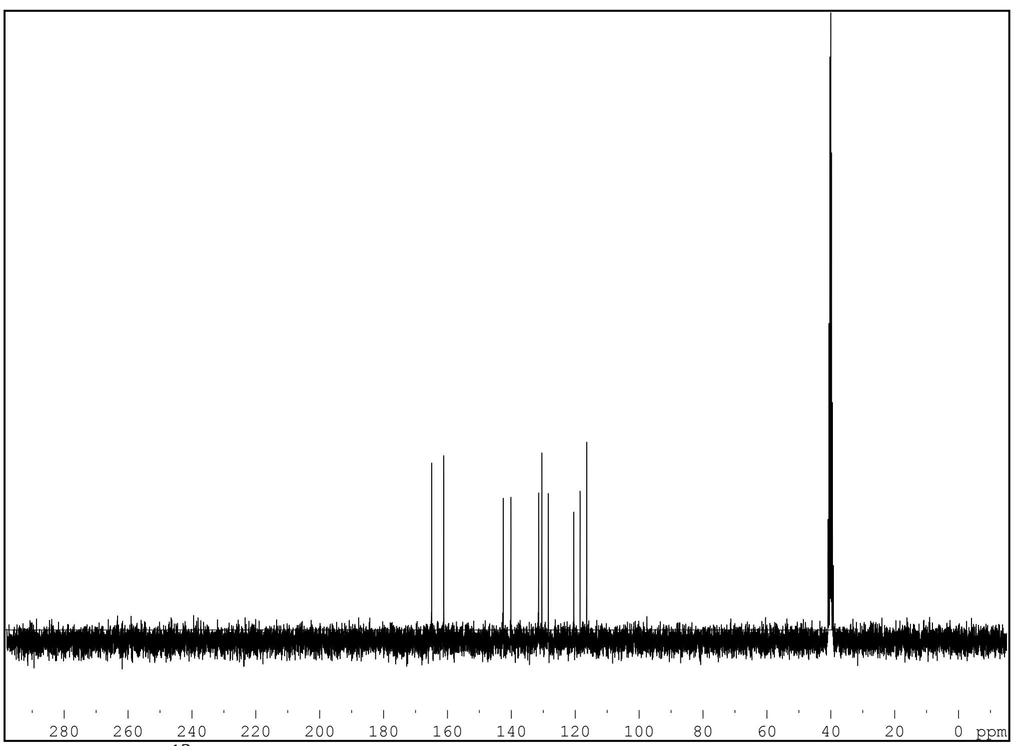


Figure 3.30: ^{13}C-NMR spectrum of **(XII)** in DMSO-d_6

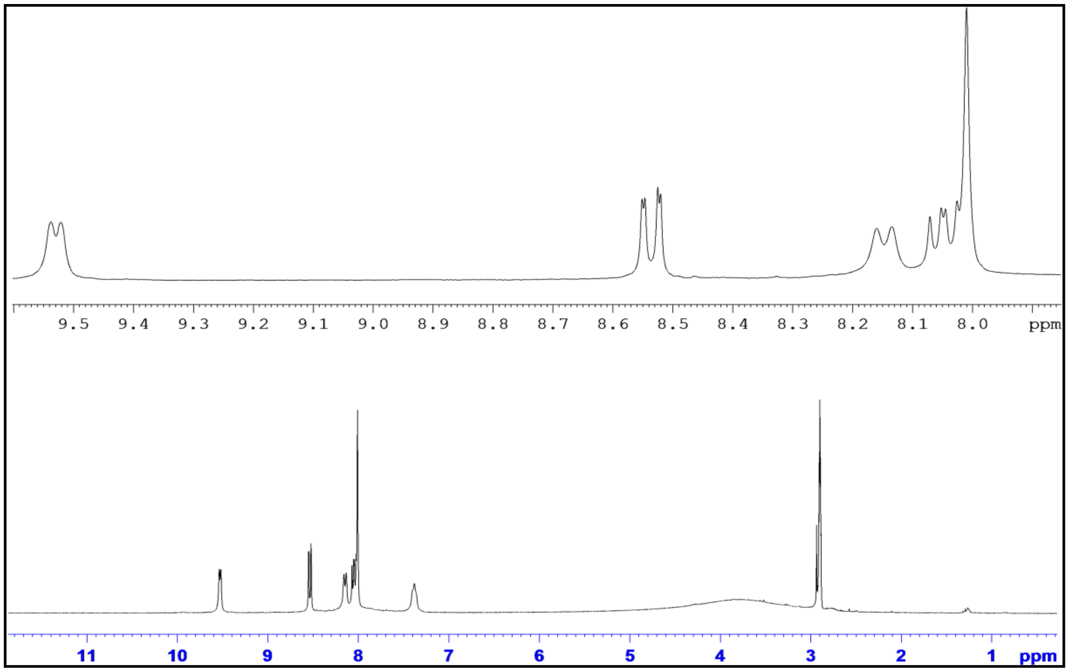


Figure 3.31: [1]H-NMR spectrum of $Ru(V)_2(NCS)_2$ in DMF

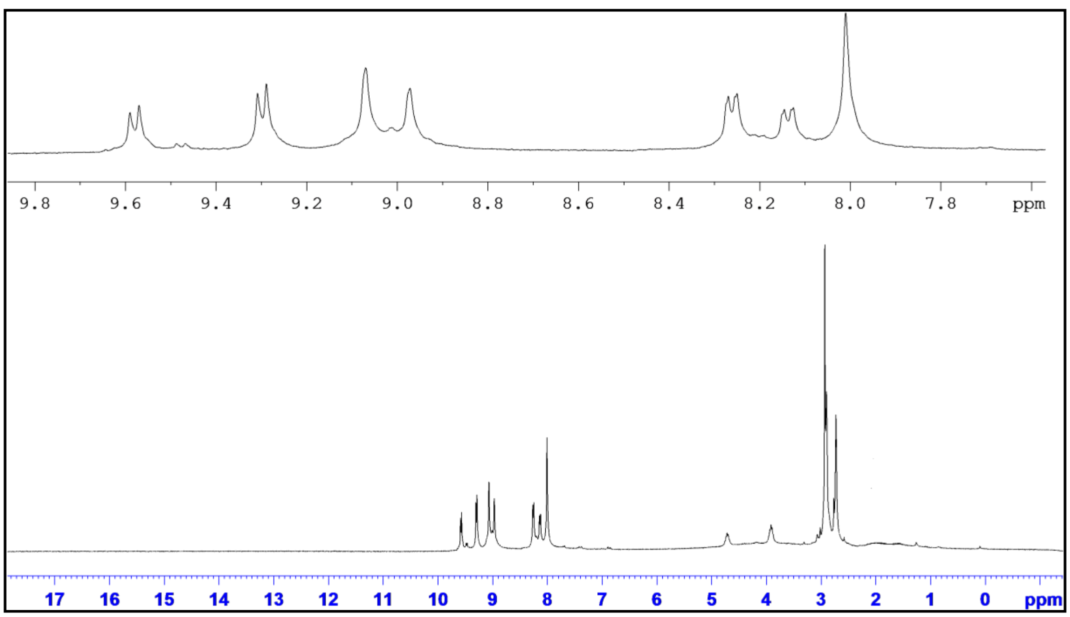


Figure 3.32: [1]H-NMR spectrum of $Ru(VI)_2(NCS)_2$ in DMF

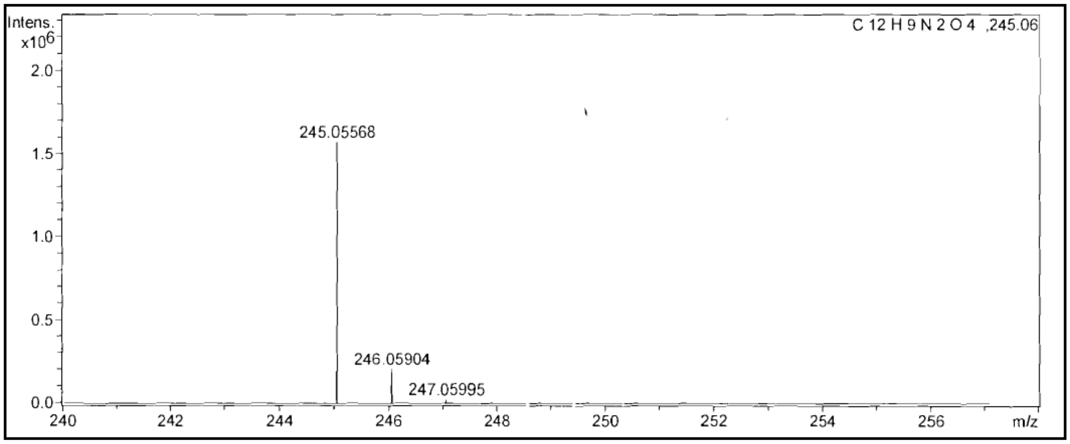


Figure 3.33: Mass spectrum of **(V)**

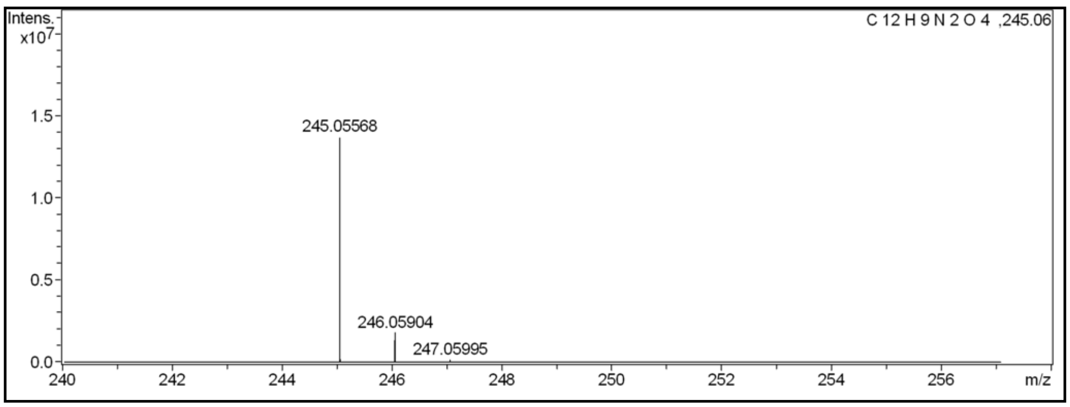


Figure 3.34: Mass spectrum of **(VI)**

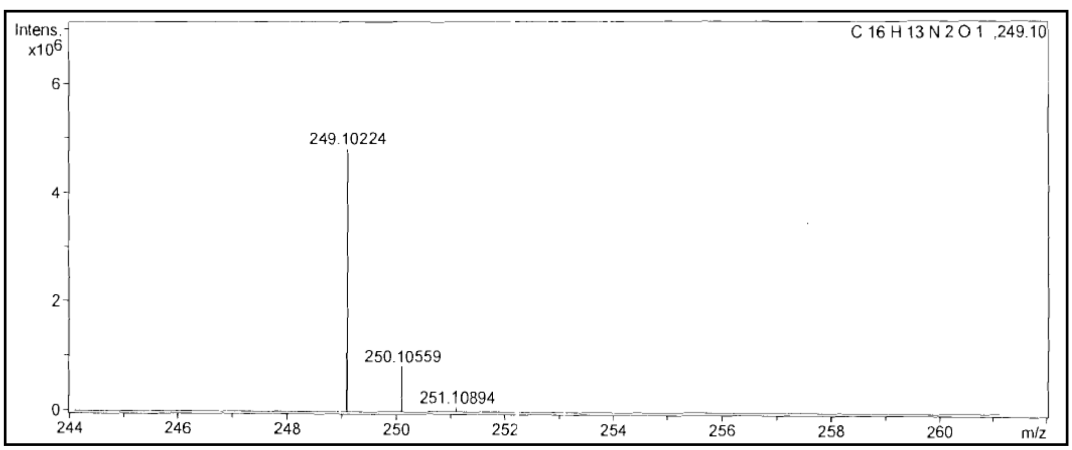


Figure 3.35: Mass spectrum of **(VII)** Schiff base ligand

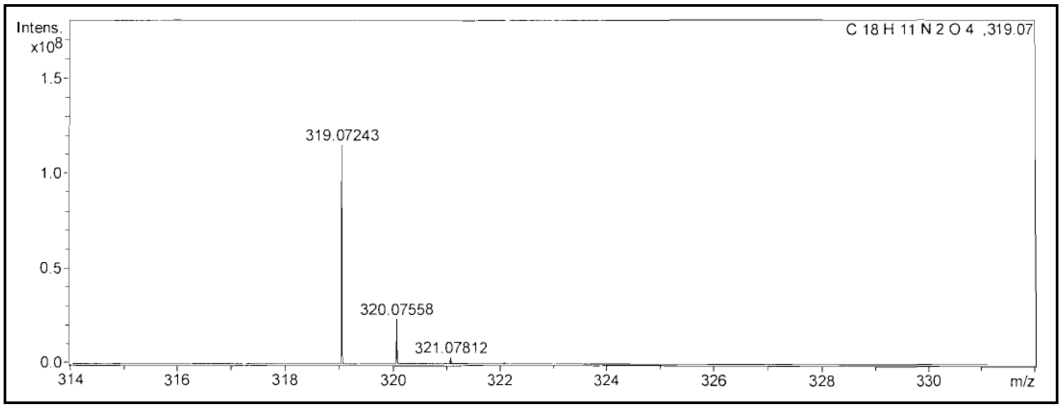


Figure 3.36: Mass spectrum of **(IX)** Schiff base ligand

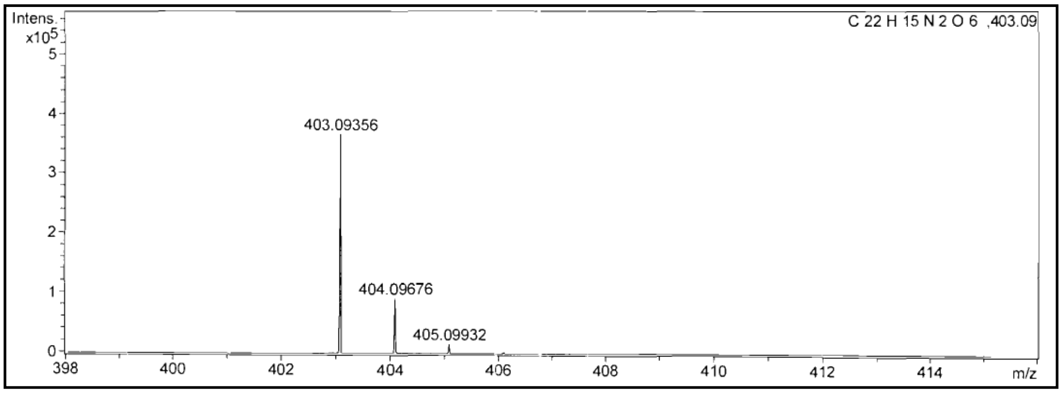


Figure 3.37: Mass spectrum of **(X)** Schiff base ligand

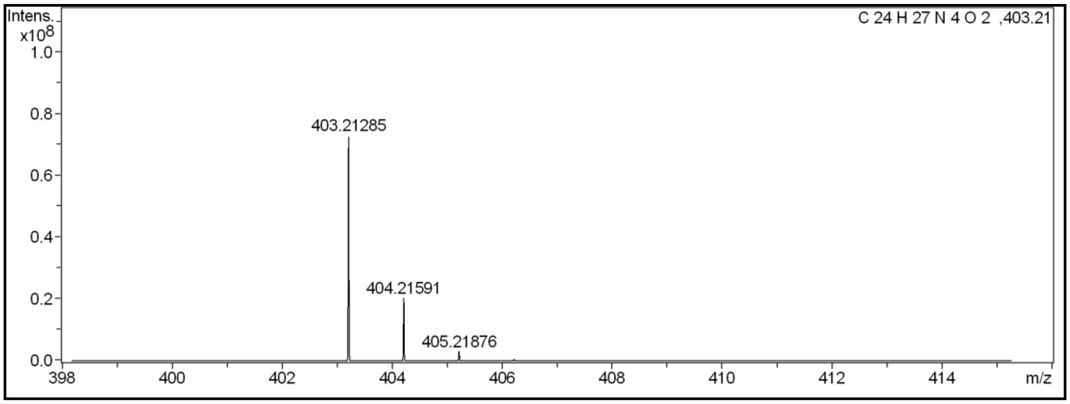


Figure 3.38: Mass spectrum of **(XI)** Schiff base ligand

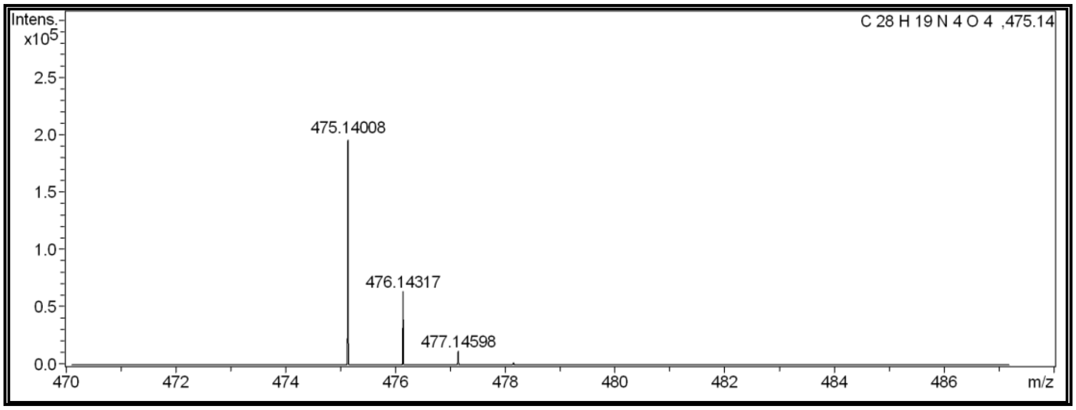


Figure 3.39: Mass spectrum of **(XIII)** Schiff base ligand

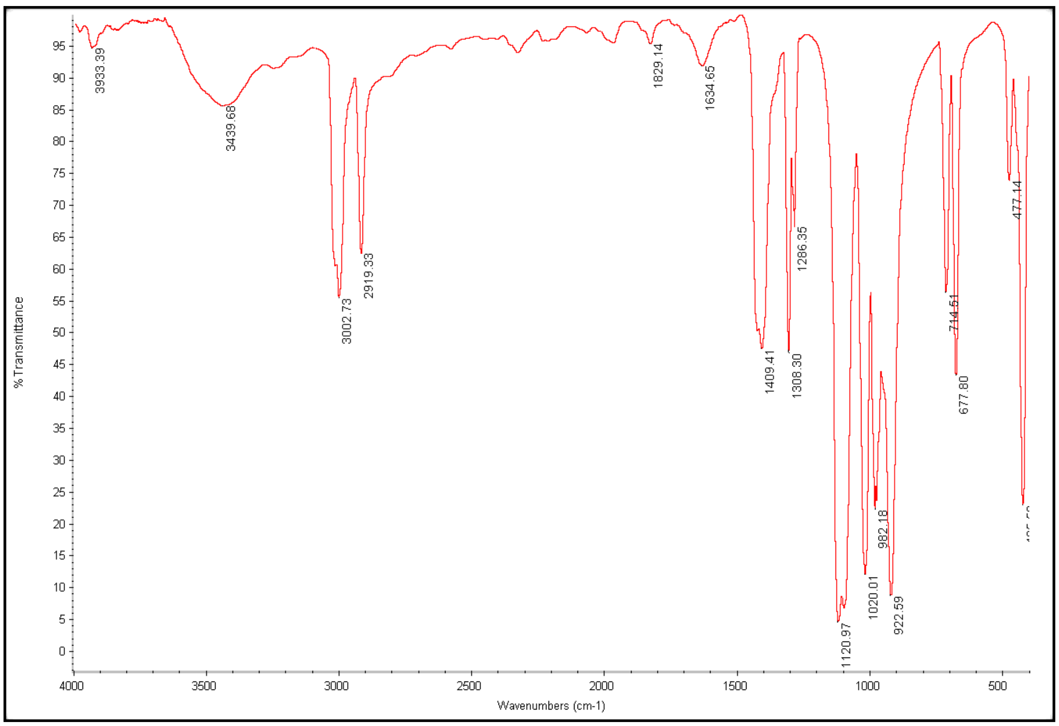


Figure 3.40: FT-IR spectrum of $RuCl_2(DMSO)_4$

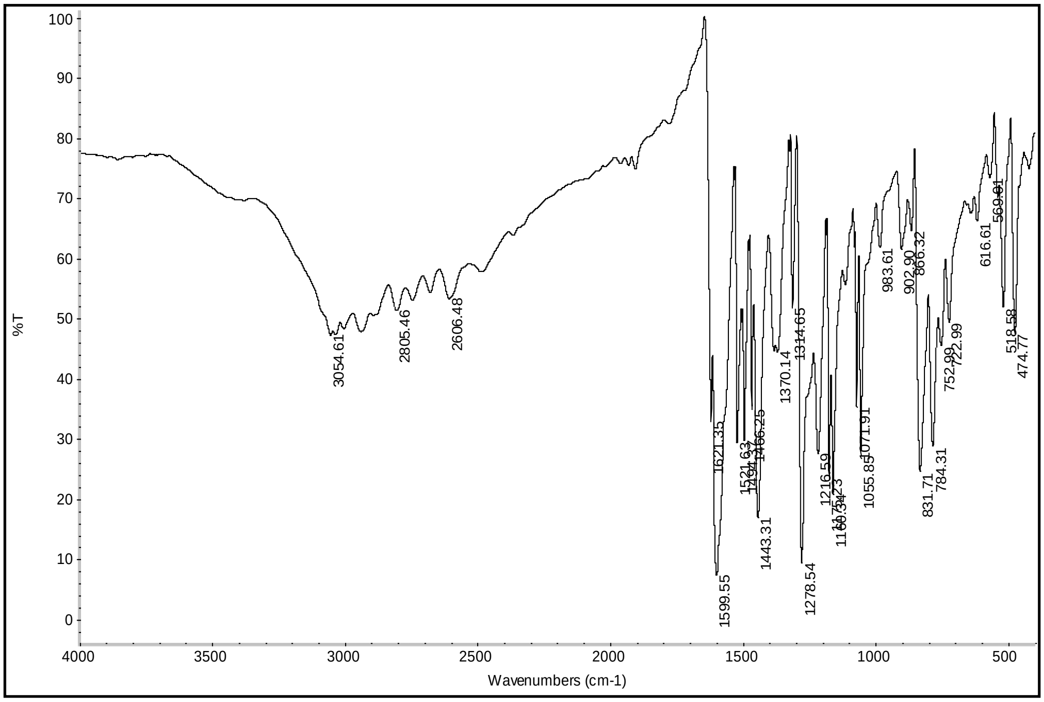


Figure 3.41: FT-IR spectrum of **(VII)**

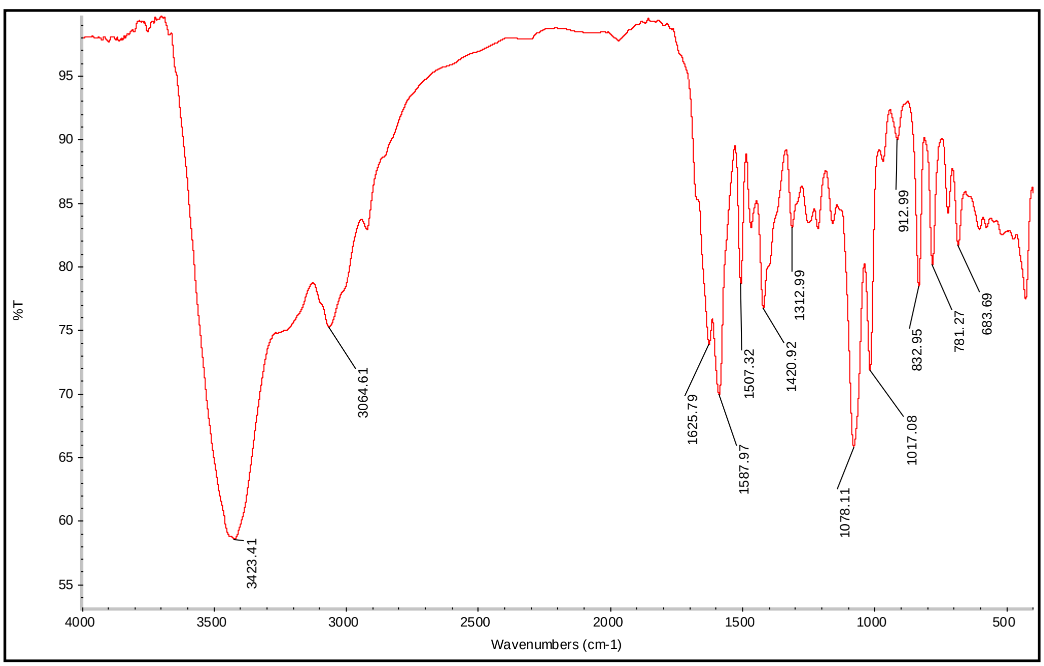


Figure 3.42: FT-IR spectrum of [Ru(VII)(AQ)Cl_2].5H_2O

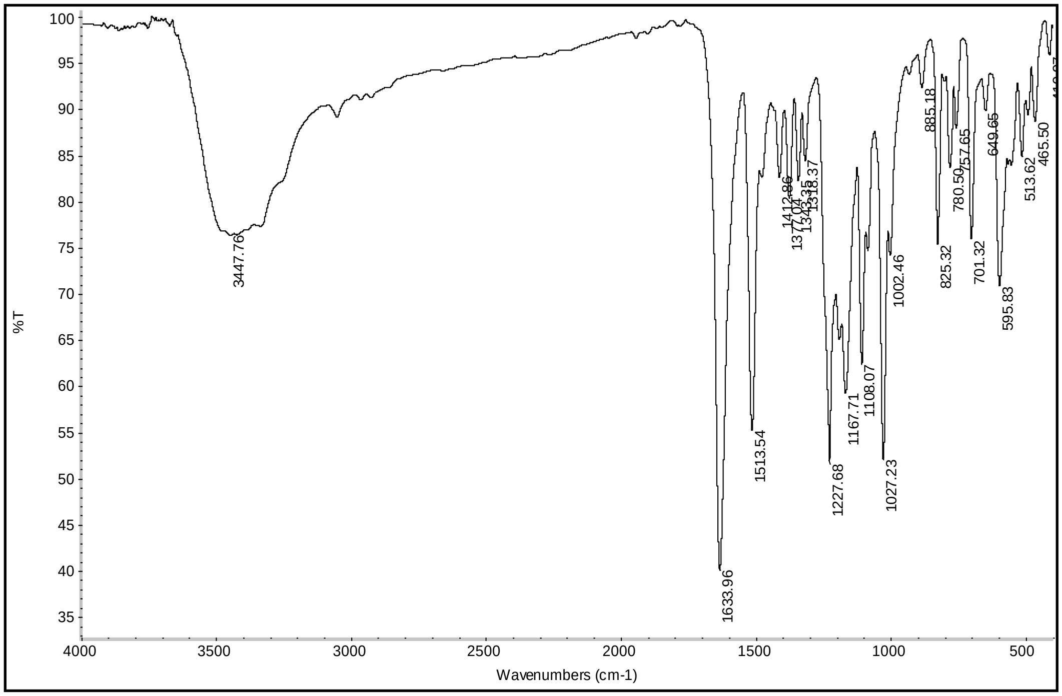


Figure 3.43: FT-IR spectrum of **(VIII)**

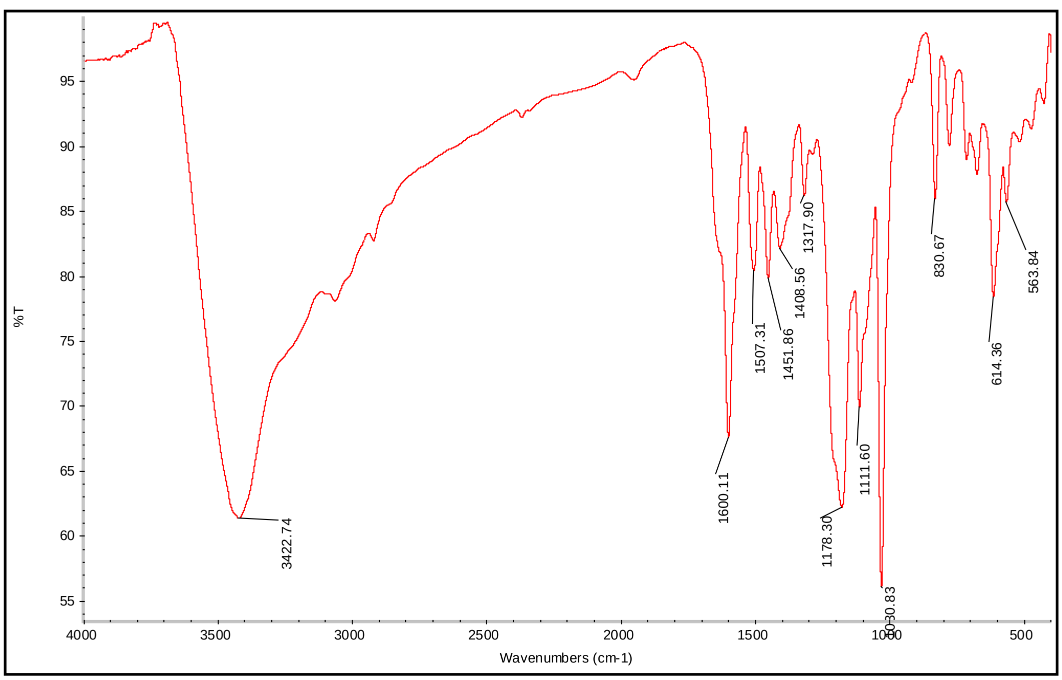


Figure 3.44: FT-IR spectrum of $[Ru(VIII\text{-}H)_2].4H_2O$

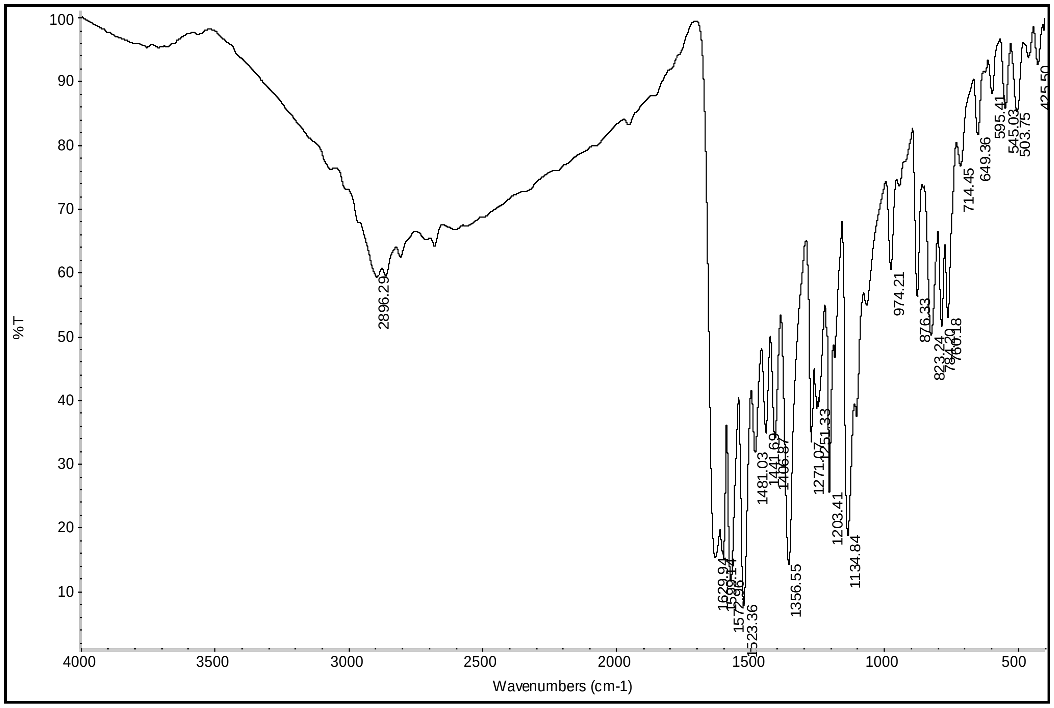


Figure 3.45: FT-IR spectrum of **(X)**

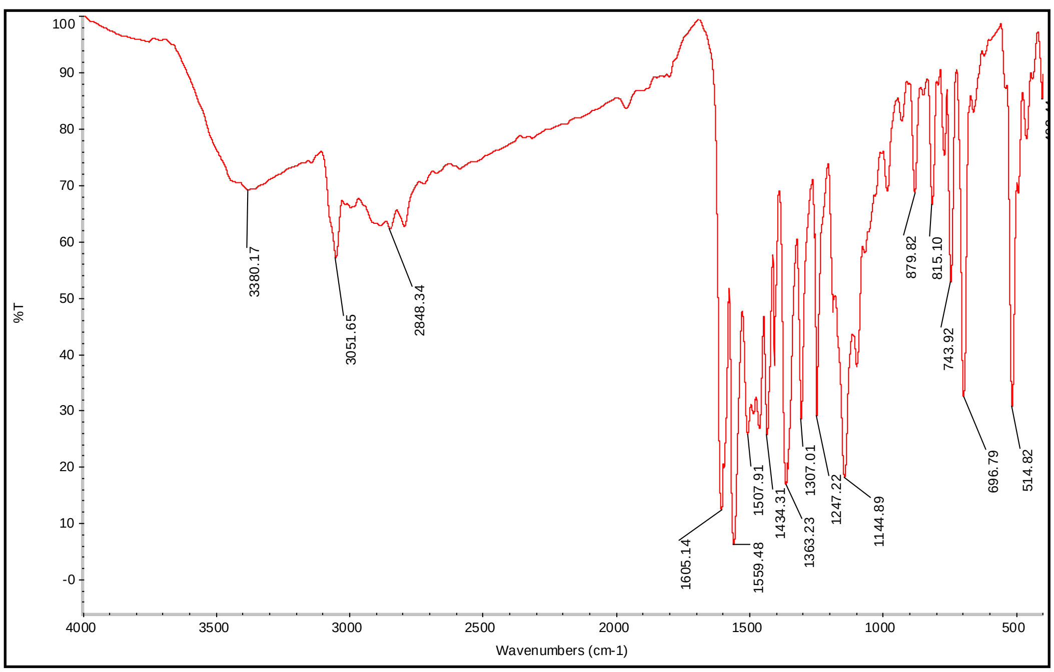


Figure 3.46: FT-IR spectrum of $[Ru(X\text{-}2H)(PPh_3)(H_2O)].3H_2O$

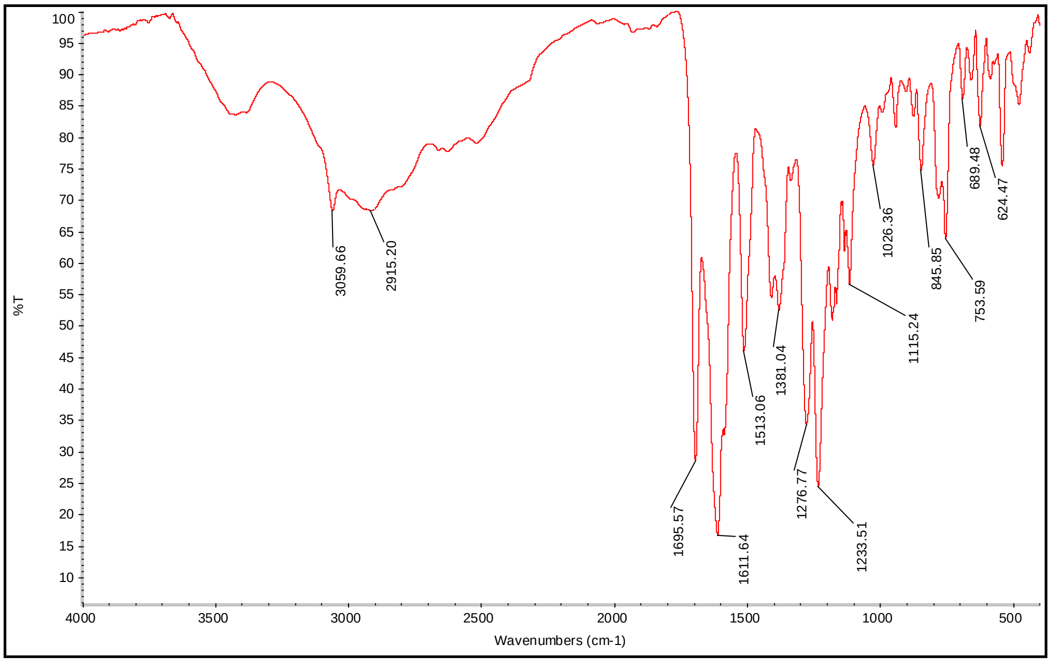


Figure 3.47: FT-IR spectrum of **(XI)**

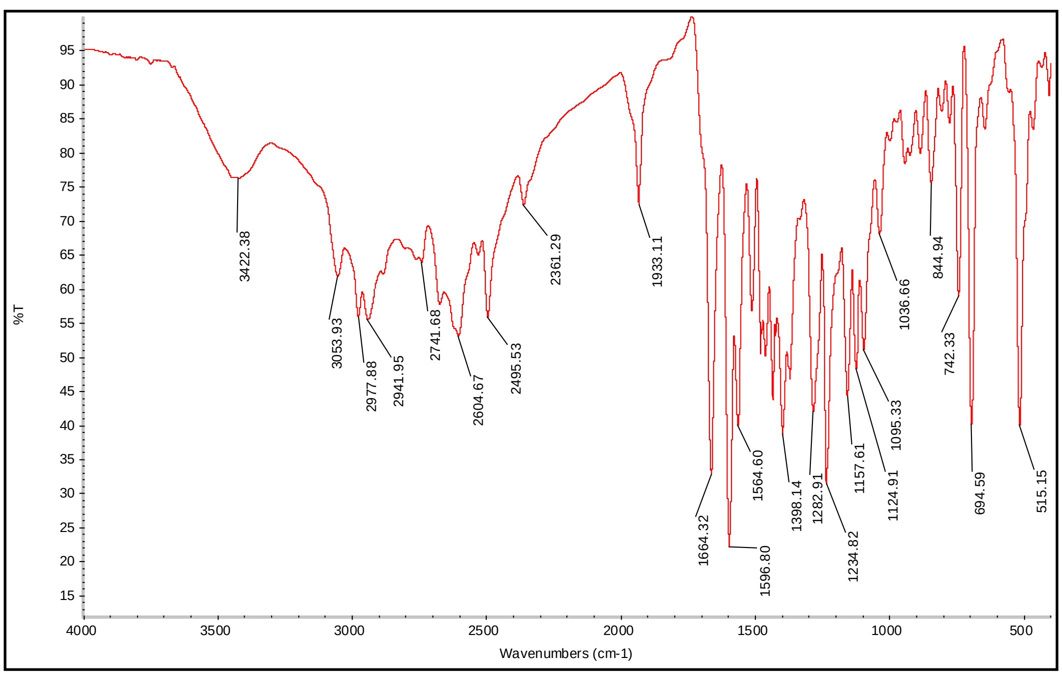


Figure 3.48: FT-IR spectrum of Ru(XI-3H)(PPh_3)(H_2O)

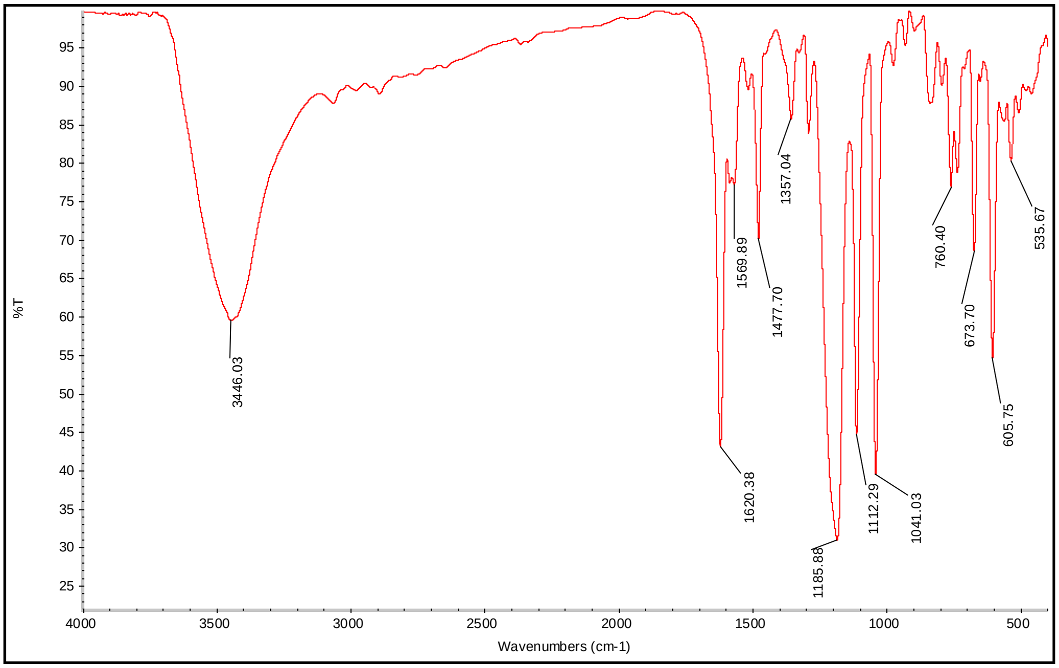


Figure 3.49: FT-IR spectrum of **(XII)**

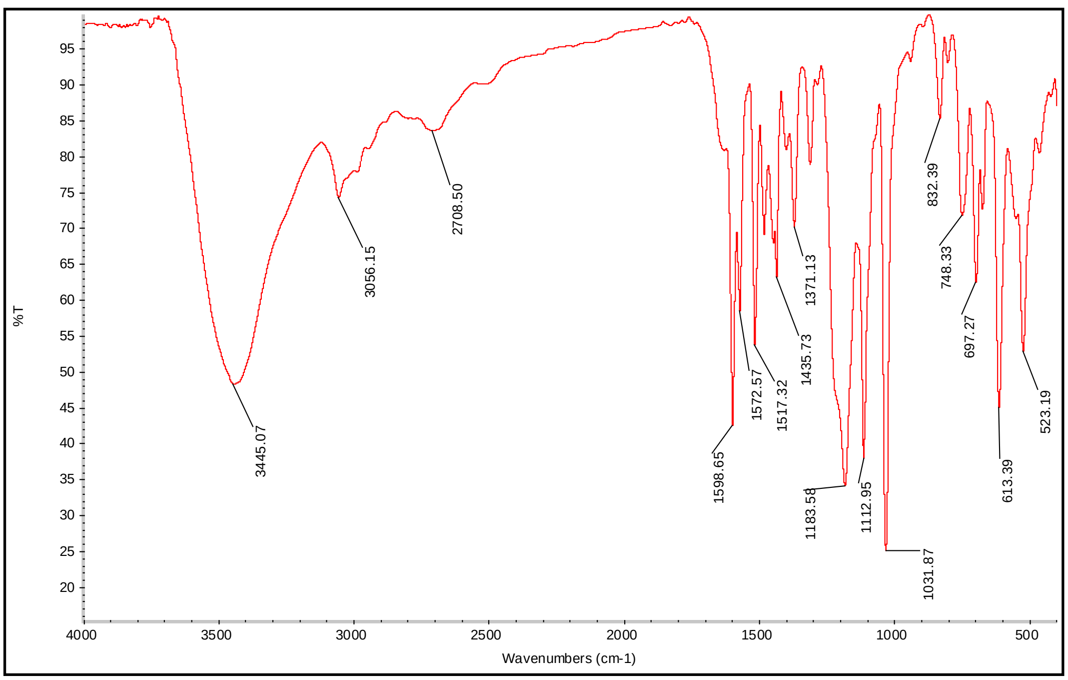


Figure 3.50: FT-IR spectrum of [Ru(XII-2H)(PPh_3)(NEt_3)].$3H_2O$

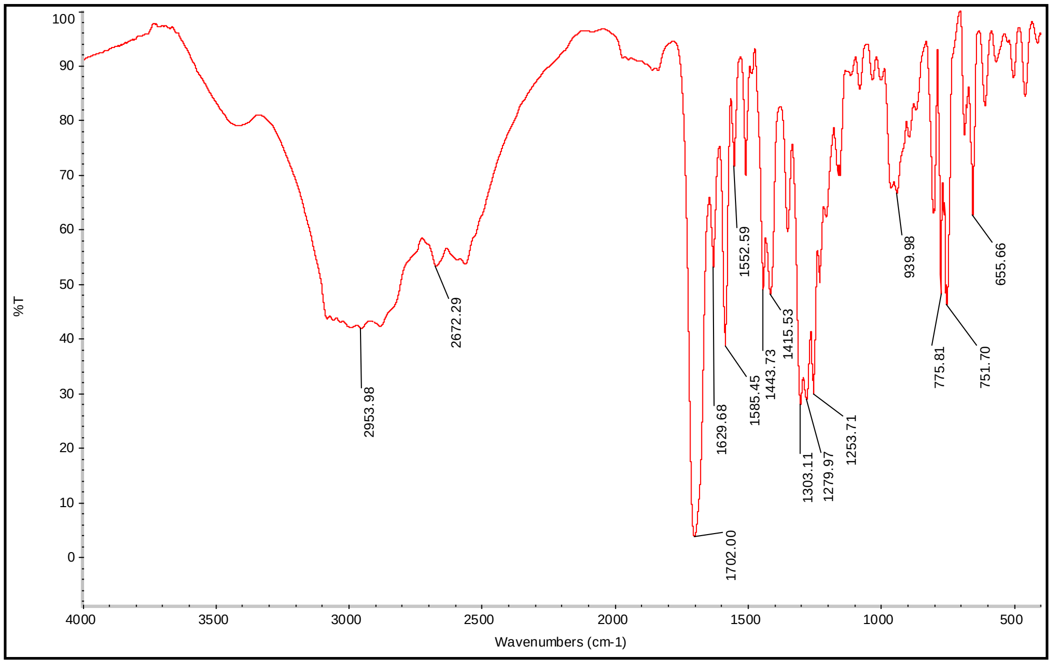


Figure 3.51: FT-IR spectrum of **(XIII)**

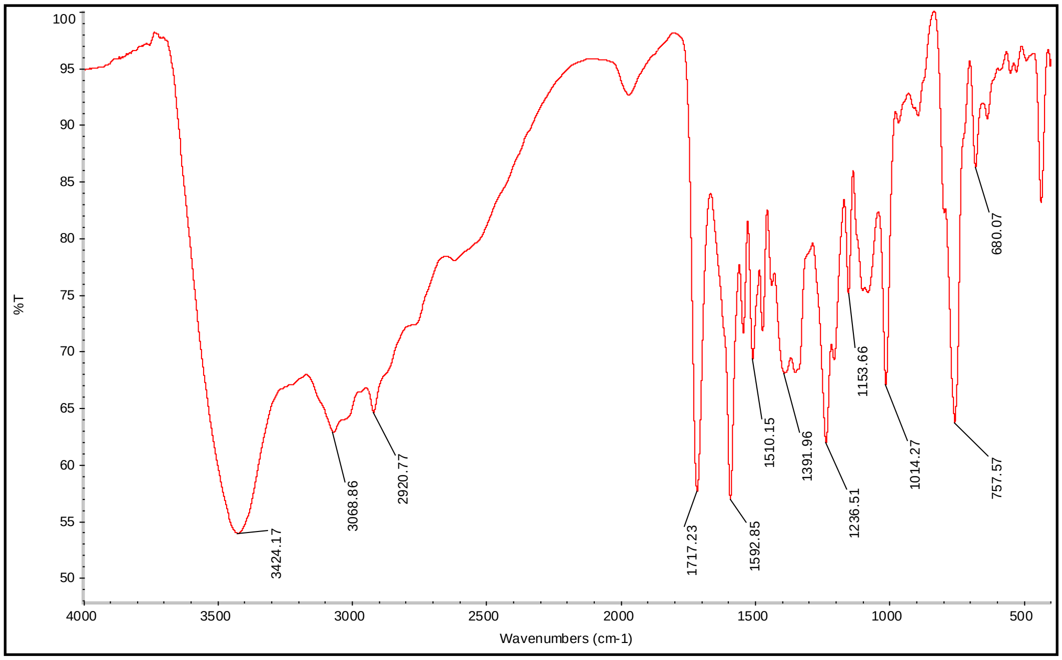


Figure 3.52: FT-IR spectrum of [Ru(XIII)Cl_2].3H_2O

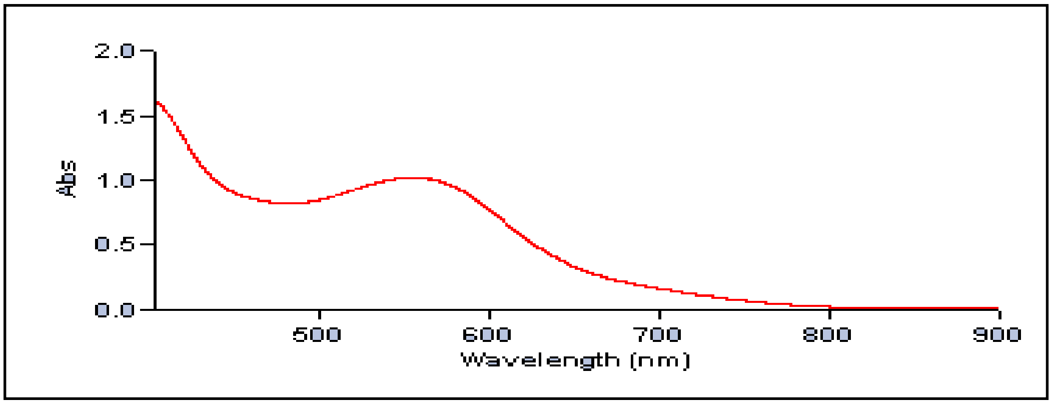


Figure 3.53: UV-Visible spectrum of $Ru(VI)_2(NCS)_2$

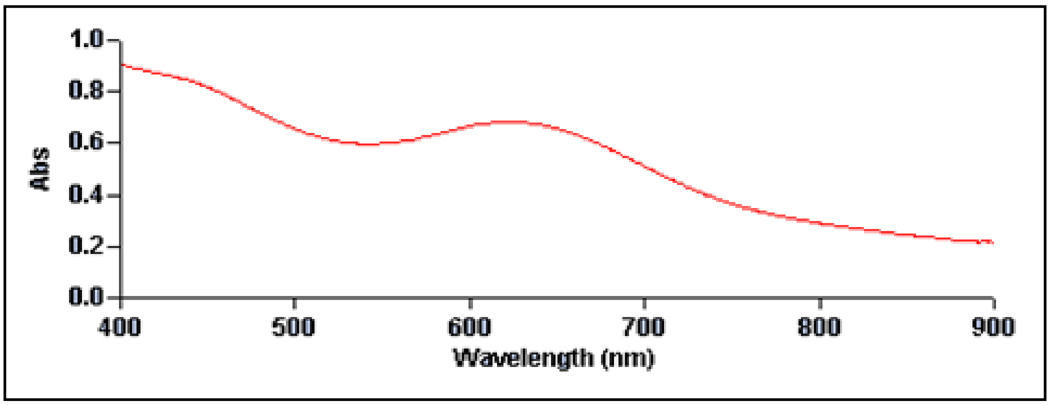


Figure 3.54: UV-Visible spectrum of $[Ru(VII)(AQ)Cl_2].5H_2O$

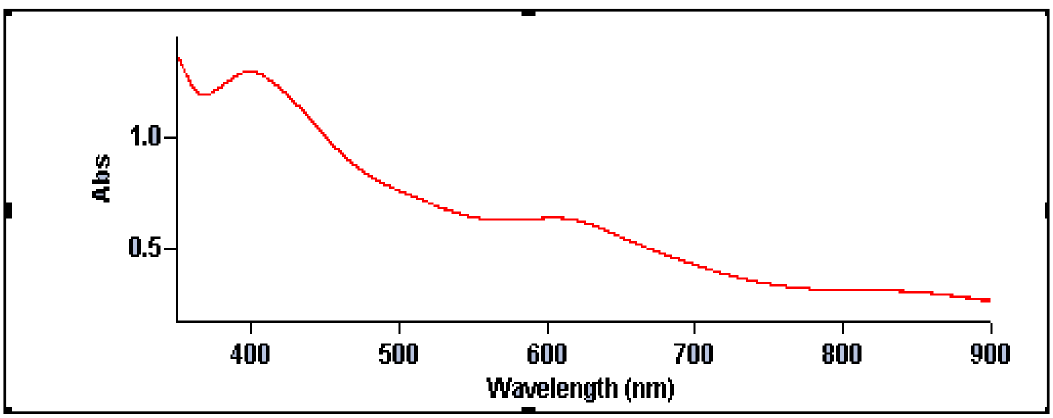


Figure 3.55: UV-Visible spectrum of $[Ru(VIII\text{-}H)_2].4H_2O$

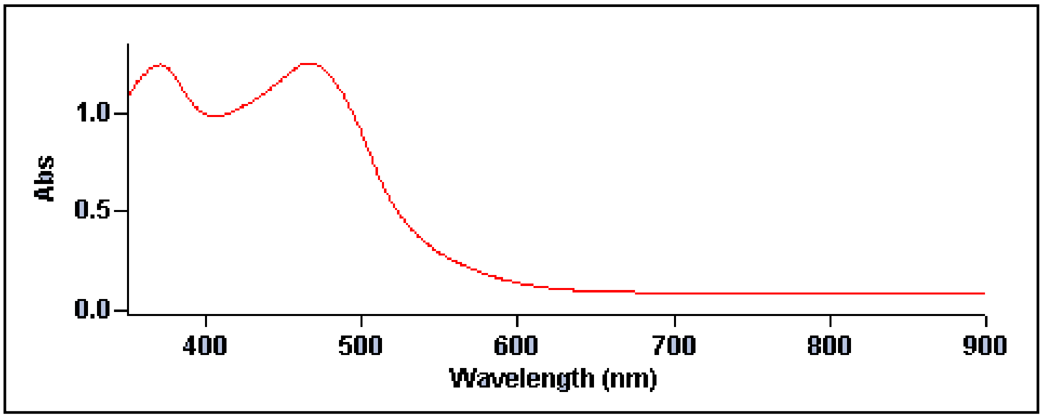


Figure 3.56: UV-Visible spectrum of $[Ru(X\text{-}2H)(PPh_3)(H_2O)].3H_2O$

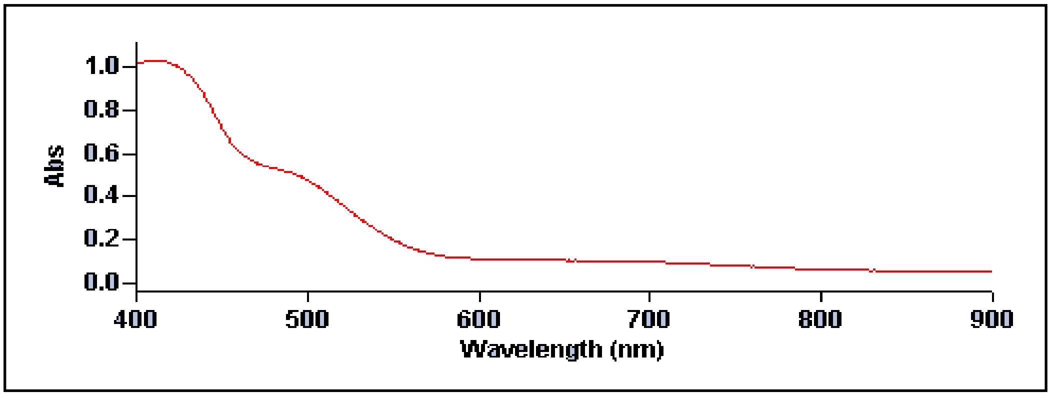


Figure 3.57: UV-Visible spectrum of $[Ru(XI\text{-}3H)(PPh_3)(H_2O)]$

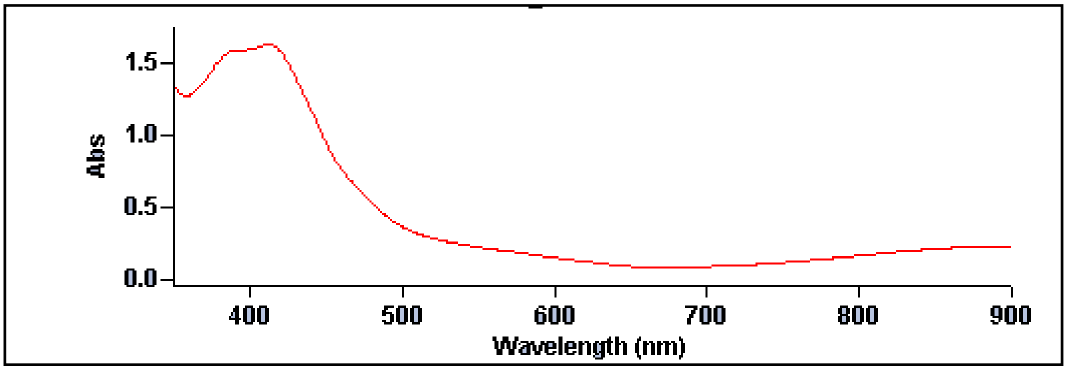


Figure 3.58: UV-Visible spectrum of $[Ru(XII\text{-}2H)(PPh_3)(NEt_3)].3H_2O$

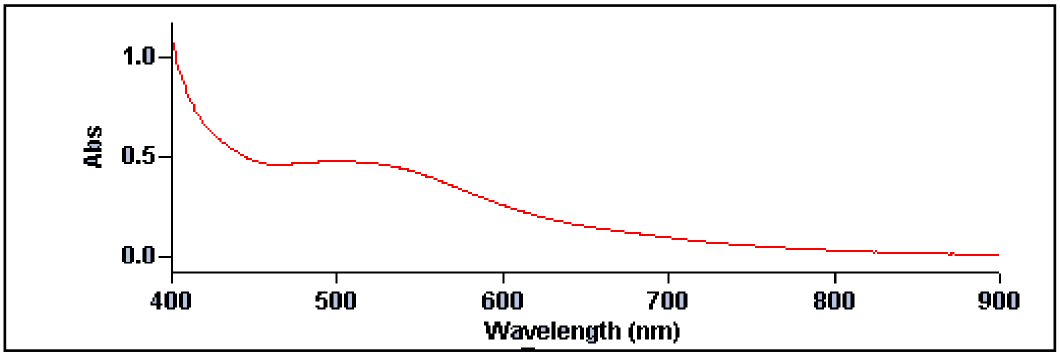


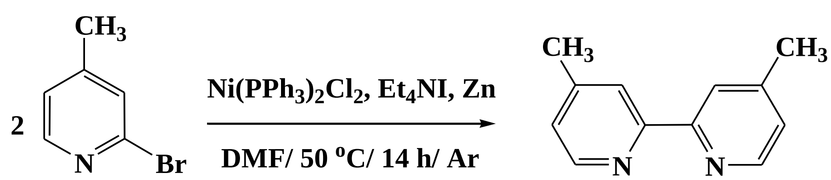
Figure 3.59: UV-Visible spectrum of [Ru(XIII)Cl_2].$3H_2O$

4. DISCUSSION

4.1 preparation of starting material

4.1.1 Preparation of 4,4`-dimethyl-2,2`-biyridine (I)

This compound was prepared following literature procedure (Rajalakshmanan and Alexander, 2005) with some modification (Eq. 2). According to the above reference the preparation of this compound should be carried out in dry THF. In fact, all the attempts to prepare the compound using THF as solvent were unsuccessful. However, when DMF was used as a solvent, it was possible to isolate the product in relatively good yield. This could be due to higher solubility of the used catalyst in DMF.



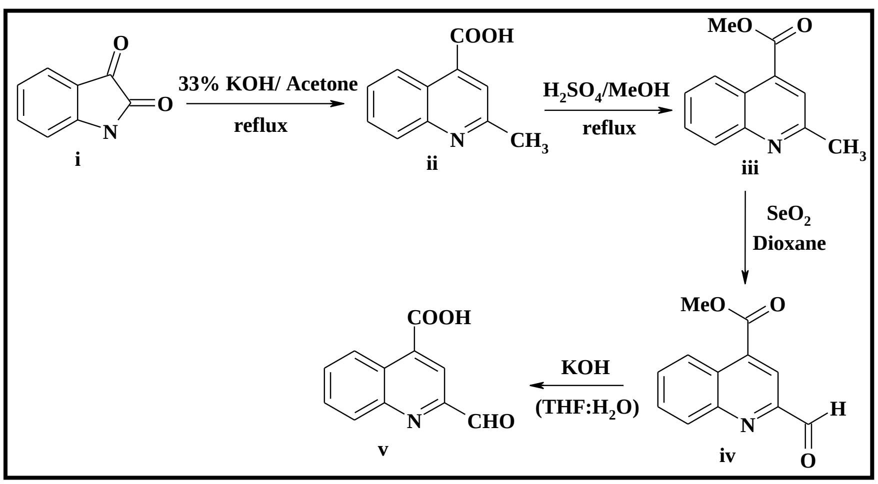
………….. (2)

The compound was characterized by comparison of its ^{1}H-NMR (Table 3.6) and ^{13}C-NMR (Table 3.7) spectroscopy with literature data. The ^{1}H-NMR spectrum (300 MHz, $CDCl_3$); Figure 3.1, shows a singlet at δ = 2.39 ppm, which corresponds to (-C**H**$_3$) protons. Bipyridyl protons show a singlet at δ = 8.19 ppm, and two doublets centered at δ = 8.49 ppm and at δ = 7.09 ppm. The ^{13}C-NMR spectrum (75 MHz, $CDCl_3$); Figure 3.2, shows a signal at δ = 21.2 ppm, which corresponds to (-**C**H$_3$) carbon. Bipyridyl carbons show a signals at δ (in ppm) =

156.0, 148.9, 148.2, 124.7 and 122.0. All these data are in agreement with the reported data.

4.1.2 Preparation of 2-formyl-4-quinolinecarboxylic acid (II)

This compound was prepared as shown in Scheme 4.1. The first step according to (Tietze, 2000), involves the reaction of Isatin with acetone in the presence of aqueous solution of alkali (33% KOH) to give the salt of 2-methyl-4-quinolinecarboxylic acid; which upon acid treatment gives compound (ii). The second step according to (Sarkis and Axamawaty, 2003), involves the esterification of (ii) with methanol in presence of acid to give (iii), which is then subjected to partial oxidation via SeO_2 followed by hydrolysis with base to give the required compound.



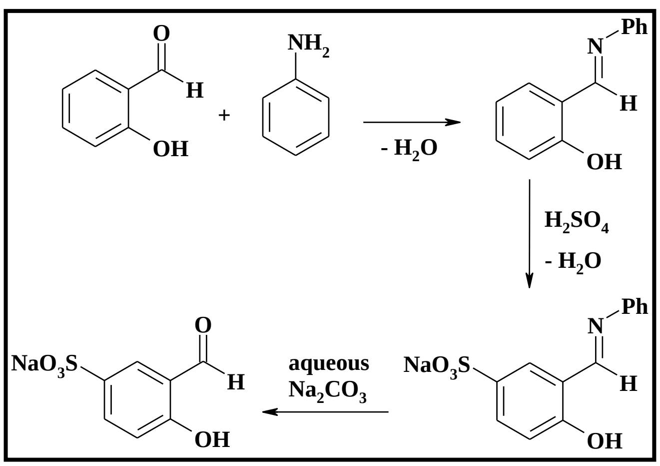
Scheme 4.1: Synthesis of 2-formyl-4-quinolinecarboxylic acid

Compound **(II)** was characterized by its mass spectroscopy (m/z = 200.03), ^{1}H-NMR (Table 3.6) and ^{13}C-NMR (Table 3.7) spectroscopy. ^{1}H-NMR spectrum (300 MHz, DMSO-d_6); Figure 3.3, shows two signals, singlet at δ = 10.10 ppm,

which corresponds to (-COO**H**) proton and doublet centered at δ = 8.78 ppm, which corresponds to (-C**H**O) proton. Quinoline protons show a doublet centered at δ = 8.26 ppm, and multiplet at δ = 7.83-7.96 ppm.^{13}C-NMR spectrum (75 MHz, DMSO-d_6), Figure 3.4, shows two signals at δ = 193.6 ppm, which corresponds to (-**C**HO) carbon, and at δ = 167.4 ppm, corresponds to (-**C**OOH) carbon. Quinoline carbons show signals at δ (in ppm) = 152.2, 148.1, 138.2, 131.5, 131.2, 131.1, 126.7, 126.3 and 118.3.

4.1.3 Preparation of sodium salt of salicylaldehyde-5-sulfonic acid (III)

Sodium salt of salicylaldehyde-5- sulfonic acid was prepared as shown in Scheme 4.2. The first step involves a protection of the aldehyde group via condensation with aniline to form N-phenylsalicylaldimine. Sulfonation of this product affords N-phenylsalicylaldimine-5-sulfonic acid which is hydrolyzed by base to give the sodium salt of salicylaldehyde-5-sulfonic acid (**Na-SSA**).

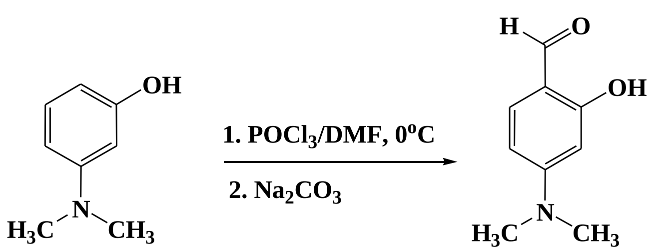


Scheme 4.2: Synthesis of sodium salt of Salicylaldehyde-5-sulfonic acid

This compound was characterized by its ^{1}H-NMR (Table 3.6) and ^{13}C-NMR (Table 3.7) spectroscopy. ^{1}H-NMR (300 MHz, D_2O) spectrum; Figure 3.5, shows a singlet at δ = 9.76 ppm, which corresponds to the (-C**H**O) proton. The aromatic protons show two doublets centered at δ = 7.73 ppm and at 6.87 ppm, and singlet at δ = 7.91 ppm. ^{13}C-NMR (75 MHz, D_2O) spectrum; Figure 3.6, shows signal at δ = 196.6 ppm, which corresponds to the (-**C**HO) carbon. Aromatic carbons show signals at δ = 161.8 ppm, which corresponds to carbon attached to (-OH) group, δ = 134.6 ppm, δ = 133.9 ppm, δ = 130.8 ppm, δ = 120.3 ppm, δ = 117.9 ppm.

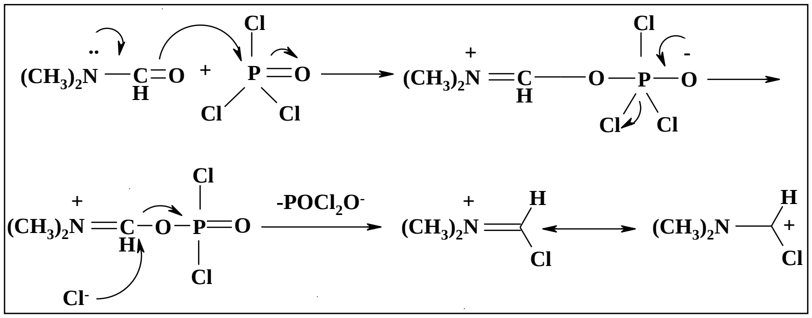
4.1.4 Preparation of 4-N,N-dimethylamino-2-hydroxybenzaldehyde (IV)

The 4-N,N-dimethylamino-2-hydroxybenzaldehyde was prepared following literature procedure (Flašík et al., 2009) with some modifications (Eq. 3). The product was prepared from the reaction of 3-N,N-dimethylaminophenol with phosphorous oxychloride ($POCl_3$) and dry N,N-Dimethyl formamide (DMF).



………………… (**3**)

At the first step N,N-Dimethyl formamide reacts with $POCl_3$ at 0^{o}C to give a reactive species (known as Vielsmeier-Haack adduct) as shown in Scheme 4.3, which in turn reacts with the 3-N,N-dimethylaminophenol to give the corresponding aldehyde.



Scheme 4.3: Mechanism of Vielsmeier-Haack adduct preparation

According to literature the ratio between the $POCl_3$ used to prepare the adduct and 3-N,N-dimethylaminophenol was 1:1 molar ratio. When this molar ratio was used the reaction product was contain a mixture of 3-N,N-dimethylaminophenol (starting material) and 4-N,N-dimethylamino-2-hydroxybenzaldehyde. Therefore, 2:1 molar ratio was used which allow the separation of a cream white product in good purity and used without further purification. This compound was characterized by comparison of its melting point, ^{1}H-NMR (Table 3.6) and ^{13}C-NMR (Table 3.7) spectroscopy with literature data. ^{1}H-NMR spectrum (300 MHz, $CDCl_3$); Figure 3.7, show a singlet at δ = 11.58 ppm, which corresponds to (-O**H**) proton, a singlet at δ = 9.47 ppm, corresponds to (-C**H**O) proton and a singlet at δ = 3.01 ppm, corresponds to (-N(C**H**$_3$)$_2$) protons. Aromatic protons show a doublet of doublet centered at δ = 6.24 ppm, and two doublets centered at δ =7.23 ppm and 6.02 ppm. ^{13}C-NMR spectrum (75 MHz, $CDCl_3$); Figure 3.8, shows a signal at δ = 192.4 ppm, corresponds to (-**C**HO) carbon, a signal at δ = 164.1 ppm, corresponds to the carbon attached to (-OH) group and a signal at δ = 40.1 ppm, corresponds to (-N(**C**H$_3$)$_2$) carbon. Aromatic carbons show signals at δ (in ppm) =

156.2, 135.2, 111.7, 104.7 and 97.2. All these data are in agreement with the reported data .

4.2 Preparation of Ligands

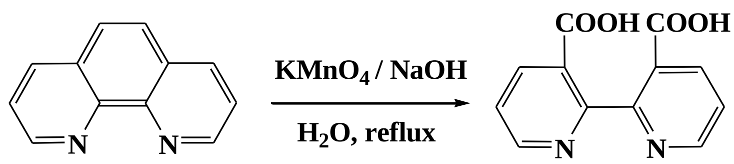
The results of elemental analysis and mass spectral data for bipyridyl and Schiff base ligands are summarized in Table 3.3 and Table 3.4, respectively. As shown in Table 3.3, the results of elemental analysis confirm the given molecular formula for the ligands. Bipyridyl and Schiff base ligands were also analyzed by high-resolution mass spectroscopy measured in either the positive ion mode or the negative ion mode of the instrument as shown in Table 3.4. The exact molar masses of the ligands were measured with high accuracy within an error range of (0.1-0.5). High intense peaks corresponding to the molar masses of the positive ion or negative ion of the ligands were clear in the mass spectra (Figure 3.33 through Figure 3.39). Small peaks for M+1 and M+2 isotopes were also observed.

These ligands were also analyzed by ^{1}H- and ^{13}C-NMR and IR spectroscopy to elucidate their structure and confirm their identity. The most important feature in the IR spectra of the Schiff base ligands is the appearance of characteristic bands for azomethine group (-RC=N-).

4.2.1 Preparation of bipyridyl ligands

Two bipyridyl ligands, 3,3`-dicarboxy-2,2`-bipyridine, **(V)**, (*Kanungo et al., 2006*) and 4,4`-dicarboxy-2,2`-bipyridine, **(VI)**, (*Hoertz et al., 2006*) were prepared.

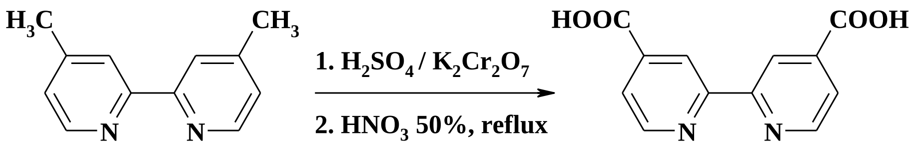
3,3`-dicarboxy-2,2`-bipyridine was prepared in one step by simple permanganate oxidation of 1,10-phenanthroline in the presence of NaOH (Eq. 4). Upon acidification with Conc. HCl a white crystalline solid was filtered off.



………………… (**4**)

Compound **(V)** was characterized by its ^{1}H- and ^{13}C-NMR spectroscopy (Table 3.8), mass spectroscopy (m/z= 245.06) and elemental analysis. ^{1}H-NMR (300 MHz, DMSO-d_6) spectrum; Figure 3.9, shows the bipyridyl protons as three doublets of doublets centered at δ = 7.48 ppm, at δ = 8.24 ppm and at δ = 8.65 ppm. ^{13}C-NMR (75 MHz, DMSO-d_6) spectrum; Figure 3.10, shows signal at δ = 167.4 ppm (s, 2C), which corresponds to (-**C**OOH) carbon. The bipyridyl carbons show signals at δ (in ppm) = 159.4 (s, 2C), 151.1 (s, 2C), 138.2 (s, 2C), 127.0 (s, 2C), 123.2 (s, 2C). All spectral data are in agreement with the reported data.

4,4`-dicarboxy-2,2`-bipyridine was prepared by oxidation of 4,4`-Dimethyl-2,2`-biyridine with potassium dichromate ($K_2Cr_2O_7$) in concentrated H_2SO_4 followed by reflux in 50 % HNO_3 (Eq. 5).



……... (**5**)

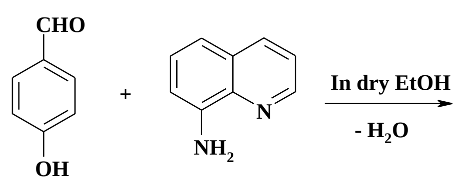
Compound **(VI)** was characterized by its ^{1}H- and^{13}C-NMR spectroscopy (Table 3.8), mass spectroscopy (m/z= 245.06) and elemental analysis. Due to its poor solubility in NMR solvents, a small amount of **(VI)** was treated with NaOH to get its sodium salt, which is water soluble. ^{1}H-NMR (300 MHz, D_2O) spectrum; Figure 3.11, shows the bipyridyl protons as doublet centered at δ = 8.59 ppm, doublet centered at δ = 7.68 ppm and singlet at δ = 8.19 ppm. ^{13}C-NMR (75 MHz, D_2O) spectrum; Figure 3.12, shows signal at δ = 172.9 ppm (s, 2C), which corresponds to (-**C**OOH) carbon. The bipyridyl carbons show signals at δ (in ppm) = 155.7 (s, 2C), 149.7 (s, 2C), 146.3 (s, 2C), 123.3 (s, 2C) and 121.2 (s, 2C). All these data are in agreement with the reported data.

4.2.2 Preparation of Schiff base ligands

The Schiff base ligands that have been prepared can be classified into three types; bidentate ligands (**VII** and **IX**), tridentate ligands (**VIII**) and tetradentate ligands (**X**, **XI**, **XII** and **XIII**).

4.2.2.1 Preparation of VII

This bidentate ligand was prepared from the condensation of 4-hydroxybenzaldehyde with 8-aminoquinoline; commercial materials, in equimolar ratio in dry ethanol (Eq. 6). The product was collected as fine yellow crystals and purified by recrystallization from ethanol.



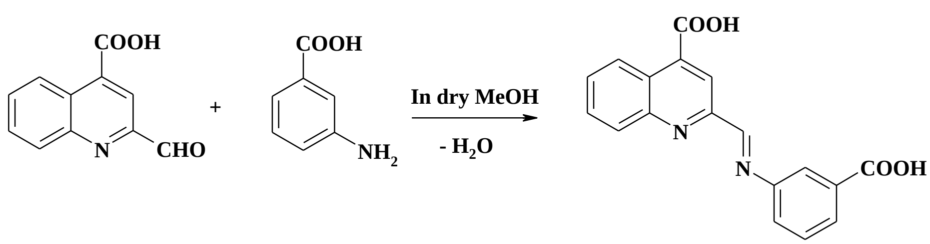
………… **(6)**

This new ligand was fully characterized by its IR, ^{1}H- and ^{13}C-NMR spectroscopy (Table 3.9), mass spectroscopy (m/z= 249.10) and elemental analysis. The IR spectrum of **(VII);** Figure 3.41, shows strong band at 1621 cm^{-1} assigned to $\nu_{C=N}$ of the azomethine group. The broad band at 3054 cm^{-1} assigned to $\nu_{O\text{-}H}$**.** The ^{1}H-NMR spectrum (300 MHz, DMSO); Figure 3.13, shows singlet at δ = 10.14 ppm, corresponds to (-O**H**) proton, singlet at δ = 8.44 ppm, corresponds to (**H**C=N) azomethine proton. The quinoline protons show, three doublets of doublets centered at δ (in ppm) = 8.83, δ = 8.33 and δ = 7.26, doublet centered at δ = 7.71 and a multiplet at δ = 7.49-7.56. The phenyl protons show, two doublets

centered at δ = 7.80 ppm and δ = 6.89 ppm. The ^{13}C-NMR spectrum (75 MHz, DMSO) of **VII**; Figure 3.14, shows two signals at δ = 162.7 ppm, which corresponds to (H**C**=N) azomethine carbon, and at δ = 161.1 ppm, which corresponds to the carbon attached to (–OH) group. Aromatic carbons show signals at δ (in ppm) = 150.7, 150.2, 141.9, 136.6, 131.3 (s, 2C), 129.3, 128.2, 127.3, 124.7, 122.1, 119.1, 116.1 (s, 2C). The above NMR spectral data were confirmed by using the Dept-135 experiment that shows disappearance of the five quaternary carbons at δ (in ppm) = 161.1, 150.7, 141.9, 129.3 and 128.2.

4.2.2.2 Preparation of IX

This bidentate ligand was prepared from the condensation of 2-formyl-4-quinolinecarboxylic acid with 3-aminobenzoic acid (commercial material), in equimolar ratio in dry methanol (Eq. 7). The product was collected as white solid and purified by recrystallization from methanol.



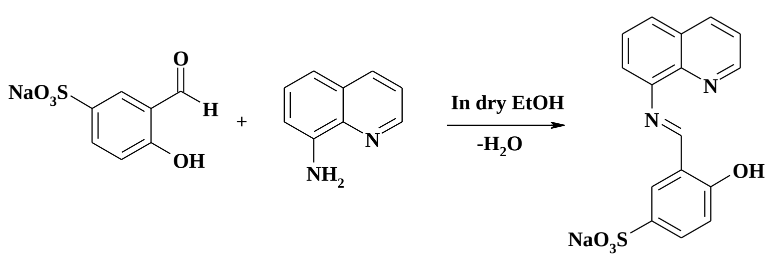
..... (7)

This new ligand was fully characterized by its IR, ^{1}H- and ^{13}C-NMR spectroscopy (Table 3.10), mass spectroscopy (m/z= 319.07) and elemental analysis. The IR spectrum, shows a strong band at 1625 cm^{-1} assigned to $\nu_{C=N}$ of the azomethine group and a strong band at 1710 cm^{-1} assigned to $\nu_{C=O}$ of the carboxyl group. The ^{1}H-NMR spectrum (300 MHz, DMSO-d_6); Figure 3.16,

shows broad singlet at δ = 13.40 ppm, corresponds to the (-COO**H**) protons and singlet at δ = 8.79 ppm, corresponds to (**H**C=N) azomethine proton. Aromatic protons show singlet at δ = 8.62 ppm, four doublets centered at δ (in ppm) = 8.75, 8.16, 7.66 and 7.58, and two multiplets at δ = 7.84-7.89 and 7.73-7.78. The ^{13}C-NMR spectrum (75 MHz, DMSO); Figure 3.17, shows two signals at δ = 167.7 ppm and 167.4 ppm, correspond to (-**C**OOH) carbons, and signal at δ = 161.7 ppm, corresponds to (H**C**=N) azomethine carbon. Aromatic carbons show signals at δ (in ppm) = 154.4, 150.7, 148.8, 137.4, 132.6, 130.9, 130.5, 130.2, 129.9, 128.4, 126.3, 126.0, 125.6, 122.8 and 119.6. The above NMR spectral data were confirmed by using the Dept-135 experiment that shows disappearance of the eight quaternary carbons at δ (in ppm) = 167.7, 167.4, 154.4, 150.7, 148.8 ppm, 137.4, 132.6 and 126.0.

4.2.2.3 Preparation of VIII

This tridentate ligand was prepared from the condensation of sodium salt of salicylaldehyde-5-sulfonic acid (**III**) with 8-aminoquinoline in equimolar ratio, in dry ethanol (Eq. 8). The product was collected as intense-orange solid and purified by recrystallization from ethanol.

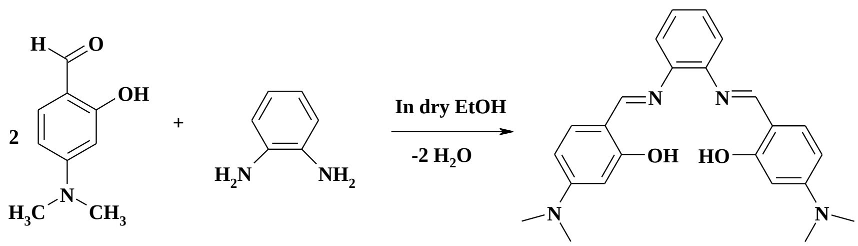


……………… **(8)**

This new ligand was fully characterized by its IR spectroscopy, ^{1}H- and ^{13}C-NMR spectroscopy (Table 3.11) and elemental analysis. The IR spectrum; Figure 3.43, shows a strong band at 1633 cm^{-1} assigned to $\nu_{C=N}$ of the azomethine group, a broad band at 3447 cm^{-1} assigned to ν_{O-H}, and a strong vibration bands at 596 cm^{-1}, 1027 cm^{-1}, 1108 cm^{-1} and 1167 cm^{-1} assigned to sulfonyl group. The ^{1}H-NMR spectrum (300 MHz, DMSO-d_6); Figure 3.19, shows two singlets, at δ = 14.18 ppm, corresponds to (-OH) proton and at δ = 9.14 ppm, corresponds to (HC=N) azomethine proton. Aromatic protons show three doublets centered at δ (in ppm) = 7.93, 7.77 and 6.89, multiplet at δ = 7.57-7.68 ppm, and three doublets of doublets centered at δ (in ppm) = 8.95, 8.40 and 7.89. The ^{13}C-NMR (75 MHz, DMSO-d_6), Figure 3.20, shows two signals at δ = 164.4 ppm, corresponds to (H**C**=N) azomethine carbon, and at δ = 162.4 ppm, corresponds to the carbon attached to (–OH) group. Aromatic carbons show signals at δ (in ppm) = 151.1, 144.8, 142.2, 139.8, 136.7, 131.6, 130.3, 129.2, 127.4, 127.1, 122.7, 118.7, 118.4 and 116.8. The above NMR spectral data were confirmed by using the Dept-135 experiment that shows disappearance of the six quaternary carbons at δ (in ppm) = 162.4, 144.8, 142.2, 139.8, 129.2 and 118.4.

4.2.2.4 Preparation of X

This tetradentate ligand was prepared from the condensation of 4-N,N-dimethylamino-2-hydroxybenzaldehyde with 1,2-phenylenediamine (commercial material), in 2:1 molar ratio, in dry ethanol (Eq. 9). The product was collected as intense-yellow solid and purified by recrystallization from ethanol.



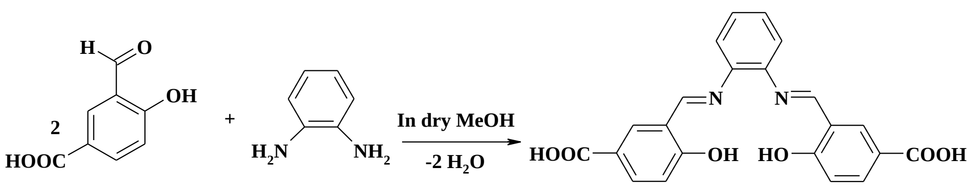
………... **(9)**

This new ligand was fully characterized by its IR spectroscopy, ^{1}H- and ^{13}C-NMR spectroscopy (Table 3.12), mass spectroscopy (m/z= 403.21) and elemental analysis. The IR spectrum of **X;** Figure 3.45, shows strong band at 1629 cm^{-1} assigned to $\nu_{C=N}$ of the azomethine group. The ^{1}H-NMR (300 MHz, DMSO-d_6) spectrum; Figure 3.22, shows singlet at δ = 13.46 ppm corresponds to (-O**H**) proton, singlet at δ = 8.62 ppm corresponds to (**H**C=N) azomethine proton and singlet at δ = 2.96 ppm corresponds to (-N(C**H$_3$**)$_2$) protons. Phenylene protons show multiplet at δ = 7.29-7.32 ppm. Other aromatic carbons show two doublets of doublets centered at δ = 7.22 ppm and 6.30 ppm, and singlet at δ = 6.06 ppm. The ^{13}C-NMR (75 MHz, DMSO-d_6); Figure 3.23, shows three signals at δ = 163.8 ppm (s, 2C), corresponds to the carbon attached to (–OH) group, at δ = 162.3 ppm (s, 2C), corresponds to (H**C**=N) azomethine carbon and at δ = 40.3 ppm (s, 4C),

corresponds to (-N(**C**H_3)$_2$) carbon. Aromatic carbons show signals at δ (in ppm) = 154.5 (s, 2C), 142.6 (s, 2C), 134.4 (s, 2C), 126.9 (s, 2C), 119.6 (s, 2C), 109.9 (s, 2C), 104.6 (s, 2C) and 98.2 (s, 2C). The above NMR spectral data were confirmed by using the Dept-135 experiment that shows disappearance of four quaternary carbons at δ (in ppm) = 163.8, 154.5, 142.6 and 109.9.

4.2.2.5 Preparation of XI

This tetradentate ligand was prepared from the condensation of 3-formyl-4-hydroxybenzoic acid with 1,2-phenylenediamine in 2:1 molar ratio, in dry methanol (Eq. 10). The product was collected as intense-orange solid and purified by recrystallization from methanol.



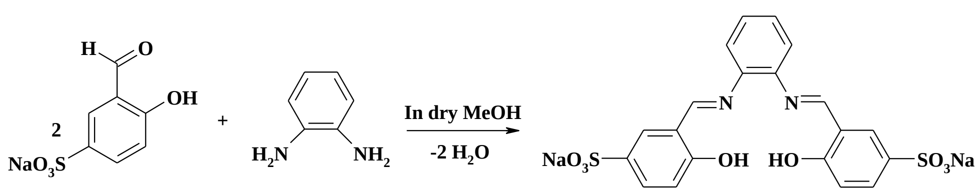
(10)

This new ligand was fully characterized by its IR, ^{1}H- and ^{13}C-NMR spectroscopy (Table 3.13), mass spectroscopy (m/z= 403.09) and elemental analysis. The IR spectrum; Figure 3.47, shows strong band at 1612 cm^{-1} assigned to $\nu_{C=N}$ of the azomethine group, strong band at 1696 cm^{-1} assigned to $\nu_{C=O}$ of the carboxyl group and broad band at 3424 cm^{-1} assigned to $\nu_{O\text{-}H}$. The ^{1}H-NMR spectrum (300 MHz, DMSO-d_6); Figure 3.25, shows singlet at δ = 13.65 ppm, corresponds to (-O**H**) proton, broad singlet at δ = 12.73 ppm, corresponds to (-COO**H**) proton and singlet at δ = 9.03 ppm, corresponds to (**H**C=N) azomethine proton. Phenylene protons show doublet centered at δ = 7.44 ppm. Other aromatic protons show two singlets at δ = 7.92 ppm and 8.31 ppm, and doublet centered at δ = 7.01. The ^{13}C-NMR (75 MHz, DMSO-d_6); Figure 3.26, shows three signals at δ = 167.1 ppm (s, 2C), corresponds to (-**C**OOH) carbon, at δ = 164.8 ppm (s, 2C), corresponds to the carbon attached to (–OH) group and at δ = 164.3 ppm (s, 2C), corresponds to

(-H**C**=N) azomethine carbon. Aromatic carbons show signals at δ (in ppm) = 142.2 (s, 2C), 135.0 (s, 2C), 134.9 (s, 2C), 128.6 (s, 2C), 122.1 (s, 2C), 120.4 (s, 2C), 119.5 (s, 2C) and 117.6 (s, 2C). The above NMR spectral data were confirmed by using the Dept-135 experiment that shows disappearance of the five quaternary carbons at δ (in ppm) = 167.1, 164.8, 142.2, 120.4 and 119.5.

4.2.2.6 Preparation of XII

This tetradentate ligand was prepared from the condensation of sodium salt of salicylaldehyde-5-sulfonic acid (**III**) with 1,2-phenylenediamine in 2:1 molar ratio, in dry methanol (Eq. 11). The product was collected as intense-yellow solid and purified by recrystallization from methanol.



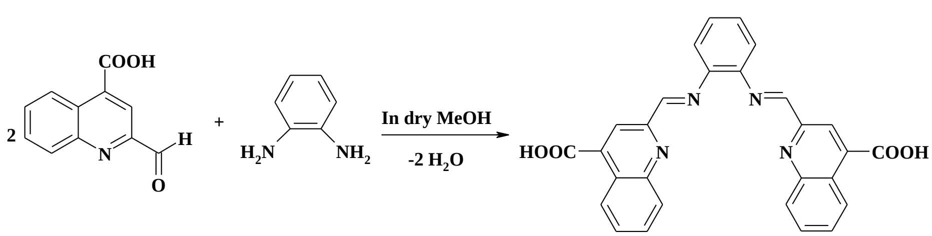
(11)

This new ligand was fully characterized by its IR, ^{1}H- and ^{13}C-NMR spectroscopy (Table 3.13) and elemental analysis. The IR spectrum; Figure 3.49, shows a strong band at 1620 cm^{-1} assigned to $\nu_{C=N}$ of the azomethine group, very broad band at 3446 cm^{-1} assigned to $\nu_{O\text{-}H}$ and a strong vibration bands at 606 cm^{-1}, 1041 cm^{-1}, 1112 cm^{-1} and 1186 cm^{-1} assigned for sulfonyl group. The ^{1}H-NMR spectrum (300 MHz, DMSO-d_6); Figure 3.29, shows singlet at δ = 13.17 ppm, corresponds to (-O**H**) proton, and singlet at δ = 8.96 ppm, corresponds to (**H**C=N)

azomethine proton. Phenylene protons show multiplet at δ = 7.36-7.49 ppm. The other aromatic protons show two doublets centered at δ = 6.88 ppm and 7.92 ppm, and doublet of doublet centered at δ = 7.60 ppm. The ^{13}C-NMR (75 MHz, DMSO); Figure 3.30, shows two signals at δ = 164.9 ppm (s, 2C), corresponds to (H**C**=N) azomethine carbon, and at δ = 161.1 ppm (s, 2C), corresponds to the carbon attached to (–OH) group. Aromatic carbons show signals at δ (in ppm) = 142.5 (s, 2C), 140.1 (s, 2C), 131.5 (s, 2C), 130.4 (s, 2C), 128.4 (s, 2C), 120.4 (s, 2C), 118.5 (s, 2C), 116.4 (s, 2C). The above NMR spectral data were confirmed by using the Dept-135 experiment that shows disappearance of the four quaternary carbons at δ (in ppm) = 161.1, 142.5, 140.1 and 118.5.

4.2.2.7 Preparation of XIII

This tetradentate ligand was prepared from the condensation of 2-formyl-4-quinolinecarboxylic acid with 1,2-phenylenediamine in 2:1 molar ratio, in dry methanol (Eq. 12). The product was collected as pale-yellow solid and purified by recrystallization from methanol. This ligand has poor solubility in most organic solvents.



…. **(12)**

This new ligand was characterized by its IR, mass spectroscopy (m/z = 475.14) and elemental analysis. IR spectrum; Figure 3.51, shows a strong band at 1629 cm^{-1} assigned to $\nu_{C=N}$ of azomethine group, a strong band at 1702 cm^{-1} assigned to $\nu_{C=O}$ of the carboxylic group, a broad band's at 2953 cm^{-1} assigned to $\nu_{C\text{-}H}$ stretching and a broad band at 2672 cm^{-1} assigned to $\nu_{O\text{-}H}$ stretching of carboxyl group. The results of elemental analysis; Table 3.3, confirms the given molecular formula for the ligands.

4.3 Preparation of Ru(II) Complexes

4.3.1 Preparation of Ru(II) Precursors

The ruthenium complexes; $RuCl_2(DMSO)_4$ (*Evans and Wilkinson, 1973*) and $RuCl_2(PPh_3)_3$ (*Hallman et al., 1970*), were prepared following literature procedures to be used as the ruthenium starting material (precursors) in the preparation of bipyridyl and Schiff base complexes.

Dichlorotetrakis(dimethyl sulphoxide)ruthenium(II) was prepared from the reaction of ruthenium(III) chloride trihydrate with dimethyl sulphoxide (Eq. 13), they were merely refluxed for a few minutes. The solution rapidly turned to orange-brown and the complex precipitated from the DMSO solution as a yellow powder with acetone.

$$\mathbf{RuCl_3.3H_2O \xrightarrow[\text{reflux}]{\text{DMSO}} Ru(DMSO)_4Cl_2} \quad \ldots\ldots\ldots\ldots\ldots\ldots\ldots\ldots \mathbf{(13)}$$

The complex was characterized by comparison of its melting point and IR spectrum (Figure 3.40) with literature data. The IR spectrum shows two bands at 3002 cm^{-1} and 2919 cm^{-1} assigned to $\nu_{C\text{-}H}$, a strong band at 1120 cm^{-1} assigned to ν_{SO} S-bonded, a strong band at 922 cm^{-1} assigned to ν_{SO} O-bonded and two bands at 714 cm-1 and 677 cm-1 assigned to ν_{CS} . All these data are in agreement with the reported data.

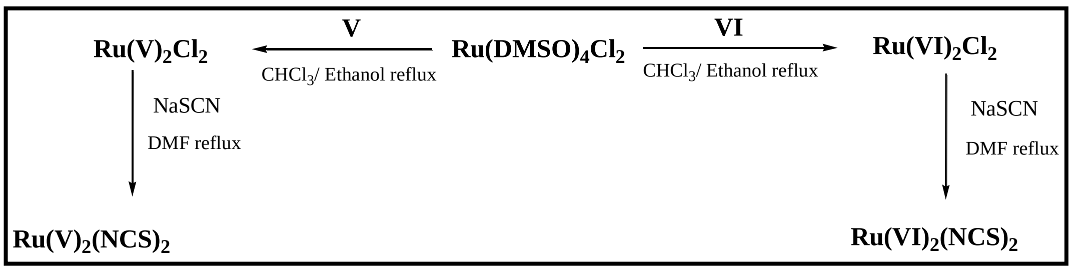
Dichlorotris(triphenylphosphine)ruthenium(II) was prepared from reaction of ruthenium(III) chloride trihydrate with sixfold excess of triphenylphosphine (Eq.

14). The complex was characterized by comparison of its melting point with literature data.

$$\mathbf{RuCl_3.3H_2O + (C_6H_5)_3P \longrightarrow RuCl_2(P(C_6H_5)_3)_3} \quad \ldots\ldots\ldots\ldots\ldots\ldots \mathbf{(14)}$$

4.3.2 Preparation of Ru(II) bipyridyl complexes

Two ruthenium(II) bipyridyl complexes; cis-di(thiocyanato)-N,N-bis(2,2`-bipyridyl-4,4`-dicarboxylic acid)ruthenium(II) (**star photosensitizer**) and cis-di(thiocyanato)-N,N-bis(2,2`-bipyridyl-3,3`-dicarboxylic acid)ruthenium(II) were prepared following literature procedures (*Xie et al., 2000* ;*Nazeeruddin et al., 1993*). These two complexes were prepared as shown in Scheme 4.4.



Scheme 4.4: Synthesis of cis-$Ru(V)_2(NCS)_2$ and cis-$Ru(VI)_2(NCS)_2$

At the first step, $Ru(DMSO)_4Cl_2$ and bipyridyl ligand; **V** or **VI**, have been refluxed (under reduced light) in a mixture of solvent (chloroform and ethanol) in 1:2 molar ratio. The $Ru(V)_2Cl_2$ and $Ru(VI)_2Cl_2$ complexes have been obtained as purple-red and red powder, respectively. The isothiocyanate complexes; $Ru(V)_2(NCS)_2$ and $Ru(VI)_2(NCS)_2$, were prepared by replacement of chloride in $Ru(V)_2Cl_2$ and $Ru(VI)_2Cl_2$ complexes, by refluxing them in DMF solution in the presence of aqueous solution of NaSCN under reduced light. The isothiocyanate complexes were characterized by comparison of their ^{1}H-NMR spectral data with literature data. ^{1}H-NMR spectrum (300 MHz, DMF) of $Ru(V)_2(NCS)_2$; Table 3.17 (Figure 3.31), shows three doublets centered at δ = 9.53 ppm, 8.54 ppm and 8.15 ppm, and a multiplet at δ = 8.07-8.01 ppm. ^{1}H-NMR spectrum of $Ru(VI)_2(NCS)_2$

(300 MHz, DMF); Table 3.17 (Figure 3.32), shows two singlets at δ = 9.07 ppm and at δ = 8.97 ppm, and four doublets centered at δ (in ppm) = 9.58, 9.30, 8.27 and 8.13. All these data are in agreement with the reported data.

4.3.3 Preparation of Ru(II) Schiff base complexes

The ruthenium(II) Schiff base complexes that have been prepared can be classified into three types: ruthenium complexes containing bidentate Schiff base ligands, tridentate Schiff base ligands and tetradentate Schiff base ligands. All the complexes were prepared under inert atmosphere and reduced light. Two ruthenium precursors, $Ru(DMSO)_4Cl_2$ and $Ru(PPh_3)_3Cl_2$, have been used as starting materials for the preparation of ruthenium complexes.

All the new ruthenium Schiff base complexes are diamagnetic (μ_{eff} ~ 0.1-0.2 BM), indicating the presence of ruthenium in the +2 oxidation state. The molar conductance values of these complexes were determined in DMF solution, where all exhibited low values; less than 40 $S.cm^2.mol^{-1}$, suggesting non-electrolytic nature of the complexes. The colors and melting points (or decomposition points) for these complexes are listed in (Table 3.19). The ruthenium Schiff base complexes are insoluble in most of organic solvents (Table 3.20).

In order to confirm the binding modes of the Schiff bases to ruthenium ions in the new complexes, the characteristic IR spectral data of the free ligands were compared with those of the ruthenium(II) complexes (Table 3.21). The free Schiff bases show very strong absorption in the region 1590-1633 cm^{-1} in their IR spectra, which is characteristic of the azomethine group ($\nu_{C=N}$). In the IR spectra of all the new complexes, the absorption due to ($\nu_{C=N}$) group was observed at lower values (1580-1610 cm^{-1}) indicating coordination of the azomethine nitrogen of the Schiff base to ruthenium.

The analytical data (elemental analysis) of the new Schiff base complexes (Table 3.18) agree well with the proposed molecular formula. Due to poor solubility of these complexes in most of organic solvents, their ^{1}H-NMR spectra in DMF were not strong enough to be used to confirm their structures. However, for the ruthenium complexes containing the tridentate (NNO) Schiff base ligand and tetradentate (NNOO) Schiff base ligands, the complete absence of signals due to OH protons in ^{1}H-NMR spectra of these complexes suggests, deprotonation and coordination of oxygen to the metal center.

The electronic (UV-Vis) spectra of the ruthenium Schiff base complexes were studied in DMF solution over a wavelength range from 350 nm to 900 nm, (Table 3.21, Figure 3.53 through 3.58). The ground state of ruthenium(II) arising from the t_{2g}^{6} configuration in an octahedral environment is $^{1}A_{1g}$. The excited states corresponding to the above configuration were $^{1}T_{1g}$ and $^{1}T_{2g}$. Hence, two spin-allowed d-d transitions $^{1}A_{1g} \rightarrow {}^{1}T_{1g}$ and $^{1}A_{1g} \rightarrow {}^{1}T_{2g}$ are expected to appear in the UV-Vis spectra of the ruthenium complexes.

4.3.3.1 Ruthenium complexes containing bidentate Schiff base ligands

Attempts to prepare ruthenium complex with the bidentate Schiff base ligand **(IX)**, lead to the formation of unidentified mixture of ruthenium complexes as shown by their elemental analysis. This is probably due to Schiff base hydrolysis.

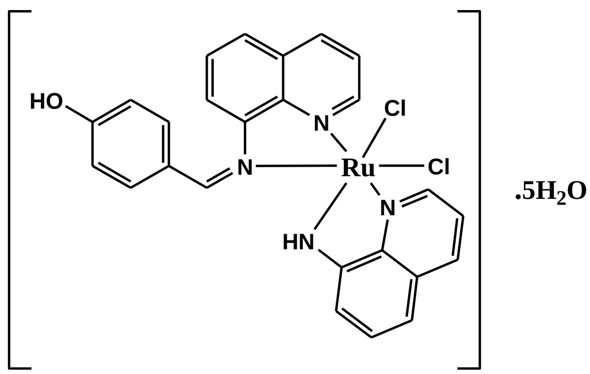
4.3.3.1a Preparation of $[Ru(VII)(AQ)Cl_2].5H_2O$

This complex was prepared from the reaction of $Ru(DMSO)_4Cl_2$; as a source of ruthenium ions, with **(VII)** Schiff base ligand in 1:2 molar ratio, under inert conditions and reduced light in dry 2-methoxyethanol. This complex was precipitated as a green solid from the concentrated solution of 2-methoxyethanol upon addition of diethyl ether.

Conductivity measurements of the above complex in DMF solvent indicate a non-electrolyte nature of the complex. The ratio of metal-to-ligand in the above mentioned complex was confirmed by the result of elemental analysis as shown in Table 3.18.

This complex was characterized by its IR spectroscopy. The IR spectrum; Figure 3.42, shows a strong band at 1587 cm^{-1} assigned to $\nu_{C=N}$ azomethine group. As compared with the free ligand ($\nu_{C=N}$ 1599 cm^{-1}), this stretching frequency shows a shift to lower frequency by about 12 cm^{-1}, indicating the coordination of the azomethine group nitrogen of the Schiff base to ruthenium ion. A strong and broad band at 3423 cm^{-1} is due to the presence of water molecules.

Magnetic susceptibility measurements for [Ru(VII)(AQ)Cl_2].5H_2O indicate a diamagnetic behavior of this complex which is consistent with low-spin, d^6 octahedral geometry. UV-Vis spectrum for this complex (Figure 3.54), shows absorption band at λ= 623 (ε = 6834 $L.mol^{-1}.cm^{-1}$). The microelemental analysis indicate the presence of one molecule of the Schiff base and one molecule of 8-aminoquinoline in the molecular formula of the complex. In view of the above data the proposed structure of [Ru(VII)(AQ)Cl_2].5H_2O is:



4.3.3.2 Ruthenium complexes containing tridentate Schiff base ligand

4.3.3.2a Preparation of $[Ru(VIII\text{-}H)_2].4H_2O$

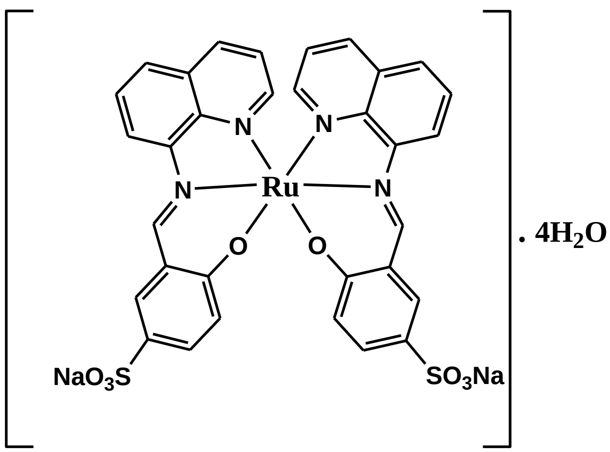
This complex was prepared from the reaction of $Ru(DMSO)_4Cl_2$ with **(VIII)** Schiff base ligand in 1:2 molar ratio (Eq. 15). The reaction was performed in dry 2-methoxyethanol in presence of triethylamine (NEt_3) under inert atmosphere and reduced light. The complex was precipitated as shiny black solid from the concentrated solution of 2-methoxyethanol upon the addition of diethyl ether.

$$\mathbf{Ru(DMSO)_4Cl_2 + 2\ VIII + 2NEt_3 \xrightarrow[\text{refluxed, 8 h}]{\text{2-methoxyethanol}} [Ru(VIII\text{-}H)_2].4H_2O + 2Et_3NH^+Cl^-} \quad \mathbf{....15}$$

Conductivity measurements of the above complex in DMF solvent indicate a non-electrolyte nature of the complex. This ruthenium complex is soluble in water, and has a partial solubility in DMSO and DMF. The ratio of metal-to-ligand in the above mentioned complex was confirmed by the result of elemental analysis as shown in Table 3.18.

This complex was characterized by its IR spectroscopy. The IR spectrum; Figure 3.44, shows a strong band at 1600 cm^{-1} assigned to $\nu_{C=N}$ azomethine group. As compared with the free ligand ($\nu_{C=N}$ 1620 cm^{-1}), this stretching frequency shows a shift to lower frequency by about 20 cm^{-1}, indicating the coordination of the azomethine group nitrogen of the Schiff base to ruthenium ion. The strong vibration bands at 614 cm^{-1}, 1030 cm^{-1}, 1111 cm^{-1} and 1178 cm^{-1} assigned for sulfonyl group. A strong and broad band at 3422 cm^{-1} is due to the presence of water molecules. Magnetic susceptibility measurements for $[Ru(VIII\text{-}H)_2].4H_2O$

indicate a diamagnetic behavior of this complex which is consistent with low-spin, d^6 octahedral geometry. UV-Vis spectrum (Figure 3.55), show two absorption bands at λ= 630 nm (ε = 6310 $L.mol^{-1}.cm^{-1}$) and a strong band at λ = 399 nm (ε = 13,012).In view of the above data the proposed structure of [Ru(VIII-$H)_2$].$4H_2O$ is:



4.3.3.3 Ruthenium complexes containing tetradentate Schiff base ligands

4.3.3.3a Preparation of [Ru(X-2H)(PPh_3)(H_2O)].3H_2O

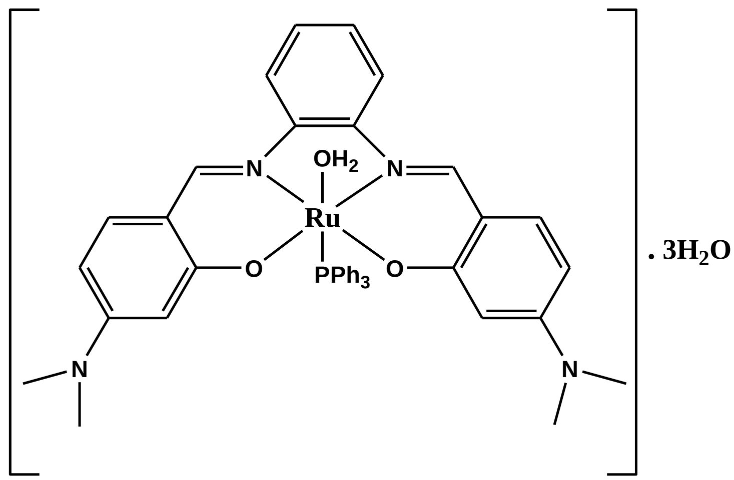
This complex was prepared from the reaction of Ru(PPh_3)$_3$$Cl_2$; as a source of ruthenium ions, with **(X)** Schiff base ligand in 1:1 molar ratio, in the presence of NEt_3, under inert conditions and reduced light in dry 2-methoxyethanol (Eq. 16). The complex was precipitated as red solid from the concentrated solution of 2-methoxyethanol upon addition of diethyl ether.

$$\mathbf{Ru(PPh_3)_3Cl_2 + X + 3NEt_3 \xrightarrow[\text{reflux, 4 h}]{\text{2-methoxyethanol}} [Ru(X\text{-}2H)(PPh_3)(H_2O)].3H_2O + 2PPh_3 + 2Et_3NH^+Cl^- + NEt_3} \quad ....16$$

Conductivity measurements of the above complex in DMF solvent indicate a non-electrolyte nature of the complex. The ratio of metal-to-ligand in the above mentioned complex was confirmed by the result of elemental analysis as shown in Table 3.18.

This complex was characterized by IR spectroscopy. The IR spectrum; Figure 3.46, shows a strong band at 1609 cm^{-1} assigned to $\nu_{C=N}$ azomethine group. As compared with the free ligand ($\nu_{C=N}$ 1629 cm^{-1}), this stretching frequency shows a shift to lower frequency by about 20 cm^{-1}, indicating the coordination of the azomethine group nitrogen of the Schiff base to ruthenium ion. A strong band at 3421 cm^{-1} is due to the presence of water molecules. The absence of signal due to Ph-O**H** proton in ^{1}H-NMR spectrum of this complex suggests, deprotonation and coordination of oxygen to the ruthenium ion. Magnetic susceptibility measurements for [Ru(X-2H)(PPh_3)(H_2O)].3H_2O indicate a diamagnetic behavior

for this complex which is consistent with low-spin, d^6 octahedral geometry. UV-Vis spectrum (Figure 3.56), shows two strong absorption bands at λ = 466 nm (ε = 12,585 $L.mol^{-1}.cm^{-1}$) and at λ = 371 nm (ε = 12,484 $L.mol^{-1}.cm^{-1}$). In view of the above data the proposed structure of $[Ru(X\text{-}2H)(PPh_3)(H_2O)].3H_2O$ is:



4.3.3.3b Preparation of Ru(XI-3H)(PPh_3)(H_2O)

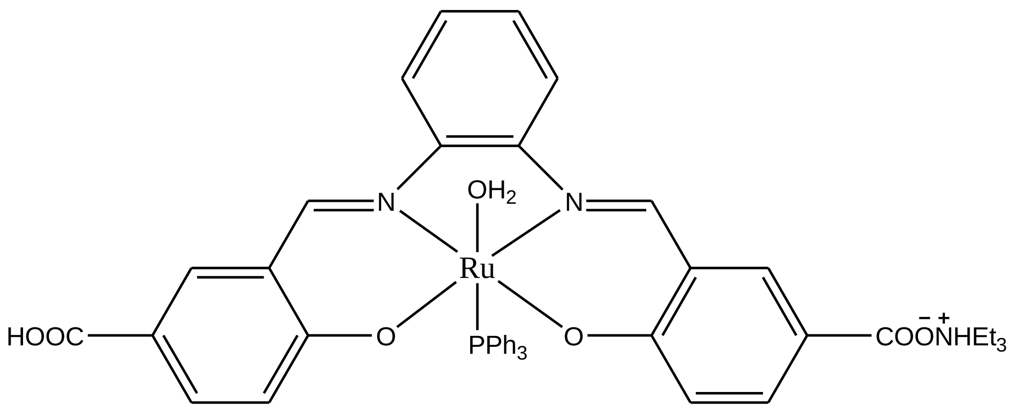
This complex was prepared from the reaction of $Ru(PPh_3)_3Cl_2$ with **(XI)** Schiff base ligand in 1:1 molar ratio, in the presence of NEt_3, under inert conditions and reduced light in dry 2-methoxyethanol (Eq. 17). This complex was precipitated as a brown solid from the concentrated solution of 2-methoxyethanol upon the addition of diethyl ether.

$$\mathbf{Ru(PPh_3)_3Cl_2 + XI + 3Et_3N \xrightarrow[\text{reflux, 4 h}]{\text{2-methoxyethanol}} Ru(XI\text{-}2H)(PPh_3)(H_2O) + 2PPh_3 + 2Et_3NH^+Cl^-} \quad \text{....17}$$

Conductivity measurements of the above complex in DMF solvent, indicate a non-electrolyte nature of the complex. The ratio of metal-to-ligand in the above mentioned complex was confirmed by the result of elemental analysis as shown in Table 3.18.

This complex was characterized by IR spectroscopy. The IR spectrum; Figure 3.48, shows a strong band at 1596 cm^{-1} assigned to $\nu_{C=N}$ azomethine group. As compared with the free ligand ($\nu_{C=N}$ 1611 cm^{-1}), this stretching frequency shows a shift to lower frequency by about 15 cm^{-1}, indicating the coordination of the azomethine group nitrogen of the Schiff base to ruthenium ion. The strong band at 1664 cm^{-1} assigned to $\nu_{C=O}$ of the carboxyl group. The absence of signal due to Ph-OH proton in ^{1}H-NMR spectra of this complex suggests, deprotonation and coordination of oxygen to the ruthenium ion. Also, the ^{1}H-NMR spectrum shows, two signals, triplet centered at $\delta = 1.47$ ppm and quartet centered at $\delta = 3.27$ ppm , as indication of the presence of triethylamine in the complex structure. Magnetic

susceptibility measurements for [Ru(XI-3H)(PPh_3)(H_2O)] indicate a diamagnetic behavior of this complex, which is consistent with low-spin d^6, octahedral geometry. UV-Vis spectrum for this complex (Figure 3.57), shows a strong absorption band at λ = 412 nm (ε = 10357 L.mol^{-1}.cm^{-1}). A weak absorption band at λ = 494.7 nm (ε = 5045 L.mol^{-1}.cm^{-1}) was also observed. In view of the above data the proposed structure of [Ru(XI-3H)(PPh_3)(H_2O)] is:



4.3.3.3c Preparation of [Ru(XII-2H)(PPh$_3$)(NEt$_3$)].3H$_2$O

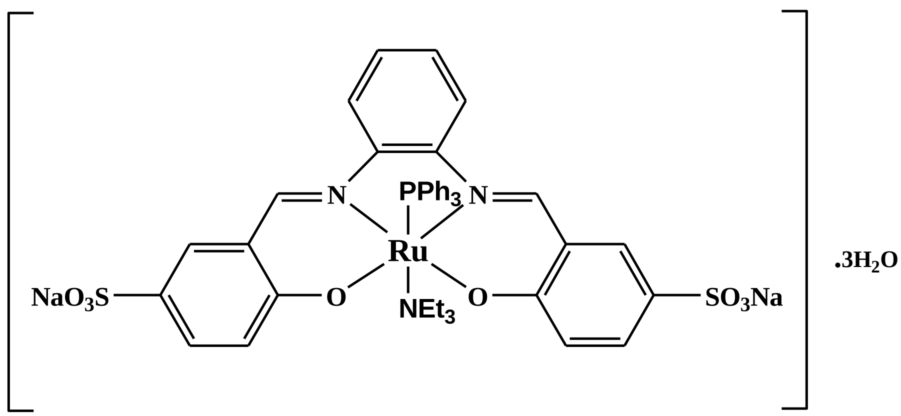
This complex was prepared from the reaction of Ru(PPh$_3$)$_3$Cl$_2$ with **(XII)** Schiff base ligand in 1:1 molar ratio, in the presence of NEt$_3$, under inert conditions and reduced light in dry 2-methoxyethanol (Eq. 18). This complex was precipitated as a brown solid from the concentrated solution of 2-methoxyethanol upon the addition of diethyl ether.

$$Ru(PPh_3)_3Cl_2 + XII + 3Et_3N \xrightarrow[\text{reflux, 4 h}]{\text{2-methoxyethanol}} Ru(XII\text{-}2H)(PPh_3)(NEt_3) + 2PPh_3 + 2Et_3NH^+Cl^- \quad ......18$$

Conductivity measurements of the above complex in DMF solvent indicate a non-electrolyte nature of the complex. This ruthenium complex is soluble in water, and has a partial solubility in DMSO and DMF. The ratio of metal-to-ligand in the above mentioned complex was confirmed by the result of elemental analysis as shown in Table 3.18.

This complex was characterized by IR spectroscopy. The IR spectrum; Figure 3.50, shows a strong band at 1598 cm^{-1} assigned to $\nu_{C=N}$ of azomethine group. As compared with the free ligand ($\nu_{C=N}$ 1620 cm^{-1}), this stretching frequency shows a shift to lower frequency by about 22 cm^{-1}, indicating the coordination of the azomethine group nitrogen of the Schiff base to ruthenium ion. The strong vibration bands at 613 cm^{-1}, 1031 cm^{-1}, 1112 cm^{-1} and 1183 cm^{-1} are assigned for sulfonyl group. A strong and broad band at 3445 cm^{-1} is due to the presence of water molecules. The absence of signal due to Ph-OH proton in ^{1}H-NMR spectra of this complex suggests, deprotonation and coordination of oxygen to the

ruthenium ion. Magnetic susceptibility measurements for Ru[(XII-2H)(PPh_3)(NEt_3)].3H_2O indicate a diamagnetic behavior for this complex which is consistent with low-spin d^6, octahedral geometry. UV-Vis spectrum for this complex (Figure 3.58), shows a strong absorption band at λ = 413 nm (ε = 16,553 $L.mol^{-1}.cm^{-1}$). In view of the above data the proposed structure [Ru (XII-2H)(PPh_3)(NEt_3)].3H_2O is:



4.3.3.3d Preparation of [Ru(XIII)Cl_2].3H_2O

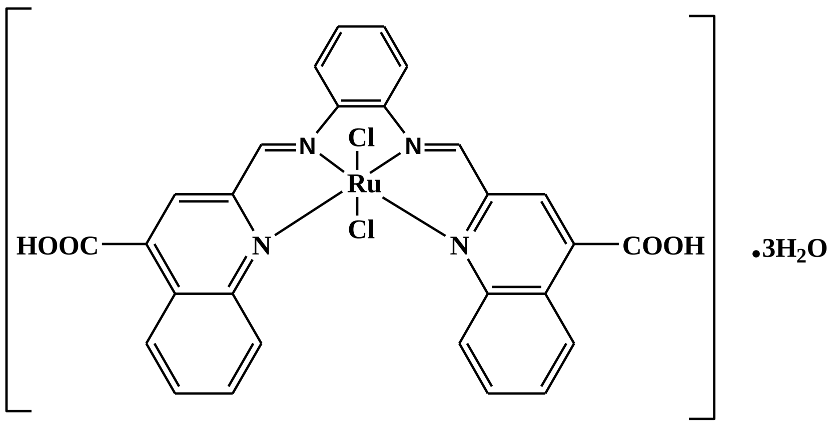
This complex was prepared from the reaction of Ru$(DMSO)_4Cl_2$ as a source of ruthenium ions with **(XIII)** Schiff base ligand in 1:1 molar ratio, under inert conditions and reduced light in dry 2-methoxyethanol (Eq. 19). This complex was precipitated as a violet solid from the concentrated solution of 2-methoxyethanol upon addition of diethyl ether.

$$\mathbf{Ru(DMSO)_4Cl_2 + XIII \xrightarrow[\text{reflux, 4 h}]{\text{2-methoxyethanol}} [Ru(XIII)Cl_2].\,3H_2O + 4DMSO} \quad .....19$$

Conductivity measurements of the above complex in DMF solvent, indicate a non-electrolyte nature of the complex. The ratio of metal-to-ligand in the above mentioned complex was confirmed by the result of elemental analysis as shown in Table 3.18.

This complex was characterized by IR spectroscopy. The IR spectrum; Figure 3.52, shows a strong band at 1592 cm^{-1} assigned to $\nu_{C=N}$ azomethine group. As compared with the free ligand ($\nu_{C=N}$ 1629 cm^{-1}), this stretching frequency shows a shift to lower frequency by about 37 cm^{-1}, indicating the coordination of the azomethine group nitrogen of the Schiff base to ruthenium ion. The strong band at 1717 cm^{-1} assigned to $\nu_{C=O}$ of the carboxyl group. A strong and broad band at 3424 cm^{-1} is due to the presence of water molecules.

Magnetic susceptibility measurements for [Ru(XIII)Cl_2].3H_2O indicate a diamagnetic behavior for this complex which is consistent with low-spin d^6, octahedral geometry. UV-Vis spectrum (Figure 3.59), shows absorption band at λ= 499 nm (ε = 4786 L.mol^{-1}.cm^{-1}). In view of the above data the proposed structure of [Ru(XIII)Cl_2].3H_2O is:



5. Conclusion

In this work three types of Schiff base ligands: bidentate, tridentate and tetradentate ligands have been prepared and characterized. The bidentate and the tridentate ligands include quinoline ring within their structure. However, the tetradentate ligands are based on the condensation of phenylenediamine with different substituted aldehydes.

The above ligands were designed to have conjugation close to bipyridyl ligands, and having different anchoring groups such as –COOH, -OH and SO_3^-.

The work also involves the preparation of ruthenium complexes with all the prepared Schiff base ligands. The bidentate Schiff base ligands undergo hydrolysis in the presence of ruthenium precursor, which leads to the formation of impure samples. The instability of these ligands towards hydrolysis limits their use as photosensitizer in dye-sensitized solar cells. However the tridentate and tetradentate Schiff base ligands appears to be stable towards hydrolysis in the reaction medium. This is could be due the extended conjugation in these ligands compared with the bidentate ligands.

All the prepared ruthenium Schiff base complexes are hygroscopic as confirmed by their elemental analysis and IR spectra, and consistent with literature observations.

The all prepared ruthenium Schiff base complexes show poor solubility in organic solvents. The solubility could be enhanced by the reduction of azomethine

bond (C=N), but that will reduce the conjugation which can be compensated by π-system substituent such as thiophene or phenyl rings.

In this work we have used $[Ru(DMSO)_4Cl_2]$ and $[Ru(PPh_3)_3Cl_2]$ as precursors for ruthenium ions. In the case of the first precursor, the complete removal of DMSO was a challenging task due to the strong bonding of DMSO with Ru-metal. In the case of the second precursor, we faced the difficulty in substituting all the triphenylphosphine ligands. Accordingly, we suggest the use of another precursors that do not contain DMSO or PPh_3. A good candidate is the polymeric complex $[Ru(COD)Cl_2]_n$ (where COD = 1,5-cyclooctadiene).

All the ruthenium Schiff base complexes show absorption in the UV-Vis region. In particular the complexes $[Ru(VII)(AQ)Cl_2].5H_2O$ and $[Ru(VIII\text{-}H)_2].4H_2O$ show absorption extended to 623 nm and 630 nm, respectively. These results are very close to absorption of the model compound $[Ru(VI)_2(NCS)_2]$. The complexes $[Ru(X\text{-}2H)(PPh_3)(H_2O)].3H_2O$, $[Ru(XI\text{-}3H)(PPh_3)(H_2O)]$, and $[Ru(XII\text{-}2H)(PPh_3)(NEt_3)].3H_2O$, show a strong absorption at λ = 466 nm (ε = 12,585 $L.mol^{-1}.cm^{-1}$), 412 nm (ε = 10,357 $L.mol^{-1}.cm^{-1}$), and 413 nm (ε = 16,553 $L.mol^{-1}.cm^{-1}$), respectively. Although these complexes show absorption in the edge of the visible region but they show relatively high molar extinction coefficients.

REFERENCES

Altobello, S., Bignozzi, C. A., Caramori, S., Larramona, G., Quici, S., Marzanni, G. and Lakhmiri, R. (2004), Sensitization of TiO_2 with ruthenium complexes containing boronic acid functions, **Journal of Photochemistry and Photobiology, A**, 166, 91-98.

Anderson, P. A., Strouse, G. F., Treadway, J. A., Keene, F. R. and Meyer, T. J. (1994), Black MLCT Absorbers, **Inorganic Chemistry**, 33, 3863-3864.

Anderson, S., Constable, E., Dare-Edwards, M., Goodenough, J., Hamnett, A., Seddon, K. and Wright, R. (1979), Chemical modification of titanium(IV) oxide electrode to give stable dye sensitization without a supersensitizer**, Nature**, 280, 571-573.

Ardo, S. and Meyer, G. J. (2009), Photodriven heterogeneous charge transfer with transition metal compounds anchored to TiO_2 semiconductor surfaces, **Chemical Society Reviews**, 38, 115-164.

Armaroli N. and Balzani V. (2007), The Future of Energy Supply: Challenges and Opportunities, **Angewandte Chemie, International Edition,** 46, 52-66.

Balzani, V., Juris, A., Venturi, M., Campagna, S., and Serroni, S. (1996), Luminescent and Redox-Active Polynuclear Transition Metal Complexes, **Chemical Reviews**, 96, 759-833.

Berry, K., Moya, F., Murray, K.,Van den Berge, A. and West, B. (1982), Water-soluble cobalt(II) complexes of N,N`-subistituted bis(salicylidimine-5-sulphonic acid). Oxygen carrying properties and conversion into cobalt(III) organometallic compounds, **Journal of Chemical Society, Dalton Transactions**, 109-116.

Bhowon, M. G., Wah, H. L., Dosieah, A., Ridana, M., Ramalingum, O. and Lacour, D. (2004), Synthesis, Characterization and Catalytic Activity of Metal Schiff Base Complexes Derived from pyrrole-2-carboxaldehyde, **Synthesis and Reactivity in Inorganic and Metal-Organic Chemistry**, 34, 1-16.

Bhowon, M. G., Wah, H. L. and Narain, R. (1999), Schiff base complexes of ruthenium(II) and their use as catalytic oxidants, **Polyhedron**, 18, 341-345.

Bosi, M., and Pelosi, C. (2007), The potential of III-V semiconductors as terrestrial photovoltaic devices, **Progress in Photovoltaics: Research and Applications**, 15, 51–68.

Botsivali, M., Evans, D. F., Missen, P. H. and Upton, M. W. (1985), Studies of singlet oxygen in aqueous solution part 2. Water-soluble square-planar complexes as quenchers, **Journal of Chemical Society, Dalton Transactions,** 1147-1149

Bozic-Weber, B., Constable, E. C., Housecroft, C. E., Neuburger, M. and Price, J. R. (2010), Sticky complexes: carboxylic acid-functionalized N-phenylpyridin-2-ylmethanimine ligands as anchoring domains for copper and ruthenium dye-sensitized solar cells, **Dalton Transactions**, 39, 3585-3594.

Case, F. H. (1946), The Synthesis of Certain Substituted 2,2`-Bipyridyls, **Journal of American Chemical Society**, 68, 2574-2577.

Chapin, D. M., Fuller, C. S. and Pearson, G. L. (1954), A new silicon p-n junction photocell for converting solar radiation into electrical power, **Journal of Applied Physics**, 25, 676-677.

Cotton, F. A., Faut, O. D. and Goodgame, D. M. (1961), Preparation, Spectra and Electronic structures of Tetrahedral Nickel(II) Complexes Containing Triphenylphosphine and Halide Ions as Ligands, **Journal of American Chemical Society**, 83, 344-351.

Eisenberg E. and Nocera D. G. (2005), Preface: Overview of the Forum on Solar and Renewable Energy, **Inorganic Chemistry**, 44, 6799-6801.

Evans, I. P., Spencer, A. and Wilkinson, G. (1973), Dichlorotetrakis(dimethylsulphoxide)ruthenium(II) and its Use as a Source Material for Some New Ruthenium(II) Complexes, **Journal of Chemical Society, Dalton Transactions,** 2, 204-209.

Flašík, R., Stankovičová, H., Gáplovský, A. and Donovalová, J. (2009), Synthesis and Study of Novel Coumarin Derivatives Potentially Utilizable as Memory Media, **Molecules,** 14, 4838-4848.

Gaffney, J. S. and Marely, N. A. (2009), Impacts of combustion emissions on air quality and climate – From coal to biofuels and beyond, **Atmospheric Environment**, 43, 23-36.

Galoppini, E. (2004), Linkers for anchoring sensitizers to semiconductor nanoparticles, **Coordination Chemistry Reviews**, 248, 1283-1297.

Ghoniem A. F. (2011), Needs, resources and climate change: clean and efficient conversion technologies, **Progress in Energy and Combustion Science**, 37, 15-51.

Goetzberger A., Luther J. and Willeke G. (2002), Solae Cells: past, present, future, **Solar Energy Materials and Solar Cells**, 74, 1-11.

Goncalves, L, Bermudes, V., Ribeiro, H. and Mendes, A. (2008), Dye-Sensitized Solar Cells, A safe bet for the Future, **Energy and Environment Science**, 1, 655-667.

Gowri, S., Priya, J., Muthukumar, M. and Viswanathamurthi, P. (2009), Synthesis, spectral and catalytic studies of ruthenium(II) unsymmetrical Schiff base complexes, **Journal of Coordination Chemistry**, 62, 1320-1326.

Gratzel M. (2009), Recent Advances in Sensitized Mesoscopic Solar Cells, **Accounts Of Chemical Research**, 42, 1788-1798.

Gratzel, M. (2007), Photovoltaic and photoelectrochemical conversion of solar energy, **Philosophical Transactions of The Royal Society**, 365, 993-1005.

Gratzel M. (2001), Photoelectrochemical Cells, **Nature**, 414, 338-344.

Gratzel, M. (2000), Perspectives for Dye-Sensitized Nanocrystalline Solar Cells, **Progress in Photovoltaics: Research and Applications**, 8, 171-185.

Gratzel, M. (2005), Solar Energy Conversion by Dye-Sensitized Photovoltaic Cells, **Inorganic Chemistry**, 44, 6841-6851.

Green M. A., Emery K., Hishikawa Y. and Warta W. (2010), Solar cell efficiency tables (version 35), **Progress in Photovoltaics: Research and Applications**, 88, 144-150.

Grossmann W. D., Grossmann I. and Steininger K., (2010), Indicators To Determine Wining Renewable Energy Technologies With an Application to Photovoltaics, **Environmental Science and Technology**, 44, 4849-4855.

Hagfeldt, A. and Gratzel, M. (2000), Molecular Photovoltaics, **Accounts of Chemical Research**, 33, 269-277.

Hagfeldt, A. and Gratzel, M. (1995), Light-Induced Redox Reactions Nanocrystalline Systems, **Chemical Reviews**, 95, 49-68.

Hagfeldt, A., Boschloo, G., Sun, L., Kloo, L. and Pettersson, H. (2010), Dye-Sensitized Solar Cells, **Chemical Reviews**, 110, 6595-6663.

Hallman, P. S., Stephenson, T. A. and Wilkinson, G. (1970), Tetrakis(triphenylphosphine)dichlororuthenium(II) and Tris(triphenylpho-sphine)dichlororuthenium(II), **Inorganic Syntheses**, 12, 237-240.

Haque, S., Palomares, E., Cho, B., Green, A., Hirata, N., Klug, D. and Durrant, J. (2005), Charge separation versus recombination in dye-sensitized nanocrystalline solar cells: the minimization of kinetic redundancy, **Journal of American Chemical Society**, 127, 3456-3462.

Hara, K., Sugihara, H., Tachibana, Y., Islam, A., Yanagida, M., Sayama, K. and Arakawa, H. (2001), Dye-sensitized nanocrystalline TiO_2 solar cells based on ruthenium(II) phenanthroline complex photosensitizers, **Langmuir**, 17, 5992-5999.

Hoertz, P. G., Staniszewski, A., Marton, A., Higgins, G. T., Incarvito, C. D., Rheingold, A. L. and Meyer, G. J. (2006), Toward Exceeding the Shockley-Queisser Limit: Photoinduced Interfacial Charge Transfer Processes that Store Energy in Excess of the equilibrated Excited State, **Journal of American Chemical Society**, 128, 8234-8245.

Hou, Y., Xie, P., Zhang, B., Cao, Y., Xiao, X. and Wang, W. (1999), Influence of the attaching group and substituted position in the photosensitization behavior of ruthenium polypyridyl complexes, **Inorganic Chemistry**, 38, 6320-6322.

Ito, S., Zakeeruddin, S. M., Humphry-Baker, R., Liska, P., Charvet, R., Comte, P., Nazeeruddin, M. K., Pechy, P., Takata, M. and Miura, H. (2006), High-efficiency

organic-dye-sensitized solar cells controlled by nanocrystalline-TiO_2 electrode thickness, **Advanced Materials**, 18, 1202-1205.

Jose, R., Thavasi, V. and Ramakrishna, S. (2009), Metal Oxides for Dye-Sensitized Solar Cells, **Journal of American Ceramic Society**, 92, 289-301.

Juris, A., Balzani, V., Barigelletti, F., Campagna, S., Belser, P. and Von Zelewsky, A. (1988), Ruthenium(II) polypyridine complexes: photophysics, photochemistry, electrochemistry, and chemiluminescence, **Coordination Chemistry Reviews**, 84, 85-277.

Kalyanasundaram, K.; Gratzel, M. (1998), Applications of functionalized transition metal complexes in photonic and optoelectronic devices, **Coordination Chemistry Reviews**, 77, 347-414.

Kang, M., Kim, J. H., Kim, Y. J., Won, J., Park, N. and Kang, Y. S. (2005), Dye-sensitized solar cells based on composite solid polymer electrolytes, **Chemical Communications**, 7, 889-891.

Kanungo, B. K., Baral, M., Bhattacharya, S. and Sahoo, Y. (2003), Synthesis of New Macrocycles with 2,2`-Bipyridyl and Polyamine Functions, **Synthetic Communications**, 33, 3159-3164.

Klein, C., Nazeeruddin, M. K., Liska, P., Di Ceno, D., Hirata, N., Palomares, E., Durrant, J. R. and Gratzel, M. (2005), Engineering of a Novel Ruthenium Sensitizer and Its Application in Dye-Sensitized Solar Cells for Conversion of Sunlight into Electricity, **Inorganic Chemistry**, 44, 178-180.

Kuang, D., Ito, S., Wenger, B., Klein, C., Moser, J., Humphry-Baker, R., Zakeeruddin, S. and Gratzel, M. (2006), High Molar Extinction Coefficient Heteroleptic Ruthenium Complexes for Thin Film Dye-Sensitized Solar Cells, **Journal of American Chemical Society**, 128, 4146-4154.

Kuang, D., Klein, C., Ito, S., Moser, J., Humphry-Baker, R., Evans, N., Duriaux, F., Gratzel, C., Zakeeruddin, S. and Gratzel, M. (2007), High-efficiency and stable Mesoscopic dye-sensitized solar cells based on a high molar extinction coefficient ruthenium sensitizer and nonvolatile electrolyte, **Advanced Materials**, 19, 1133-1137.

Kuciauskas, D., Monat, J. E., Villahermosa, R., Gray, H. B., Lewis, N. S. and Mccusker, J. K. (2002), Transient Absorption Spectroscopy of Ruthenium and Osmium Polypyridyl Complexes Adsorbed onto nanocrystalline TiO_2 Photo electrodes, **Journal of Physical Chemistry B**, 106, 9347-9358.

Kuznetsov, V. L. and Edwards, P. P. (2010), Functional Materials for Sustainable Energy Technologies: Four Case Studies, **Chem. Sus. Chem.**, 3, 44-58.

Longo, C. and De Paoli, M. (2003), Dye-Sensitized Solar Cells: A Successful Combination of Materials, **J. Braz. Chem. Soc**., 14, 889-901.

Luque, A. and Hegedus, S. (2003), **Handbook of Photovoltaic Science and Engineering**, First Edition, UK, John Wiley and Sons Ltd.

Markvart, T. and Castaner, L. (2005), **Solar Cells, Materials, Manufacture and Operation,** First Edition, UK, Elsevier.

McEvoy, A. J. and Gratzel, M. (1994), Sensitization in photochemistry and photovoltaics, **Solar Energy Materials and Solar Cells**, 32, 221-227.

Naskar, S., Naskar, S., Drew, M., Gorelsky, S., Lassalle-Kaiser, B., Aukauloo, A, Mishra, D. and Chattopadhyay, S. (2009), Structural and spectroscopic properties of Ru(II) complexes of 4(aryl)thiosemicarbazones of thiophen-2-carbaldehyde, **Polyhedron**, 28, 4101-4109.

Nazeeruddin, M. K. and Gratzel, M. (2007), Transition Metal Complexes for Photovoltaic and light emitting Applications, **Struct. Bond**, 123, 113-175.

Nazeeruddin, M. K., Kay, A., Rodicio, I., Humphry-Baker, R., Muller, E., Liska, P.,Vlachopoulos, N. and Gratzel, M. (1993), Conversion of Light to Electricity by cis-X2Bis(2,2`-bipyridyl-4,4`-dicarboxylate)ruthenium(II) Charge-Transfer Sensitizers (X = Cl-, Br-, I-, CN-, and SCN-) on nanocrystalline TiO2 Electrodes, **Journal of American Chemical Society**, 115, 6382-6390.

Nazeeruddin, M. K., Pechy, P., Renouard, T., Zakeeruddin, S. M., Humphry-Baker, R., Comte, P., Liska, P., Cevey, L., Costa, E. and Shklover, V. (2001), Engineering of efficient panchromatic sensitizers for nanocrystalline TiO2-based solar cells, **Journal of American Chemical Society**, 123, 1613-1624.

Nazeeruddin, M. K., Wang, Q., Cevey, L., Aranyos, V., Liska, P., Figgemeier, E., Klein, C., Hirata, N., Koops, S. and Haque, S. A. (2006), DFT-INDO/S Modeling of New High Molar Extinction Coefficient Charge Transfer Sensitizers for Solar Cell Applications, **Inorganic Chemistry**, 45, 787-797.

Nazeeruddin, M. K., Zakeeruddin, S. M., Humphry-Baker, R., Jirousek, V., Fischer, C., Liska, P., Vlachopoulous, N., Shklover, V. and Gratzel, M. (1999), Acid-Base Equilibria of (2,2`-Bipyridine-4,4`-dicarboxylic acid)ruthenium(II) complexes and the effect of protonation on charge transfer sensitization of Nanocrystalline Titania, **Inorganic Synthesis**, 36, 6298-6305.

Omer, A. M. (2009), Energy use and environmental impacts: A general review, **Journal of Renewable and sustainable Energy**, 1, 053101-053129.

O`Regan, B. and Gratzel, M. (1991), A low cost high efficiency solar cell based on dye sensitized colloidal titanium dioxide films, **Nature**, 353, 737-740.

Perrin, D. D. and Armarego, W. L. (1988), **Purification of Laboratory Chemicals**, Third edition, U.S.A, Pergamon Press.

Polo, A. S., Itokazu, M. K. and Iha, N. Y. (2004), Metal complex sensitizers in dye-sensitized solar cells, **Coordination Chemistry Reviews**, 248, 1343-1361.

Rajalakshmanan, E. and Alexander, V. (2005), Synthesis of Dimethylbipyridines by the Reductive Coupling of 2-Halomethylpyridines with Nickel Catalyst, **Synthetic Communications**, 35, 891-895.

Ribeiro, H. A., Sommeling, P. M., Kroon, J. M., Mendes, A. and Costa, C. A. (2009), Dye-Sensitized Solar Cells: Novel Concepts, Materials and State-of-the-Art Performances, **International Journal of Green Energy**, 6, 245-256.

Robertson, N. (2006), Optimizing Dyes for Dye-Sensitized Solar Cells, **Angewandte Chemie, International Edition,** 45, 2338-2345.

Sarkis, G. Y. and Axamawaty, M. T. (2003), Synthesis and biological activity of some new 4-carbomethoxyquinoline-2-carboxaldehyde thiosemicarbazones and their Co(II), Ni(II), Cu(II) and Fe(II) complexes, **Dirasat: Pure Sciences**, 30, 182-190.

Sathya, N., Raja, G., Priya, N. P. and jayabalakrishnan, C. (2009), Ruthenium(II) complexes incorporating tridentate Schiff base ligands: synthesis, spectroscopic, redox, catalytic and biological properties, **Applied Organometallic Chemistry**, 24, 366-373.

Shah, A., Torres, P., Tscharner, R., Wyrsch, N. and Keppner, H. (1999), Photovoltaic Technology: The Case for Thin-Film Solar Cells, **Science**, 285, 692-698.

Singh, K. S., Carroll, P. J. and Kollipara, M. (2005), Pentamethylcyclopentadienyl ruthenium(II) complexes of para-substituted N-(pyrid-2-ylmethylene)-phenylamine ligands: syntheses, spectral and structural studies, **Polyhedron**, 24, 391-396.

Sivoththaman, S. and Baroughi, M. F. (2006), Cost-Effective, Silicon-Based Solar Cells: Material and Technology Issues, **International Journal of Green Energy**, 3, 1-15.

Tsubomura, H., Matsumura, M., Nomura, Y. and Amamiya, T. (1976), Dye sensitized zinc oxide: aqueous electrolyte: platinum photocell, **Nature**, 261, 402-403.

Venanzi, L. M. (1958), Tetrahedral Nickel(II) Complexes and the Factors Determining Their Formation. Part I. Bistriphenylphosphine Nickel(II) Compounds, **Journal of American Chemical Society**, 719-724.

Vernon, A. and Sheard, J. (1948), The solubility of Tetraethylammonium iodide in benzene-ethylene dichloride mixtures, **Journal of American Chemical Society**, 70, 2035-2036.

Wang, P., Klein, C., Moser, J., Humphry-Baker, R., Cevey-Ha, N., Charvet, R., Comte, P., Zakeeruddin, S. and Gratzel, M. (2004), Amphiphilic Ruthenium Sensitizer with 4,4`-Diphosphonic Acid-2,2`-bipyridine as Anchoring Ligand for Nanocrystalline Dye Sensitized Solar Cells, **Journal of Physical Chemistry B**, 108, 17553-17559.

Wang, Z., Huang, C., Zhang, B., Hou, Y., Xie, P., Qian, H. and Kurash, I. (2000), Highly efficient charge transfer from a trans-ruthenium bipyridine complex to nanocrystalline TiO2 particles, **New Journal of Chemistry**, 24, 567-568.

Xie, P. and Guo, F. (2007), Molecular Engineering of Ruthenium Sensitizers in Dye-Sensitized Solar Cells, **Current Organic Chemistry**, 11, 1272-1286.

Xie, P., Hou, Y. J., Wei, T. X., Zhang, B. W., Cao, Y. and Huang, C. H. (2000), Synthesis and photoelectric studies of Ru(II) polypyridyl sensitizers, **Inorganica Chemica Acta**, 308, 73-79.

Zakeeruddin, S. M., Nazeeruddin, M. K., Humphry-Baker, R. and Gratzel, M. (1999), Synthesis and photophysical properties of trans-dithiocyanato bis(4,4`-dicarboxylic acid-2,2`-bipyridine) ruthenium(II) charge transfer sensitizer, **Inorganica Chimica Acta**, 296, 250-253.

تحضير بعض معقدات الروثينيوم (II) لاستخدامها في الخلايا الشمسية ذات الصبغات الحساسة

إعداد

رشا خالد الشويكي

إشراف

الدكتور

الأستاذ حمد الله الهودلي

ملخص

خلال هذا البحث تم تحضير عدد من قواعد شيف من الأنواع التالية: (أ) تكثيف 8-أمينوكوينولين مع 4-هيدروكسي بنزألدهيد (**1**) أو مع ملح الصوديوم التابع لسالسلدهيد-5-سلفونيك أسيد (**2**) . (ب) تكثيف 3- أمينوبنزويك أسيد مع 2- فورميل -4- كوينولين كربوكسيلك أسيد (**3**). (ج) تكثيف 1,2- فينيلين ثنائي الأمين مع 3- فورميل -4- هيدروكسي بنزويك أسيد (**4**) و مع 4- ثنائي ميثيل أمينو-2- هيدروكسي بنزالدهيد (**5**) و مع ملح الصوديوم التابع لسالسلدهيد -5- سلفونيك أسيد (**6**) ومع 2- فورميل -4- كوينولين كربوكسيلك أسيد (**7**). و لقد تم تشخيص المتصلات المحضرة بواسطة التحاليل الدقيقة للعناصر و أطياف الأشعة تحت الحمراء (IR) وطيف الرنين المغناطيسي للهيدروجين و لنظير الكربون-13 (^{13}C NMR and ^{1}H NMR) و أطياف الكتلة. ونتج عن تفاعل 1 و 2 و 7 مع ثنائي كلورو- رباعي(ثنائي ميثيل السلفوكسايد) روثينيوم (II), $RuCl_2(DMSO)_4$, المعقدات التالية: $[Ru(1)(AQ)Cl_2].5H_2O$ و $[Ru(2\text{-}H)_2].4H_2O$ و $[Ru(7)Cl_2].3H_2O$. و نتج عن تفاعل 4 ,5 و 6 مع ثنائي كلورو- ثلاثي(فينيل

فوســـفين) روثينيـــوم (II), $RuCl_2(PPh_3)_3$, أعطـــى المعقـــدات التاليـــة -[Ru(4
و [$Ru(5-2H)(PPh_3)(H_2O)].3H_2O$ و $3H)(PPh_3)(H_2O)$]
[$Ru(6-2H)(PPh_3)(NEt_3)].3H_2O$ بالترتيب. و قد تم التعرف على هذه المعقدات من خلال التحاليل الدقيقة للعناصر و أطياف الأشعة تحت الحمراء (IR) وقياسات الموصلية الكهربائية و قياسات القابلية المغناطيسية لهذه المعقدات. و قد أظهرت جميع المعقدات المحضرة القدرة على امتصاص الأشعة في المنطقة المرئية و فوق البنفسجية.

و بشكل خاص أظهرت المعقدات: [$Ru(1)(AQ)Cl_2].5H_2O$ و [$Ru(2-H)2].4H_2O$ امتصاص يمتد إلى 623 نانوميتر و 630 نانوميتر, بالترتيب. أما المعقدات:
[$Ru(4-3H)(PPh_3)(H_2O)$] و [$Ru(6-2H)(PPh_3)(NEt_3)].3H_2O$ و [$Ru(5-2H)(PPh_3)(H_2O)].3H_2O$ أظهرت امتصاصاً قوياً عند الأطوال الموجية التالية 466 نانوميتر (معامل الامتصاص =12.585 لتر/مول.سم) و 412 نانوميتر (معامل الامتصاص = 10.357لتر/مول.سم) و 413 نانوميتر (معامل الامتصاص =16.553 لتر/مول.سم) بالترتيب.